

6-26-2017

Synthesis of Gemcitabine Analogues with Silicon-Fluoride Acceptors for ^{18}F Labeling

Cesar Gonzalez-Espinoza
cgonz042@fiu.edu

DOI: 10.25148/etd.FIDC001927

Follow this and additional works at: <https://digitalcommons.fiu.edu/etd>

Recommended Citation

Gonzalez-Espinoza, Cesar, "Synthesis of Gemcitabine Analogues with Silicon-Fluoride Acceptors for ^{18}F Labeling" (2017). *FIU Electronic Theses and Dissertations*. 3469.
<https://digitalcommons.fiu.edu/etd/3469>

This work is brought to you for free and open access by the University Graduate School at FIU Digital Commons. It has been accepted for inclusion in FIU Electronic Theses and Dissertations by an authorized administrator of FIU Digital Commons. For more information, please contact dcc@fiu.edu.

FLORIDA INTERNATIONAL UNIVERSITY

Miami, Florida

SYNTHESIS OF GEMCITABINE ANALOGUES WITH SILICON-FLUORIDE
ACCEPTORS FOR ^{18}F LABELING

A dissertation submitted in partial fulfillment of

the requirements for the degree of

DOCTOR OF PHILOSOPHY

in

CHEMISTRY

by

Cesar Gonzalez

2017

To: Dean Michael R. Heithaus
College of Arts, Sciences and Education

This dissertation, written by Cesar Gonzalez, and entitled Synthesis of Gemcitabine Analogues with Silicon-Fluoride Acceptors for ^{18}F Labeling, having been approved in respect to style and intellectual content, is referred to you for judgment.

We have read this dissertation and recommend that it be approved.

David Chatfield

Watson Lees

Kevin O'Shea

John Makemson

Stanislaw F. Wnuk, Major Professor

Date of Defense: June 26, 2017

The dissertation of Cesar Gonzalez is approved.

Dean Michael R. Heithaus
College of Arts, Sciences and Education

Andrés G. Gil
Vice President for Research and Economic Development
and Dean of the University Graduate School

Florida International University, 2017

© Copyright 2017 by Cesar Gonzalez

All rights reserved.

DEDICATION

I would like to dedicate this dissertation to everyone that helped through this period of my life, specially my family which always encouraged me during the good and the not so good times. Always keep it tight, keep it alright.

ACKNOWLEDGMENTS

I would like to thank my committee members, Watson Lees, Kevin O'Shea, David Chatfield and John Makemson for their support and advice throughout my graduate studies. I also like to extend my gratitude towards everyone at the Department of Chemistry and Biochemistry at Florida International University.

I would also like to thank all my collaborators whom their great help have made this dissertation what it is. I would like to thank Dr. Cheppail Ramachandran from the Department of Pathology at Nicklaus Children's Hospital for studying the cytostatic activities of my 4-*N*-modified gemcitabine analogues in his L1210 cell line. Also, thank you to Dr. Alejandro Barbieri at FIU's department of Biological Sciences for providing cell and fluorescence studies with his HEK 293 cell line in order to have a better understanding of cellular uptake on my 4-*N*-modified gemcitabine analogues. A very special and appreciated thank you to Dr. Michael van Dam and his coworkers from the Crump Institute for Molecular Imaging in the University of California Los Angeles for their work in ¹⁸F labeling and PET imaging of my 4-*N*-modified gemcitabine analogues in WT C57BL/6 mice.

Finally, I would like to thank my advisor, Dr. Stanislaw F. Wnuk, for all his guidance and always keeping my in the right track. I would like to thank all of my lab mates, previous and current, for their advice and friendship.

ABSTRACT OF THE DISSERTATION
SYNTHESIS OF GEMCITABINE ANALOGUES WITH SILICON-FLUORIDE
ACCEPTORS FOR ^{18}F LABELING

by

Cesar Gonzalez

Florida International University, 2017

Miami, Florida

Professor Stanislaw F. Wnuk, Major Professor

Gemcitabine (dFdC) is an effective chemotherapeutic nucleoside analogue for treatment of cancers and solid tumors. Gemcitabine's chemotherapeutic effect is limited by its rapid intracellular deamination by cytidine deaminase into the inactive uracil derivative. Herein, I designed and synthesized two sets of gemcitabine analogues: i) a 4-*N*-alkyl gemcitabine analogue containing a β -keto sulfonate moiety, and ii) clickable analogues possessing silicon-fluoride acceptor building blocks. Both of these sets of analogues undergo efficient fluorination, including fluorination protocols compatible with ^{18}F labeling.

The synthesis of the 4-*N*-alkyl gemcitabine analogue bearing β -keto sulfonate moiety began with reaction of 4-*N*-tosylgemcitabine with 1-amino-10-undecene, followed by a series of oxidation and sulfonation steps which yielded the β -keto sulfonate analogues.

The coupling of gemcitabine with carboxylic acids using peptide coupling conditions afforded 4-*N*-alkanoyl analogues with a terminal alkyne or azido moiety. Click reaction of these 4-*N*-alkanoyl analogues with dialkylsilyl building blocks gave 4-*N*-alkanoylsilanegemcitabine analogue. Reaction of 4-*N*-tosylgemcitabine with

functionalized azidoalkyl amines provided 4-*N*-alkylgemcitabine with a terminal azido group. Coupling of the latter with dialkylsilyl building block provided 4-*N*-alkylsilanegemcitabine. Fluorination of 4-*N*-alkyl gemcitabine analogues with β -keto sulfonate moieties and of the trisubstituted silane derivatives with KF and 18-Crown-6 ($\text{CH}_3\text{CN}/75^\circ\text{C}/0.5\text{-}1\text{h}$), gave the corresponding fluorinated 4-*N*-alkyl and alkanoyl gemcitabine analogues under conditions that are compatible with protocols for positron emission tomography (PET) ^{18}F labeling. The [^{18}F] 4-*N*-alkyl and alkanoyl silane gemcitabine analogues were successfully synthesized on microscale and macroscale radiochemical protocols. The biodistribution of [^{18}F] 4-*N*-alkyl gemcitabine analogue was analyzed via PET imaging. The cytotoxicity activity of the silane gemcitabine analogues were studied in cancer L1210 and HEK 293 cell lines and their cellular uptake were investigated using HPLC analysis and fluorescence microscopy.

Reduction of ribono-1,4-lactones and gulono-1,4-lactone as well as ribono-1,5-lactone and glucono-1,5-lactones with LTBH (1.2 equiv.) in CH_2Cl_2 at 0°C for 30 min provided the corresponding pentose or hexose hemiacetals in chemoselective fashion and in high yields. Commonly used in carbohydrate chemistry protecting groups such as trityl, benzyl, silyl, acetals and to some extent acyls are compatible with this reduction.

TABLE OF CONTENTS

CHAPTER	PAGE
1. INTRODUCTION	1
1.1. Gemcitabine: Chemistry and biological activity	1
1.1.1. Gemcitabine: Anti-cancer mechanism of action and inhibition	1
1.1.2. Gemcitabine: Design and synthesis of prodrugs	3
1.1.3. Gemcitabine: Theranostic image-guided tumor agents	5
1.2. Positron emission tomography (PET)	11
1.2.1. Radiochemistry: Fluorination	11
1.2.2. Positron emitting ¹⁸ F radiotracers for anticancer therapy	13
1.2.3. Silicon ¹⁸ F radiochemistry	16
1.3. Reduction of lactones to hemiacetals	19
1.3.1. Synthetic significance of reduction of lactones to hemiacetals	19
1.3.2. Reducing agents for reduction of lactones to hemiacetals	22
2. RESEARCH OBJECTIVES	26
3. RESULTS AND DISCUSSION	28
3.1. Design and synthesis of 4- <i>N</i> -alkanoyl and 4- <i>N</i> -alkyl gemcitabine analogues	28
3.1.1. 4- <i>N</i> -Alkyl β-keto sulfonate gemcitabine analogue	28
3.1.1.1. 4- <i>N</i> -Alkyl β-keto sulfonate gemcitabine analogue: Rationale	28
3.1.1.2. 4- <i>N</i> -Alkyl β-keto sulfonate gemcitabine analogue: Synthesis	29
3.1.1.3. 4- <i>N</i> -Alkyl β-keto sulfonate gemcitabine analogue: Fluorination studies	34
3.1.2. 4- <i>N</i> -Alkyl and alkanoyl gemcitabine analogues with silicon-fluoride acceptors	39
3.1.2.1. Silicon-fluoride acceptors gemcitabine analogues: Rationale	39
3.1.2.2. Silicon-fluoride acceptors gemcitabine analogues: Synthesis	40
3.1.2.3. Silicon-fluoride acceptors gemcitabine analogues: Fluorination studies	43
3.1.2.4. Silicon-fluoride acceptors gemcitabine analogues: Stability studies	46
3.1.2.5. Biological evaluation of the 4- <i>N</i> -alkyl & alkanoyl gemcitabine analogues	50
3.1.2.6. [¹⁸ F]-Labeling of 4- <i>N</i> -alkanoyl and alkyl gemcitabine radioligands	57
3.1.2.7. Biological and PET evaluation of [¹⁸ F]-4- <i>N</i> -alkyl gemcitabine radioligand 96	61
3.2. Reduction of sugar lactones to hemiacetals using lithium triethylborohydride	65
3.2.1. Reduction with LTBH: Rationale	65
3.2.2. Reduction optimization and study of parameters	66
3.2.3. Reaction profile of reduction of lactone 97 to hemiacetal 98	68
3.2.4. Reduction of several sugar lactones	70
4. EXPERIMENTAL	76

4.1. General Procedures	76
4.2. Synthesis of 4- <i>N</i> -Alkyl β -keto sulfonate gemcitabine analogues	76
4.3. Synthesis of 4- <i>N</i> -alkanoyl and 4- <i>N</i> -alkyl clickable gemcitabine analogues with silicon-fluoride acceptors	89
4.4. Reduction of sugar lactones to hemiacetals with LTBH.....	98
4.4.1. Typical procedure for reduction of the sugar lactones to hemiacetals with LTBH and selected products ¹⁵⁰	98
4.4.2. ¹ H NMR reaction profile for reduction of sugar lactone 97	100
4.5. Biological evaluation and studies for 4- <i>N</i> -alkanoyl and alkyl gemcitabine analogues	101
4.6. Radiosynthesis of ¹⁸ F Fluoro-silane probes.....	104
4.7. Biological and PET evaluation of [¹⁸ F]-4- <i>N</i> -alkyl gemcitabine radioligand 96 ..	111
5. CONCLUSION.....	114
REFERENCES	117
VITA.....	127

LIST OF TABLES

TABLE	PAGE
1. <i>In vitro</i> cytostatic activity of 4- <i>N</i> -Modified gemcitabine analogues 7-10 on the tumor cell lines L1210, HeLa, and MCF-7.....	5
2. Fluorination reactions with different conditions.....	35
3. Stability studies of fluoro β -keto model compound 75.....	36
4. Summary of model fluorination studies.....	43
5. <i>In vitro</i> cytostatic activity of 4- <i>N</i> -modified gemcitabine analogues on L1210 cell line.....	52
6. ^{18}F radiosynthetic yields of 4- <i>N</i> -modified gemcitabine analogues 94 and 96.....	58
7. Effect of various reaction parameters on reduction of 97 with LTBH.....	68
8. Reduction of various sugar lactones with LTBH to lactols.....	71
9. Details of ELIXYS radiosynthesis program.....	107
10. Details of reagent positions in ELIXYS cassette.....	108

LIST OF FIGURES

FIGURE	PAGE
1. Structure of gemcitabine.....	2
2. Gemcitabine mode of action & inhibition.....	2
3. 4- <i>N</i> -modified gemcitabine prodrugs with enhanced anti-cancer activity.....	4
4. 4- <i>N</i> -modified gemcitabine analogues synthesized by Pulido <i>et al</i> ²⁸	5
5. Structure of H-gemcitabine ³¹	6
6. Structure of GnRH-gemcitabine conjugate ³⁹	7
7. Fluorescent theranostic prodrug synthesized by Bhuniya <i>et al</i> ^{59, 60}	9
8. Fluorescent theranostic prodrug synthesized by Liu <i>et al</i> ⁶²	10
9. Examples of ¹⁸ F-aliphatic and aromatic nucleophilic substitutions ^{71, 73, 74}	12
10. Selected ¹⁸ F radiotracers for anticancer therapy.....	14
11. Hydrolysis half-lives (<i>t</i> _{1/2}) of selected organofluorosilanes under aqueous buffer (pH 7) and ambient temperature reported by Hhne <i>et al</i> ⁹¹	17
12. Silicon-fluoride acceptors in octreotate ⁹⁶ 32 and thymidine derivatives ⁹⁹ 33.....	19
13. Catalytic cycle and transition state proposed by Buchwald <i>et al</i> ¹²¹	23
14. Proposed structures of 4- <i>N</i> -alkanoyl and 4- <i>N</i> -alkyl gemcitabine analogues.....	26
15. Key structural differences between β -keto A and 4- <i>N</i> -alkyl 10 gemcitabine analogues.....	29
16. Fluorination of 4- <i>N</i> -alkyl 73 (chromatogram A: 73 standard, chromatogram B: Crude fluorination reaction) in 50% CH ₃ CN/H ₂ O.....	38
17. Fluorination of 4- <i>N</i> -alkyl 72 (chromatogram A: 72 standard, chromatogram B: Crude fluorination reaction) in 50% CH ₃ CN/H ₂ O.....	38
18. General synthetic goal of gemcitabine silicon-fluoride acceptors analogues.....	40

19. Stability of 4- <i>N</i> -alkanoyl 90 (chromatogram A: 1, chromatogram B: 90 after 30 min) in 35 %CH ₃ CN /0.1% TFA.....	47
20. Stability of 4- <i>N</i> -alkanoyl 94 (chromatogram A: 1, chromatogram B: 94 after 2 h) in 35% CH ₃ CN/0.1% TFA.....	47
21. Stability of 4- <i>N</i> -alkyl 92 (chromatogram A: 1, chromatogram B: 92 after 8 h) in 25% CH ₃ CN/0.1% TFA.....	48
22. Analysis of stability of 4- <i>N</i> -alkyl 96 (chromatogram A: 96 after 1 h, chromatogram B: 96 after 3 h) in 25%CH ₃ CN/0.1% TFA.....	49
23. Analysis of stability of 4- <i>N</i> -alkyl 96 (chromatogram A: 1, chromatogram B: 96 after 3 h) in 25%CH ₃ CN/H ₂ O (NO TFA).....	49
24. <i>In vitro</i> cytotoxicity curve of 4- <i>N</i> -alkanoyl and 4- <i>N</i> -alkyl gemcitabine analogues on L1210 mouse leukemic cell lines. Cells were treated with analogues for 72 h before the viability of treated cells was determined by MTT assay. Results represent the mean of triplicates with error bars indicating standard deviation.....	51
25. <i>In vitro</i> cytotoxicity graph of 4- <i>N</i> -alkanoyl and 4- <i>N</i> -alkyl gemcitabine analogues on HEK 293 cell lines. Cells were treated with analogues for 48 h before the viability of treated cells was determined by MTT assay. Results represent the mean of triplicates.....	53
26. HPLC chromatograph of 86 in 20% CH ₃ CN/H ₂ O.....	54
27. HPLC analysis of 86 in CH ₃ CN/H ₂ O after incubation in HEK 293 cell line (chromatogram A: cell blank, chromatogram B: supernatant after 24 h, chromatogram C: cell sample after 24 h) in 20% CH ₃ CN/H ₂ O.....	55
28. General fluorescence labeling experiment.....	56
29. Labeling of 86 in HEK 293 cells for 24 h, followed by fixation and addition of Fluor 488 alkyne and copper(I).....	57
30. Macroscale radiosynthesis of 4- <i>N</i> -alkanoyl [¹⁸ F]94 (chromatogram A: UV detector, chromatogram B: radio detector, radiolabeled product in green) in 80% CH ₃ CN/0.1% TFA.....	59
31. Macroscale radiosynthesis of 4- <i>N</i> -alkyl [¹⁸ F]96 (chromatogram A: UV detector, chromatogram B: radio detector, radiolabeled product in green) in 30% CH ₃ CN/H ₂ O.....	59

32. Microscale radiosynthesis of 4- <i>N</i> -alkanoyl [¹⁸ F]94 (chromatogram A: UV detector, chromatogram B: radio detector, radiolabeled product in red) in 80% CH ₃ CN/0.1% TFA.....	60
33. Microscale radiosynthesis of 4- <i>N</i> -alkyl [¹⁸ F]96 (chromatogram A: UV detector, chromatogram B: radio detector, radiolabeled product in green) in 70% CH ₃ CN/H ₂ O....	61
34. Series of frames from dynamic PET scan of WT C57BL/6 mouse injected with [¹⁸ F]96 (up to 1 h). Images are coronal maximum intensity projections.....	63
35. Series of frames from dynamic PET scan of WT C57BL/6 mouse injected with [¹⁸ F]96 (up to 1 h). Images are sagittal maximum intensity projections.....	63
36. (Left) Dynamic biodistribution of [¹⁸ F]96 in WT C57BL/6 mouse. (Right) Maximum intensity projection at 1 h post-injection (left: coronal; right: sagittal).....	64
37. (Left) Biodistribution of [¹⁸ F]96 from 10 min static scan in WT C57BL/6 mouse at 1 h post-injection. (Right) Maximum intensity projection of 10 min static scan at 1 h post-injection (left: coronal; right: sagittal).....	64
38. Reduction of lactone 97 (36 mM) with 1.2 equiv. of LTBH (0 °C/CH ₂ Cl ₂). The profile for the reactions was measured by integrating the peaks of the ¹ H NMR spectra (e.g., disappearance of the H4 peak at 4.65 ppm for 98 and appearance of the H1 peak at 5.28 ppm for 99).....	69
39. Reduction of lactone 97 (42 mM) with 2.5 equiv. of LTBH (0 °C/CH ₂ Cl ₂). The profile for the reactions was measured by integrating the corresponding peaks of the ¹ H NMR spectra (e.g., disappearance of the H4 peak at 4.65 ppm for 97 and appearance/disappearance of the H1 peak at 5.28 ppm for 98 and appearance of the H3 peak at 4.10 ppm for 99).....	69
40. Proposed chelating of borane with exocyclic sugar oxygens.....	75
41. ¹ H NMR spectra of reaction profile with 1.2 equiv. of LTBH.....	100
42. ¹ H NMR spectra of reaction profile with 2.5 equiv. of LTBH.....	101
43. Schematic of the microdroplet radiosynthesis process.....	110

LIST OF SCHEMES

SCHEME	PAGE
1. Synthesis of gemcitabine analogue for fluorescent labeling ⁵⁸	8
2. Deoxyfluorination of phenols and heterophenols with ¹⁸ F by the Ritter group ⁷¹	13
3. Synthesis of [¹⁸ F]5-fluorouracil as a PET tracer ⁸⁴	15
4. Hydrolysis reaction of Si-F bond to Si-OH.....	18
5. Mechanism of isotopic exchange reaction between ¹⁸ F and ¹⁹ F.....	18
6. Reduction of lactones with NaBH ₄ and DIBAL-H.....	20
7. Synthesis of gemcitabine through reduction of sugar lactones.....	21
8. Synthesis of oxathiolanyl and dioxolanyl nucleoside analogues through reduction of sugar lactones ¹⁰⁸	21
9. General and specific reduction of lactones with titanocene(III) hydride ¹²²	24
10. Use of borane-based reducing agents for reduction of lactones to hemiacetals.....	24
11. Synthesis of cyclic azahemiacetals SRH analogues 53 ¹¹¹ , dihydroxyprolines 54 and functionalized prolines 55 through the use of LTBH ^{124, 125}	25
12. Reduction of sugar lactones to hemiacetals under various conditions.....	27
13. Synthesis of amino with β-keto side chain.....	30
14. Unsuccessful attempted 4- <i>N</i> -tosylgemcitabine 62 and 61 coupling reaction.....	31
15. Synthesis of fluoro β-keto side chain.....	32
16. Overall synthesis of 4- <i>N</i> -modified β-keto fluoro gemcitabine analogue.....	32
17. Synthesis of 4- <i>N</i> -(10-undecene) gemcitabine analogue.....	33
18. Overall synthesis of β-keto gemcitabine sulfonate analogue.....	34
19. Fluorination of β-keto sulfonate gemcitabine analogues and subsequent deprotection under conditions compatible with ¹⁸ F-radiolabeling protocols ^a	37

20. Synthesis of 11-azidoundecanoic acid.....	40
21. Synthesis of 4- <i>N</i> -alkanoyl gemcitabine substrates for click reactions.....	41
22. Synthesis of 7-azido-1-aminoheptane.....	42
23. Synthesis of 4- <i>N</i> -alkyl gemcitabine derivatives for click reactions.....	42
24. Synthesis of silane building blocks for click reactions.....	43
25. Synthesis of the 4- <i>N</i> -acyl/alkyl gemcitabine analogues with the silicon-fluoride acceptors.....	45
26. Radiosynthesis of [¹⁸ F] 4- <i>N</i> -alkanoyl and alkyl gemcitabine analogues with silicon-fluoride acceptors.....	58
27. Synthesis of 4C-SRH analogues involving reduction of ribonolactones with LTBH ¹¹²	66
28. Reduction of the protected ribono-1,4-lactone 97 with LTBH.....	67
29. Reduction of γ -butyrolactone with LTBH to 1,4-butanediol.....	74

LIST OF ABBREVIATIONS

Ac	acetyl
Ar	aromatic (NMR)
β	beta
Bn	benzyl
Boc	<i>tert</i> -butyloxycarbonyl
BODIPY	boron-dipyrromethene
Br	broad (NMR)
Bz	benzoyl
calcd	calculated (HRMS)
CDA	cytidine deaminase
°C	degrees Celsius
Ci	Curie(s)
d	doublet (NMR)
DAST	diethylaminosulfur trifluoride
dCK	deoxycytidine kinase
DCM	dichloromethane
dFdC	2',2'-difluoro-2'-deoxycytidine
dFdCMP	2',2'-difluoro-2'-deoxycytidine monophosphate
dFdCDP	2',2'-difluoro-2'-deoxycytidine diphosphate
dFdCTP	2',2'-difluoro-2'-deoxycytidine triphosphate
dFdU	2',2'-difluorouridine
DIBAL-H	diisobutylaluminium hydride

DIPEA	<i>N,N</i> -diisopropylethylamine
DMAP	4-dimethylaminopyridine
DMF	<i>N,N</i> -dimethylformamide
DMSO	dimethylsulfoxide
EDC	(<i>N</i> -dimethylaminopropyl)- <i>N'</i> -ethyl-carbodiimide
ESI	electrospray ionization
FAC	2'-deoxy-2'-fluoro- β -D-arabinofuranosyl
FDG	2-deoxy-2-fluoro- D-glucose
g	gram(s)
h	hour(s)
hENT	human equilibrative nucleoside transporter
HOBt	hydroxybenzotriazole
HPLC	high performance liquid chromatography
HPMA	<i>N</i> -(2-hydroxypropyl)methacrylamide
HRMS	high resolution mass spectroscopy
Hz	hertz
IC ₅₀	half maximum inhibitory concentration
ID	injected dose
<i>J</i>	coupling constant in Hz (NMR)
K ₂₂₂	Kryptofix 222
L	liter(s)
LTBH	lithium triethylborohydride

m	milli; multiplet (NMR)
M	moles per liter
min	minute(s)
mol	mole(s)
Ms	mesyl
MS	mass spectrometry
<i>m/z</i>	mass to charge ratio (MS)
NFSi	<i>N</i> -fluorobenzenesulfonimide
NMO	methylmorpholine <i>N</i> -oxide
NMR	nuclear magnetic resonance
<i>p</i>	<i>para</i>
PMMA	poly(methyl methacrylate)
PEG	polyethylene glycol
PET	positron emission tomography
PTC	phase transfer catalyst
pyr	pyridine
%	percentage
q	quartet (NMR)
QMA	quarternary methylammonium
quin	quintet (NMR)
RCY	radiochemical yield
RNR	ribonucleotide reductase
RP	reverse phase (HPLC)

rt	room temperature
s	second(s); singlet (NMR)
SPAAC	strain-promoted alkyne-azide cycloadditions
SRH	<i>S</i> -ribosylhomocysteine
t	triplet (NMR)
TBAF	tetra- <i>n</i> -butylammonium fluoride
TBDMS	<i>tert</i> -butyldimethylsilyl
<i>t</i> -Bu	<i>tert</i> -butyl
TEA	trimethylamine
TFA	trifluoroacetic acid
THF	tetrahydrofuran
TK	thymidine kinase
TLC	thin layer chromatography
TMS	trimethylsilyl
t_R	retention time (HPLC)
TPP	tetraphenylporphyrin
Ts	tosyl
μ	micro
UV	ultraviolet
VIS	visible

1. INTRODUCTION

1.1. Gemcitabine: Chemistry and biological activity

1.1.1. Gemcitabine: Anti-cancer mechanism of action and inhibition

Gemcitabine (2',2'-difluoro-2'-deoxycytidine, dFdC, Figure 1) is a chemotherapeutic cytidine analogue that is usually used as first-line therapy for pancreatic and non-small cell lung cancers.^{1, 2} The analogue was first synthesized by Hertel *et al.* in 1988.^{3, 4} Gemcitabine, like most nucleoside analogues, is hydrophilic, and its uptake across the cell membrane is facilitated by human equilibrative nucleoside transport proteins (hENT's).⁵ Once in the cell, gemcitabine is activated by deoxycytidine kinase (dCK) for monophosphorylation, which is its rate limiting step, and then subsequent phosphorylation by intracellular kinases to its di- and tri-phosphate forms (dFdCDP and dFdCTP). The triphosphate, dFdCTP, is then incorporated into DNA, inhibiting DNA polymerase by chain termination during replication and repair processes, triggering apoptosis.⁶⁻¹⁰ Also, the potentiation of the effects of the triphosphorylated gemcitabine results from its inhibition of ribonucleotide reductase(s) (RNR's). Ribonucleotide reductases are enzymes that are involved in the conversion of nucleoside diphosphates to deoxynucleoside 5'-diphosphates (dNDPs) (Figure 2).¹¹⁻¹³ The inhibition of RNR's is critical because it leads to a reduction in dNDPs and consequently to a reduction in dNTPs. The change in concentration of dNTPs reduces the competition for dFdCTP to become incorporated into DNA by DNA polymerase, increasing the chance of apoptosis.

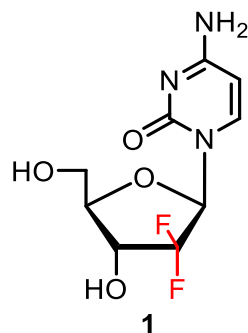


Figure 1. Structure of gemcitabine (dFdC)

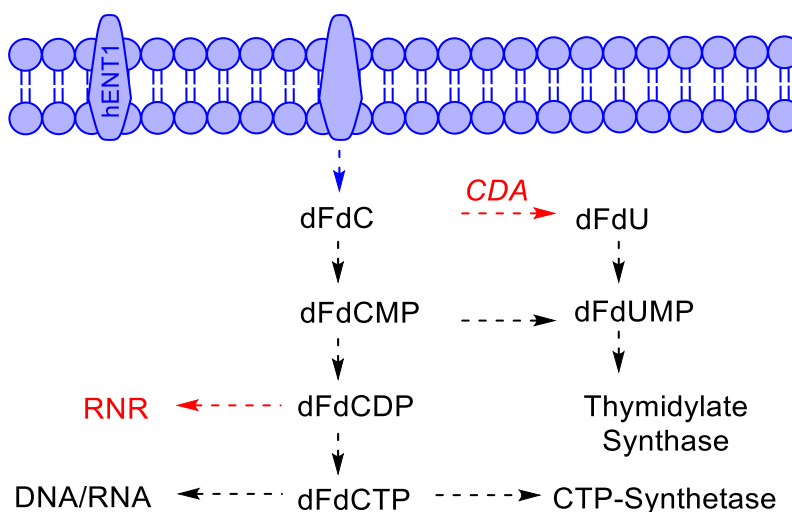


Figure 2. Gemcitabine (dFdC) mode of action & inhibition

Even though, the mechanism of gemcitabine has shown to be effective against a variety of tumor types, the efficacy of gemcitabine is diminished because of a variety of issues.⁸

¹⁴ Gemcitabine, or Gemzar® as it is known in the market, in its current form, is introduced into the body by intravenous infusion, and studies have shown that it is the optimal way for the drug to be administered.¹⁵ High-dose oral gemcitabine is cytotoxic, causing serious liver and gastrointestinal problems.^{16, 17} Studies have shown that gemcitabine, because it is hydrophilic, is excreted (>90%) in the urine. Gemcitabine also undergoes quick deamination into the inactive metabolite 2',2'-difluorouridine (dFdU) by cytidine deaminase (CDA), the enzyme which converts the cytosine base to a uracil base.¹⁸ The

transformation occurs in both the plasma and in the tissues, and it has shown to be a significant disadvantage for the potency of the drug.

1.1.2. Gemcitabine: Design and synthesis of prodrugs

In order to tackle these various issues, prodrug strategies have been developed featuring acyl modifications of different lengths on either the exocyclic 4-*N*-amine or on the hydroxyl groups of the sugar at the 3' or 5' carbon.¹⁹⁻²² These modifications have been extensively studied because, first, the addition of a lipophilic chain to gemcitabine has shown to facilitate the incorporation of the drug into cells. Second, once in the cell, the hydrolyzable acyl/amide modifications have shown to facilitate a slow conversion to the parent drug, gemcitabine. The modification increases the drug's bioavailability and uptake while also providing prolonged resistance to deamination by CDA as acyl groups are not natural substrates for the enzyme.²³ A few examples of these type of modifications include 4-*N*-stearoyl, 4-*N*-squalenoyl, and other 4-*N*-alkanoyl gemcitabine prodrugs e.g., **3-4** (Figure 3)^{21, 22, 24-31} and **7-9** (Figure 4)²⁸ as well as modifications in the 5'-hydroxyl groups (e.g. CP -4126, **2**).^{19, 29, 32-34} These designed modifications are considered the first generation of prodrugs for gemcitabine. Many of the synthesized analogues have been extensively studied in cancer cell lines as well as mice models, with the main goal of improving the overall efficacy of gemcitabine. One of these examples is LY2334737, **5**, a prodrug designed by McCarthy *et al.*²¹ This prodrug was shown to be stable between pH 4-8, and its dose resulted in prolonged gemcitabine exposure and slow deamination. Since its initial synthesis in 2009, this prodrug has undergone several pharmacokinetic evaluations, including phase 1 studies.³⁵⁻³⁷

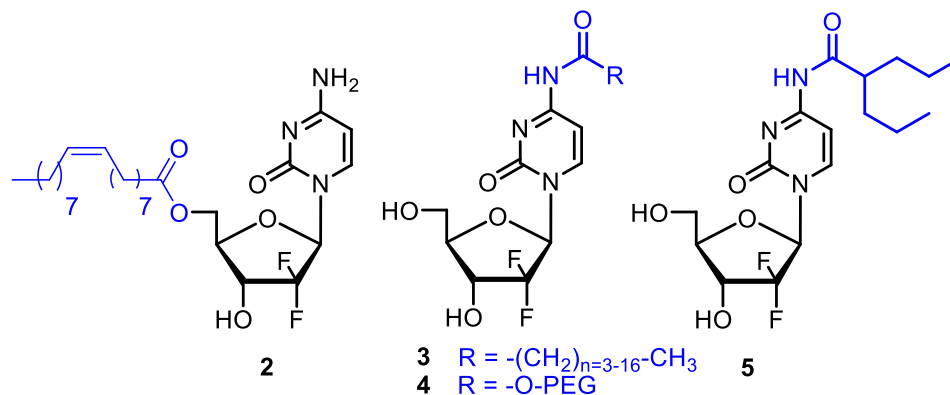


Figure 3. 4-*N*-modified gemcitabine prodrugs with enhanced anti-cancer activity

The Wnuk research group has also been interested in the synthesis of modified gemcitabine analogues.^{28, 38} Following the same design strategy of 1) increased lipophilicity, 2) slow hydrolysis to the parent drug and 3) slow deamination by CDA to inactive dFdU, Pulido *et al.* synthesized a series of 4-*N*-alkanoyl (acyl) **6-8** and alkyl gemcitabine analogues **9-10** (Figure 4) and had their cellular inhibition assessed on a panel of murine and human tumor cell lines (Table 1). Their findings correlated with previous studies on other 4-*N*-alkanoyl modified gemcitabine analogues. Their 4-*N*-alkanoyl analogues showed potent anti-proliferative activities with nanomolar range IC₅₀ values (0.0077-0.053 μM). However, the synthesized 4-*N*-alkylgemcitabine analogues showed only modest IC₅₀ values (17-29 μM). The low IC₅₀ values was hypothesized to be associated with their to low cellular uptake as well as low conversion to gemcitabine, which was shown by stability studies in rodent liver extract in PBS.

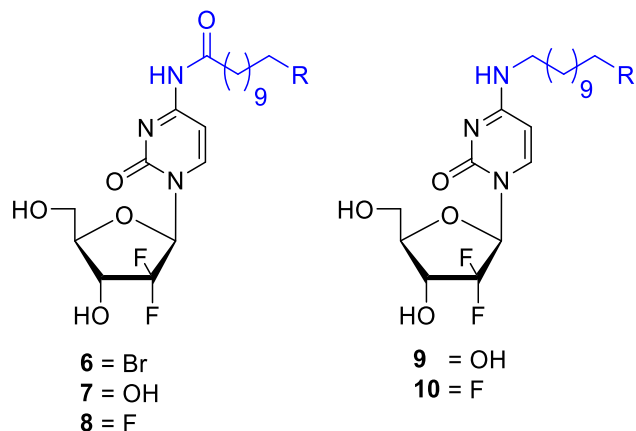


Figure 4. 4-*N*-modified gemcitabine analogues synthesized by Pulido *et al.*²⁸

Table 1. *In vitro* cytostatic activity of 4-*N*-Modified gemcitabine analogues **7-10** on the tumor cell lines L1210, HeLa, and MCF-7²⁸

Gemcitabine analogue	IC ₅₀ (μM)		
	L1210	HeLa	MCF-7
7	0.023	0.049	0.0081
8	0.053	0.011	0.0077
9	29	22	27
10	28	17	26

To my knowledge, the synthesis and biological properties of 4-*N*-alkylgemcitabine analogues have not been intensively explored. However, because of their stability and *permanent* presence of 4-*N*-alkyl chain, they can be candidates for use as ¹⁸F-PET radiotracers and metabolic labeling.

1.1.3. Gemcitabine: Theranostic image-guided tumor agents

Using the above prodrug designs as foundation, the next generation of gemcitabine prodrugs are being designed through a theranostic approach, the combination of diagnostic and therapeutic entities into one drug delivery system. These prodrugs have two goals: 1) increase the bioavailability of the drug and 2) provide increased specificity to the tumors being targeted. Approaching the same idea of acyl modification, one example is H-

gemcitabine (**11**; Figure 5), the 4-*N*-alkanoyl gemcitabine prodrug contains the Hoechst group, an extracellular DNA (E-DNA) targeting moiety, as well as a disulfide bond as an additional triggering mode of action. The Hoechst moiety binds to the E-DNA present in the core of the tumors and the disulfide bond provides a second mode of release, increasing the prodrug's time to accumulate within the tumors.³¹ H-gemcitabine then provides not only provides increased bioavailability, it also provides increased specificity to tumors with E-DNA present. The analogue H-gemcitabine also showed similar toxicity to gemcitabine. The use of disulfide bonds is also used in other gemcitabine prodrug strategies that will be discussed later in this section.

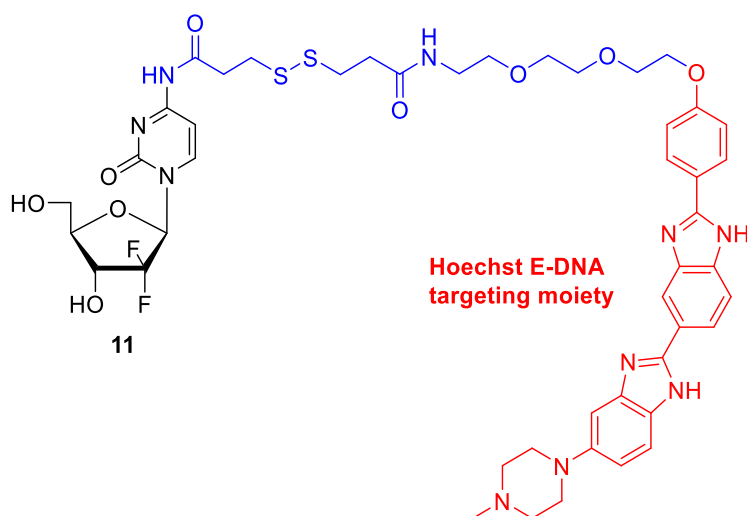


Figure 5. Structure of H-gemcitabine³¹

Another approach that has been explored is the design and synthesis of gemcitabine conjugates with receptor binding peptides for targeted delivery to specific tumors. One such example is the GnRH-gemcitabine conjugates. They have been designed to contain Gonadotropin-releasing hormone (GnRH) specific amino acids conjugated to a linker moiety attached to 5' of the sugar of gemcitabine (**12**; Figure 6).³⁹ The incorporation of the

GnRH ligand was chosen because prostate cancer tumors have shown to overexpress GnRH receptors. The conjugates were then able to provide specific target and increased bio-distribution with potent anti-cancer activity.

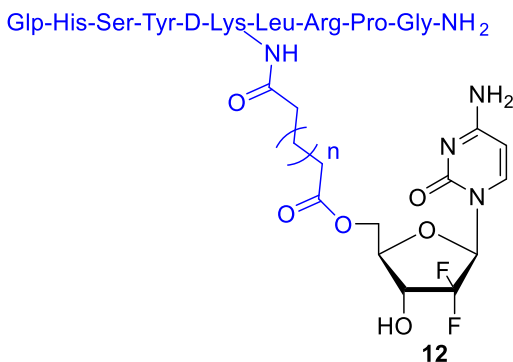


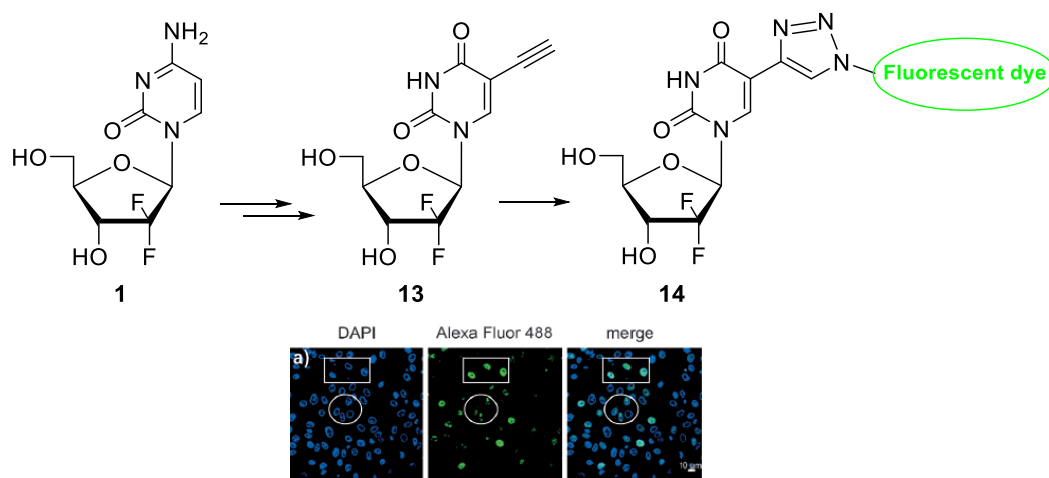
Figure 6. Structure of GnRH-gemcitabine conjugate³⁹

Another route of increasing the effectiveness of gemcitabine has been through the synthesis of nanoparticles.^{40, 41} Wang *et al.* synthesized gemcitabine–poly(methyl methacrylate) (Gem–PMMA) conjugated amphiphiles.⁴² The amphiphiles can self-assemble to form nanoscale aggregates in an aqueous environment. These nanoparticles provide high drug payload by having a controlled release. Another route that has been studied is the synthesis of copolymer and carbon nanotubes–drug conjugates containing gemcitabine.⁴³⁻⁴⁵ Hu *et al.* used gemcitabine as part of the synthesis of an azido-carbonate monomer, 2,2-bis(azidomethyl)trimethylene carbonate, which was then reacted with alkynyl compounds via click chemistry had then gemcitabine was conjugated to it.⁴³ In a similar project, Kopecek *et al.* synthesized degradable HPMA copolymer–drug conjugates containing gemcitabine for studies with human ovarian carcinoma cells.⁴⁴

Some of the example prodrugs described above have been synthesized using click chemistry,^{46-49 50, 51} through the use of copper catalyst as well as cyclooctynes (SPAAC).

Click chemistry in nucleosides and oligonucleotides, with terminal alkyne or azide has been reviewed extensively.⁵²⁻⁵⁵ These modifications have been done both at the heterocyclic base and the sugar, which then have been conjugated with modified fluorescent dyes, sugars and peptides for imaging and drug discovery.^{53, 55-57} The exploration of click chemistry in gemcitabine and its analogues is fairly recent.

Another route of click chemistry that needs mentioning is the use of gemcitabine and its analogues for imaging purposes. Luedtke *et al.* synthesized the metabolite 2',2'-difluoro analog of 5-ethynyluridine **13** to achieve pathogen-selective labeling as this analogue is selectively metabolized in HSV-1 infected cells owing to the expression of a viral thymidine kinase (TK). The analogue bearing a terminal alkyne was then treated with CuI and an azide-conjugated fluorophore to give fluorescent analogue **14**, for the visualization of cells that contained the HSV-1 infection but not uninfected cells (Scheme 1).⁵⁸



Scheme 1. Synthesis of gemcitabine analogue for fluorescent labeling⁵⁸

Additionally, extensive work has been done in the area of the synthesis of gemcitabine prodrugs with fluorescent conjugates with imaging capabilities.⁵⁹ The Kim group has

synthesized a series of theranostic gemcitabine (through C5') prodrugs that contain fluorophores connected via a disulfide bond and with biotin/folate through click chemistry to monitor drug delivery.^{60, 61} One of these prodrugs contained Coumarin as their fluorophore (not pictured) and another gemcitabine prodrug, **15**, with the near IR fluorescing BODIPY fluorophore. Another set of analogues contained heptamethine cyanine dyes with folate.⁶² In all the analogues synthesized, the disulfide bond is cleaved intracellularly by thiols, followed by hydrolysis of the ester moieties to release gemcitabine and the fluorophore. Once released from gemcitabine, the fluorophores have stronger fluorescence than when conjugated (Figure 7). The intake of gemcitabine by cells was shown by fluorescence studies of the prodrug in the presence and absence of dithiothreitol (DTT), a well-known reducing agent. The conjugates showed targeted cellular differentiation by its incorporation in biotin/folate-receptor positive tumor cells.

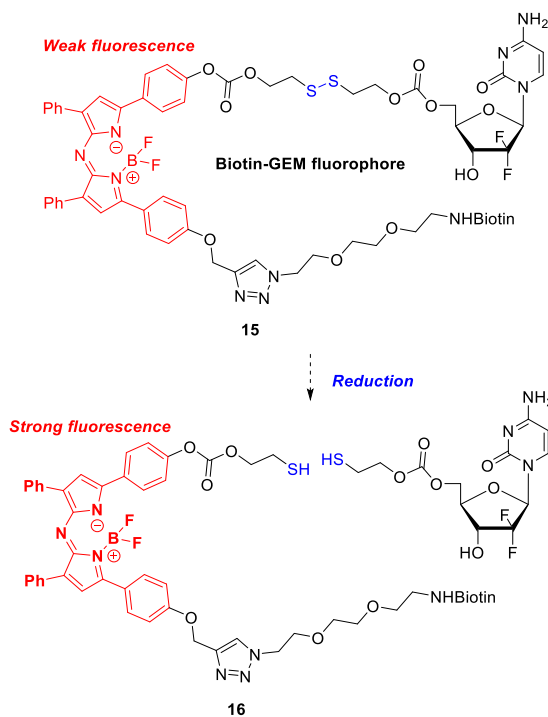


Figure 7. Fluorescent theranostic prodrug synthesized by Kim group^{60, 61}

Liu and coworkers also worked in a similar near infrared activable meso-tetraphenylporphyrin (TPP) prodrug of gemcitabine with image-guided *in situ* tumor photodynamic therapy capability known as TPP-L-GEM (Figure 8). Meso-tetraphenylporphyrin is a singlet oxygen ($^1\text{O}_2$) generator and the present thioketal linker is $^1\text{O}_2$ sensitive. The release of gemcitabine was triggered by the low energy red light induced $^1\text{O}_2$ generation in TPP followed by the $^1\text{O}_2$ mediated thioketal cleavage.⁶³

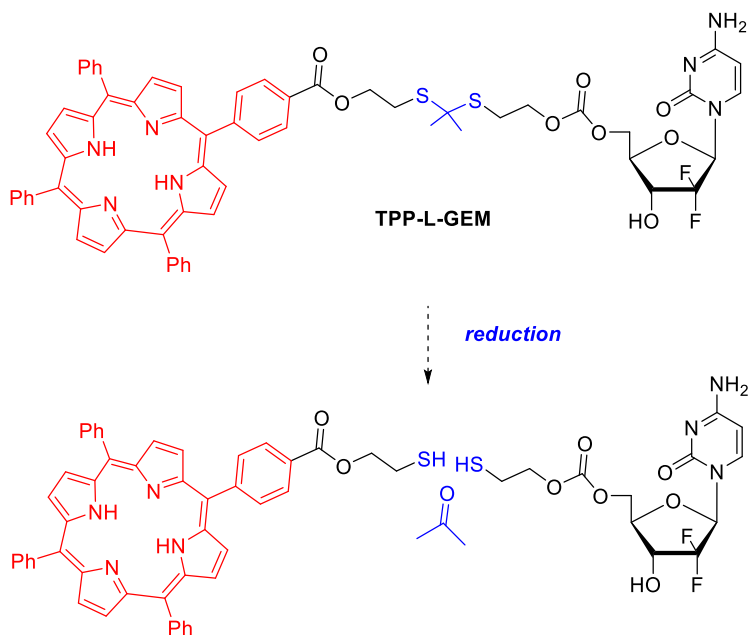


Figure 8. Fluorescent theranostic prodrug synthesized by Liu *et al.*⁶³

As discussed above, many strategies have been developed to increase gemcitabine's efficacy. Many of these strategies involve imaging capabilities, with protocols that are still in the beginning stages of development, but it shows that combinational protocols are key in understanding and advancing drug discovery. Another useful tool that we shall focused on is the use of Positron Emission Tomography (PET) as a means of theranostic imaging.

1.2. Positron emission tomography (PET)

Positron emission tomography (PET) is recognized as an important tool in modern imaging. This imaging technique uses a positron emitting radionuclide (such as fluorine-18). The radionuclide, once emitting, travels through the tissue and it comes to rest to disintegrate with emission of two diametrically opposed gamma rays of 511 keV. These created gamma rays are then detected and used for reconstruction of a 3D image.^{64, 65} The imaging technique has been used for cancer detection, metabolic disorders and cardiovascular disease among other utilizes. Fluoride-18 (^{18}F) is commonly used as a radionuclide to provide PET images of high resolution, as it has a low positron energy of 640 keV and a half-life of 109 minutes. The main focus of the use of ^{18}F is its introduction to molecules for biological purposes. The generation of ^{18}F is through a cyclotron that produces it by bombarding H_2^{18}O enriched water with protons to initiate a reaction that converts the ^{18}O atom into a ^{18}F atom.^{66, 67}

1.2.1. Radiochemistry: Fluorination

As mentioned previously, fluoride-18 has been shown to be the optimal atom for PET imaging. The radiouclide is greatly used due to its half-life of 109.8 min compared to other atoms such as ^{15}O and ^{11}C have half-lives of 2.037 and 20.38 respectively. Also, fluorine has favorable physical properties, such as small van der Waals radius (1.47 Å), high electronegativity, and strong bond formation with carbon with C–F energy bond of 112 kcal/mol, making the bond more thermally stable and oxidation resistant, which are key for PET imaging.^{68, 69}

Because of these characteristics, many nucleophilic and electrophilic fluorination reagents have been studied but only a few are used in ^{18}F fluorination available in the

market. Examples of nucleophilic fluorination reagents include KF, TBAF, DAST, PhenoFluor and Deoxo-fluor. Electrophilic reagents include NFSi and SelectFluor. Furthermore, there is a difference in nucleophilic aliphatic versus nucleophilic aromatic substitutions with fluorinating reagents.^{70, 71} Additionally, these substitutions are aided by the use of phase transfer catalysts (PTC). Kryptofix₂₂₂ and 18-Crown-6 are PTCs that enhance the solubility and nucleophilicity of the fluoride ion by complexing with the cation, usually potassium.⁷²

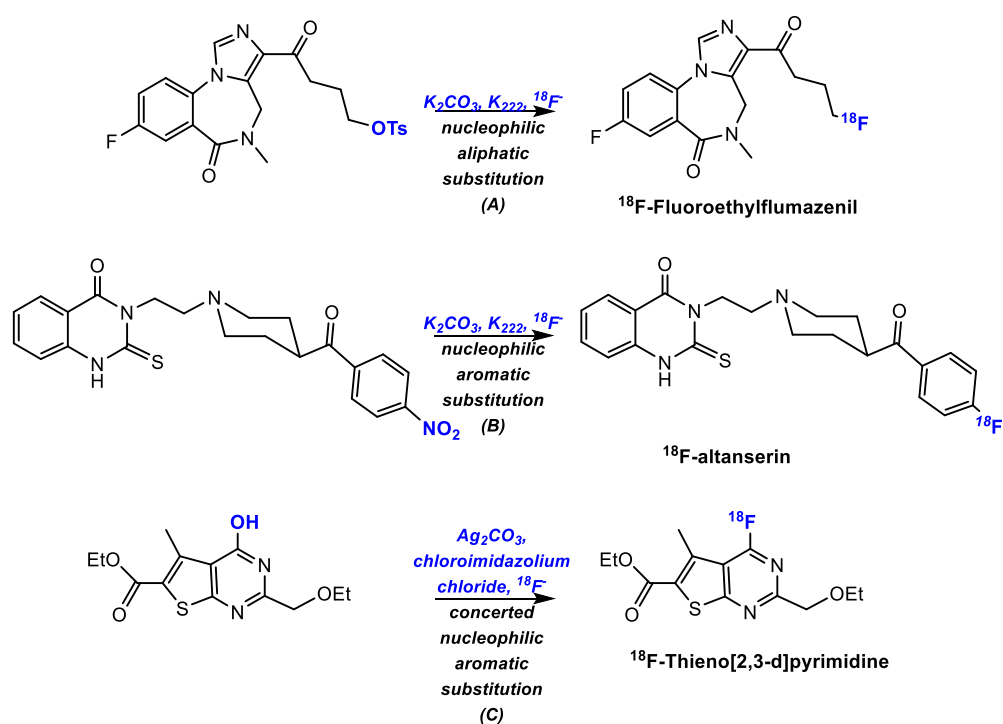
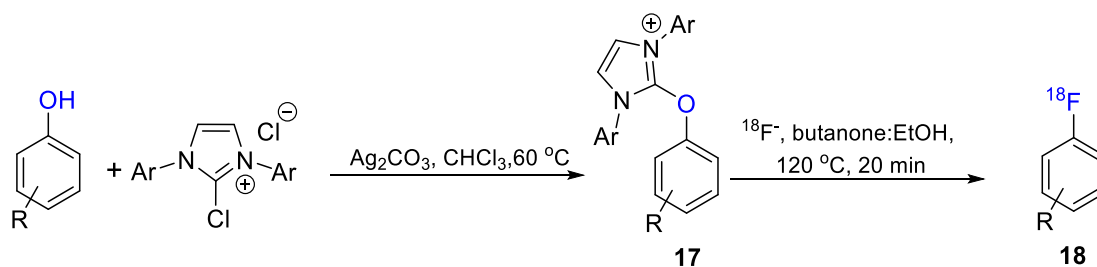


Figure 9. Examples of ^{18}F -aliphatic and aromatic nucleophilic substitutions^{71, 73, 74}

Nucleophilic aliphatic substitutions (Figure 9, **A**) are $\text{S}_{\text{N}}2$ type reactions where fluorine substitutes a leaving group. In the case for the substrates for PET imaging, the specific leaving group used is important depending on the reactivity and stability of the substrate. These aliphatic substitutions usually involve the use tosylates and mesylates with KF as the fluorine sources. Aromatic nucleophilic substitutions ($\text{S}_{\text{N}}\text{Ar}$, **B**) require electron

withdrawing group in the ortho/para position, which act as activators in these types of substitutions as well as polar aprotic solvents and high temperatures (100°C or greater). These reactions occur through addition-elimination or elimination-addition mechanisms with the formation of highly reactive Meisenheimer intermediates. One example is the Balz-Schiemann reaction, which involves a diazotization, followed by thermal decomposition of the derived tetrafluoroborate. Overall, extensive work has been done in studying these type of substitution reactions with all the focused on the carbon-fluoride bond.



Scheme 2. Deoxyfluorination of phenols and heterophenols with ^{18}F by the Ritter group⁷¹

The Ritter group showed that nucleophilic substitution to be used with ^{18}F can be done through a concerted mechanism ($\text{C}_{\text{S}_{\text{N}}\text{Ar}}$, **C**) through the deoxyfluorination reaction of phenols with the reagent PhenoFluor with both electron-rich and electron-poor substrates on the ring.⁷¹ The substitution yields an imidazolium intermediate, **17**, that undergoes a fluoride attack to give a tetrahedral intermediate followed by a concerted displacement on the arene (Scheme 2). Ritter's method works with heterocycles which are present in many bioactive compounds that are often problematic in regular $\text{S}_{\text{N}}\text{Ar}$ conditions.

1.2.2. Positron emitting ^{18}F radiotracers for anticancer therapy

Positron Emission Tomography imaging is becoming a great tool for the imaging of different types of small molecules.^{75, 76} The most extensively used radiotracer is 2-deoxy-

2-[fluorine-18]fluoro- D-glucose (^{18}F -FDG, **19**). The analogue of glucose provides valuable functional information on the basis of the increased glucose uptake and glycolysis of cancer cells and the method depicts metabolic abnormalities. The glucose analogue's ability to detect tumors depends on various factors, such as their size, metabolic activity, and distribution in some normal tissues which can affect the tumor to surrounding background ratio (Figure 10).^{64, 77} Other well studied compounds include ^{18}F -Fluoro-L-dihydroxyphenylamine (^{18}F -fluoro-L-DOPA, **20**) which is used to evaluate the in vivo activity of aromatic L-amino acid decarboxylase of dopaminergic system.⁷⁸ A structural analogue of 5- α -dihydrotestosterone, ^{18}F -16 β -Fluoro-5 α -dihydrotestosterone (FDHT, **21**), can be useful to detect metastatic and recurrent prostate cancer lesions, binding affinity and selectivity for androgen receptors⁷⁹ and ^{18}F -3-Fluoro-3-deoxy-thymidine ([^{18}F]-FLT, **22**) is a pyrimidine analogue that reveals the activities of thymidinekinase-1 during the phase S of mitoses.^{76, 80}

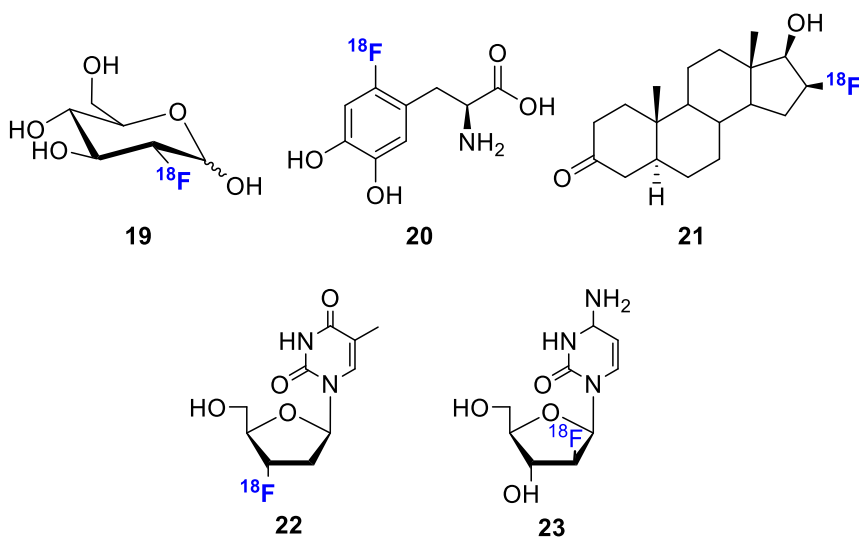
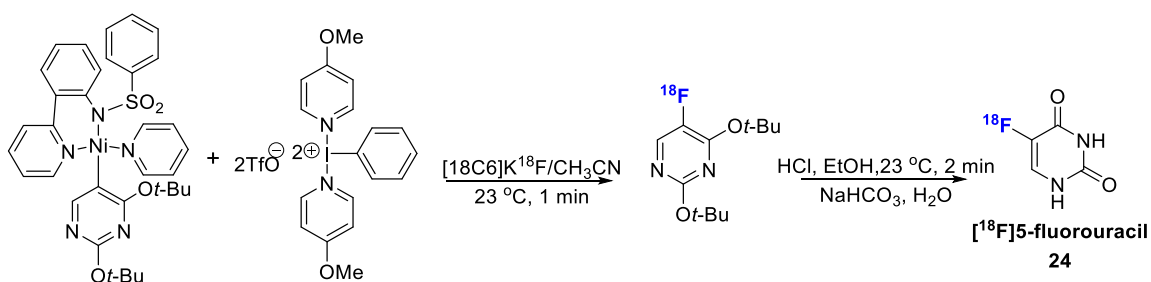


Figure 10. Selected ^{18}F radiotracers for anticancer therapy

Radu *et al.* developed 1-(2'-Deoxy-2'- ^{18}F -fluoro- β -D-arabinofuranosyl) cytosine ([^{18}F]-FAC, **23**) as a PET tracer possessing a substrate affinity for both dCK and CDA

comparable to gemcitabine (Figure 10).^{81,82} The deoxycytidine analogue bears one fluorine atom at the C2' position, instead of the two fluorine atoms in gemcitabine. The compound was synthesized with the goal of using it as a noninvasive method of dCK activity detection, which is helpful for personalized cancer therapy as a predictor of tumor response. The [¹⁸F]-FAC was tested in both tumor cell lines as well as in mice with dCK-positive and dCK-negative tumor, with selectivity for dCK-positive tumors, comparable to gemcitabine. Because of its selectivity, the incorporation of ¹⁸F proves to be useful for the diagnosis of cancer. Extensive studies of [¹⁸F]-FAC have also been done in humans.⁸³ Because it possesses similar characteristics as gemcitabine, [¹⁸F]-FAC, also has the same critical disadvantages. It is a hydrophilic nucleoside analogue that can undergo inactivation by CDA. Because of these characteristics, its role as a radiotracer has its limitations. The Ritter group has also been involved in the first production of human doses of [¹⁸F]-5-fluorouracil, **24**, a PET tracer for cancer imaging in humans, from [¹⁸F]fluoride through the use nickel(II) σ -aryl complexes by transmetalation from arylboronic acids (Scheme 3).⁸⁴



Scheme 3. Synthesis of [¹⁸F]5-fluorouracil as a PET tracer⁸⁴

The path for ¹⁸F radiolabeling has many obstacles, which include lengthy number of steps and burdensome labeling procedures. These obstacles are definitely the case for the synthesis of modified nucleosides analogues. Modification of nucleosides usually involve protection and deprotection steps. These steps, even with high conversion rates, can lead

to an overall decrease of yield. Furthermore, the synthesis of compounds bearing carbon-fluoride bond for PET imaging via substitution reactions can become troublesome with reaction conditions requiring relatively high temperatures and additives. Because of these issues, there is always the need to make this process more simple and efficient.

1.2.3. Silicon ^{18}F radiochemistry

The use of Si-F bond formation in radiochemistry has been explored since 1958,⁸⁵ with *in vivo* studies reported as early as the 1970s and 1980s.⁸⁶ The use of Si-F for labeling came from comparing C-F and Si-F bond formation, as the bond energy of Si-F bond is about 90kJ/mol higher than the C-F bond. The C-F bond is generally metabolically stable, but to be formed, through electrophilic or nucleophilic reaction, the reactions tend to be harsh at very high temperatures. Early on, it was discovered that even with this increase of bond energy, the Si-F bond is highly susceptible to hydrolysis in physiological conditions.⁸⁷ The hydrolytic stability of this bond is highly depended on the substituents attached to silicon (Scheme 4).⁸⁸ Schirmacher *et al.*, provided an alternative to the conventional ^{18}F radiopharmaceuticals that goes through the carbon-fluoride bond, prepared and tested triphenyl Si-F, diphenyl, *t*-butyl Si-F, and phenyl di-*t*-butyl-F compounds. It was noticed that having two bulky substituents in addition to one phenyl group provided the best stability for *in vivo* studies in human serum at 37.4°C and pH 7.4–7.6.⁸⁹ Ametamey *et al.* did an extensive experimental and theoretical hydrolysis study on a number of model organofluorosilanes, and they also showed that the tendency to hydrolysis can be prevented by the use of bulky substituents on the Si-atom (Figure 11). These compounds were dissolved in acetonitrile/aqueous buffer at pH 7 and incubated at ambient temperature. Several compounds were tested and they concluded that isopropyl (**28-30**) and *t*-butyl (**31**)

groups were significantly more stable than methyl groups when attached to Silicon.^{90, 91} With these extensive stability studies, it was concluded that these type of compounds, now labeled for fluoride acceptors (SiFA), are a reliable alternative for ¹⁸F PET imaging protocols.

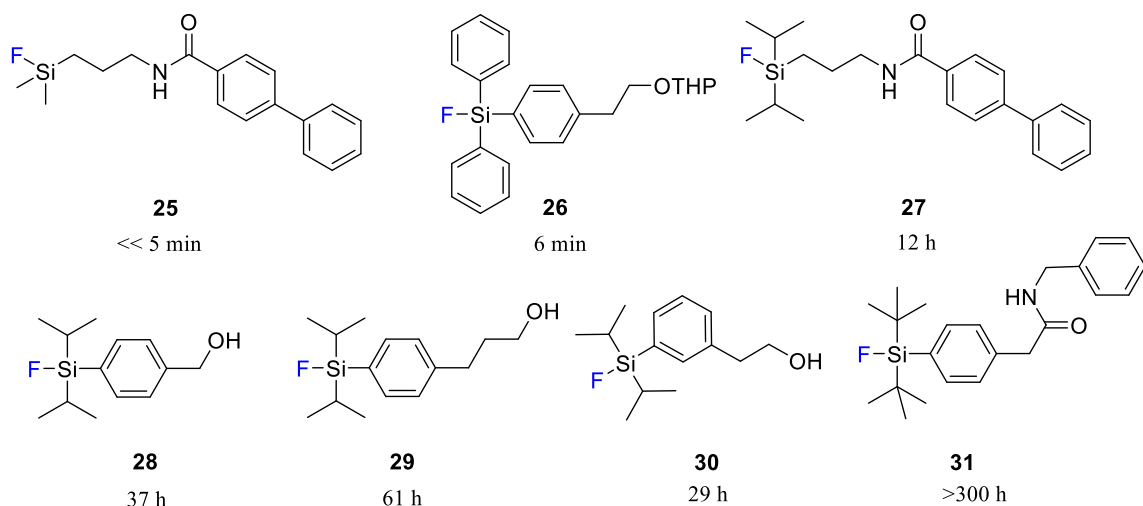
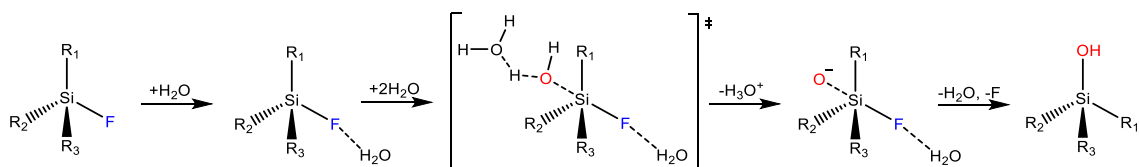


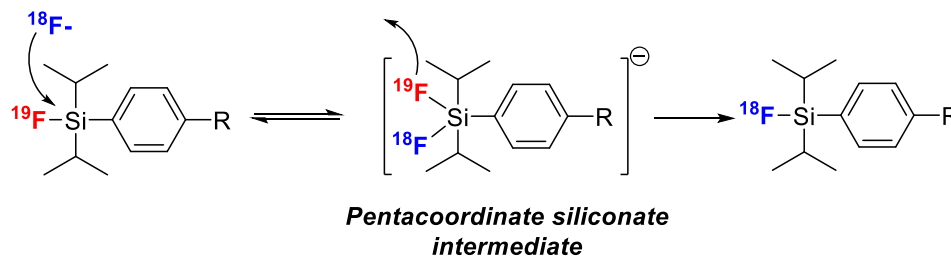
Figure 11. Hydrolysis half-lives ($t_{1/2}$) of selected organofluorosilanes under aqueous buffer (pH 7) and ambient temperature reported by Hühne *et al.*⁹¹

The Si-F hydrolysis is also affected by the leaving groups attached to the silicon atom. Early on it was noticed that the use of chloro as the leaving group was not optimal because of their strong tendency to form silanol derivatives (Si-OH), meaning it undergoes hydrolysis easily. The high tendency for hydrolysis meant that other options needed to be explored. Klar and Ametamey were able to fluorinate silane peptides with H and OH as leaving groups. These compounds, which also bear bulky groups, were fluorinated with no issue, but it was noticed that OH and alkoxy moieties requires the presence of acid for better exchange.⁹⁰



Scheme 4. Hydrolysis reaction of Si-F bond to Si-OH

Isotopic exchange reactions have been a key aspect in the study of ^{18}F radiochemistry (Scheme 5). In the case of carbon-fluorine reactions, the exchange is usually with low yields which leads to no *in vivo* applications. In addition, there is a problem with specific activity when ^{19}F -C bonds occupy receptors. In the case of Si-F, because these reactions are in higher yields, isotopic exchange can be an advantage. It has been shown that isotopic exchange reactions have occurred in high radiochemical yields with high specific activity.⁹² The labeling procedure also becomes more convenient because there is no need for purification as the labeling precursor and labeled compound are identical.



Scheme 5. Mechanism of isotopic exchange reaction between ^{18}F and ^{19}F

These silicon-fluoride acceptor building blocks are hydrophobic, which means that if they introduced in the body for imaging, they would accumulate in the liver. To prevent liver accumulation, these building blocks are usually connected to peptides and other small molecules,^{90, 92-95} which increase the overall hydrophilicity. In the case of peptides, the incorporation of silicon-fluoride acceptors involve multistep syntheses that involve the addition of linkers and auxiliaries that reduce lipophilicity. Additionally, because of the

number of amino acid residues that might react, additional protection steps need to be used. Lovkova *et al.* synthesized a set of Octreotate analogues by modifying phenylalanine with a silicon-fluoride acceptors and introducing it through solid phase peptide synthesis (**32**, Figure 12).⁹⁶ Silicon-fluoride acceptors have also been utilized in proteins for PET imaging.^{97, 98}

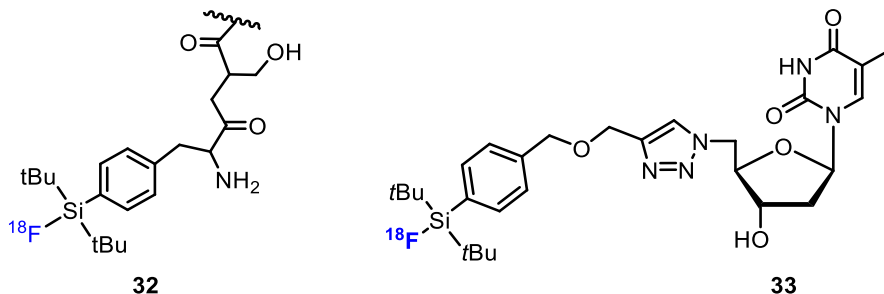


Figure 12. Silicon-fluoride acceptors in octreotate⁹⁶ **32** and thymidine derivatives⁹⁹ **33**

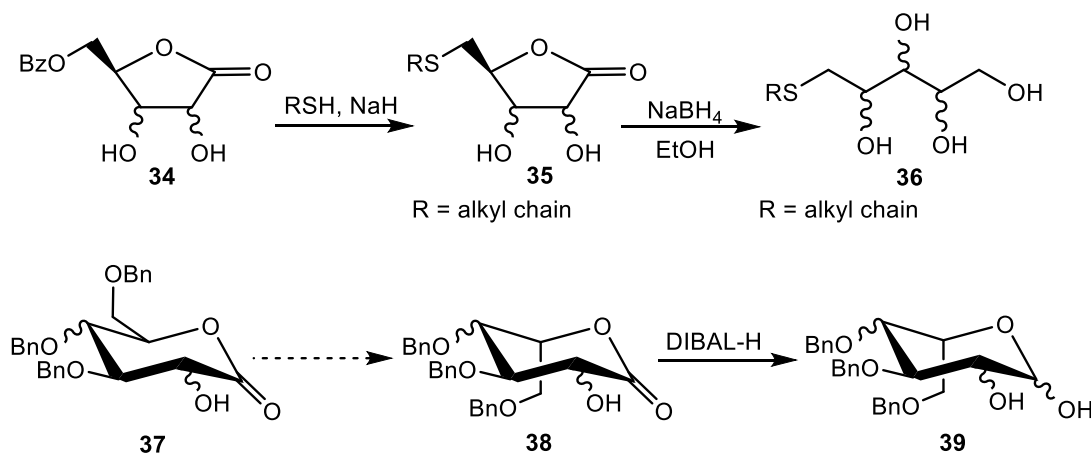
When discussing silane derivatives for their use as a tracer, to my knowledge, not much work has been done with nucleosides or nucleoside analogues. Schulz *et al.* reported a protocol for the efficient radiolabeling of nucleosides and oligonucleotides derivatives containing the silicon-fluoride acceptors building block (Figure 12).^{95, 99, 100} Schulz's work involved the use of natural nucleosides modified at the C3' and C5' (**33**) position of the sugar. As of this moment, there is no published work on the integration of nucleoside-based drugs with silicon-fluoride acceptors for PET imaging. It would be very interesting to explore their use as anti-cancer and anti-viral nucleoside theranostic agents.

1.3. Reduction of lactones to hemiacetals

1.3.1. Synthetic significance of reduction of lactones to hemiacetals

The reduction of sugar lactones to hemiacetals plays an important role in the synthesis of modified carbohydrates and nucleosides. When discussing carbohydrates, we shall focus

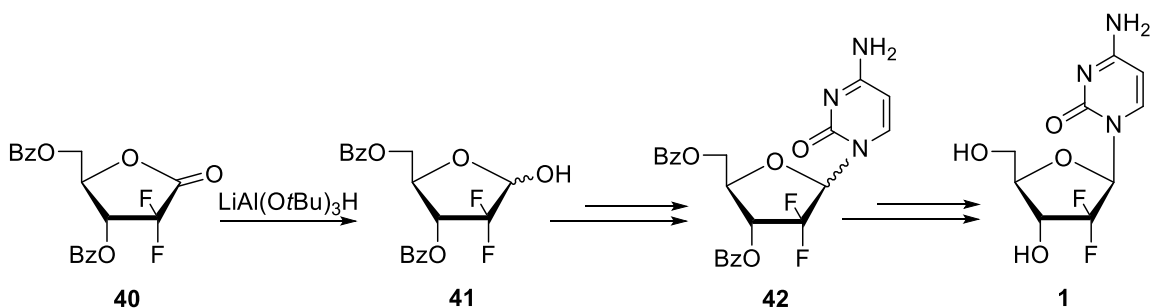
on the synthesis of modified monosaccharaides, more specifically pentoses and hexoses. Beaupere *et al.* worked on the synthesis of 5- and 6-alkyl sulfanyl derivatives.¹⁰¹⁻¹⁰³ These types of thiosugar derivatives have shown to have therapeutic potential against several diseases, including cancer.¹⁰³ These derivatives were made through the modifications of ribonolactones, (e.g., **34**) which ultimately are reduced with NaBH₄ to *S*-Alkylthiopentitol **36** (Scheme 6). Another example is the conversion of D-hexono-1,5-lactones (e.g., **37**) into cyclic hemiacetals of L-hexoses **39** through a γ -hydroxyalkoxamate derivatives using DIBAL-H.^{102, 104}



Scheme 6. Reduction of lactones with NaBH₄ and DIBAL-H

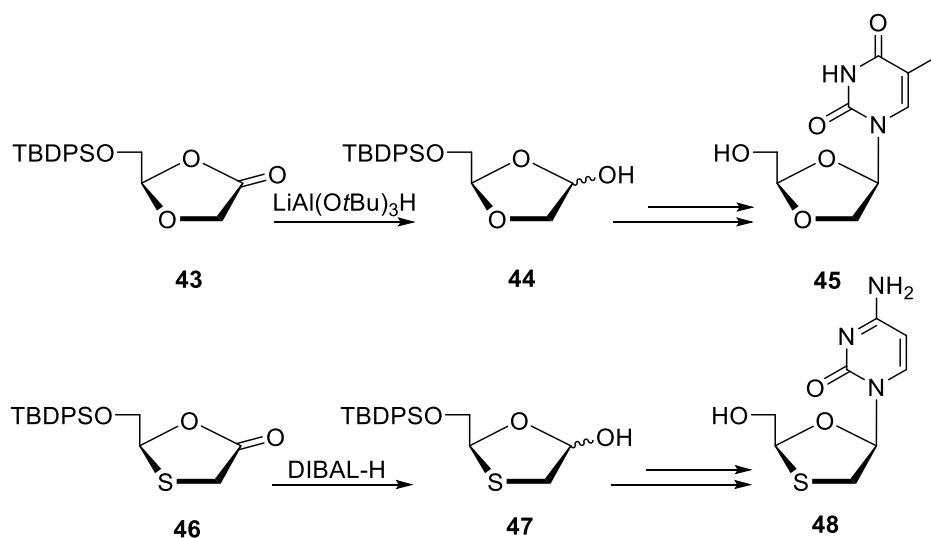
Reduction of pre-constructed sugar lactones to their corresponding lactols and their further coupling with nucleobases are often key steps in the synthesis of important nucleoside-based drugs such as the anticancer gemcitabine, anti-HIV 3TC and dideoxynucleosides among others.^{3, 105, 106} In the case of gemcitabine, **1**, there have been many routes attempted and explored but the majority of them involve the use of a modified sugar lactone for synthesis of difluororibose of carbohydrate derivatives.³ Chou *et al.*

synthesized difluororibose derivative **41** through a lactone derivative to then couple with cytosine to synthesize gemcitabine (Scheme 7).¹⁰⁷



Scheme 7. Synthesis of gemcitabine through reduction of sugar lactones

Choi *et al.* synthesized dioxolanyl **45** and oxathiolanyl **48** nucleoside analogues also by using sugar lactones which were then coupled to their respective bases. In the synthesis of dioxolanyl, Choi, utilized $\text{LiAl}(\text{O}t\text{Bu})_3\text{H}$ to reduce the lactone, while DIBAL-H for the synthesis of oxathiolanyl (Scheme 8).¹⁰⁸



Scheme 8. Synthesis of oxathiolanyl and dioxolanyl nucleoside analogues through reduction of sugar lactones¹⁰⁸

On the development of novel inhibitors of *S*-ribosylhomocysteine (SRH) hydrolase (LuxS; EC 4.4.1.21), the Wnuk group has had the challenge of reducing modified sugar

lactones to their corresponding hemiacetals. Lithium triethylborohydride (LTBH, Super-Hydride®)¹⁰⁹ has been utilized for the reduction of lactam (Scheme 10) and lactone analogues of SRH to the corresponding azahemiacetals (*N,O*-acetals)^{110,111} or lactols (*O,O*-acetals)¹¹², a method not extensively explored. Below, the commonly used reducing agents for this type of transformation will be reviewed.

1.3.2. Reducing agents for reduction of lactones to hemiacetals

The commonly used reagents for the reduction of lactones to hemiacetals include NaBH₄, and a variety of organic-soluble metal hydrides such as DIBAL-H and other boranes.¹¹³⁻¹¹⁵ Additionally, LiAlH₄, under controlled reaction conditions, has also been used for this purpose. NaBH₄ has been shown to be effective in the reduction of sugar lactones to aldoses. However, it requires aqueous acid conditions to prevent over reduction, which is problematic for nonpolar and/or acid labile protected compounds that are commonly used in nucleoside and carbohydrate chemistry.¹¹⁶⁻¹¹⁸

Diisobutyl aluminum hydride, DIBAL-H, an intensively studied organometallic reducing agent, reduces esters (including lactones) as well as nitriles to aldehydes.^{119, 120} Diisobutyl aluminum hydride has been shown to be an efficient reagent for many of the reactions discussed above, but it usually requires low temperatures (-78°C) and large excess of the reagent, which is a disadvantage for large-scale work.¹⁰⁵ In addition, extra precautions need to be taken when manipulating DIBAL-H because it is air-sensitive and pyrophoric in nature. Alternatives reagents for this transformation have been proposed. Buchwald *et al.* demonstrated the catalytic reduction of lactones to hemiacetals with generated *in situ* titanocene(III) hydride, in the presence of silanes as a hydride source (Figure 13).^{121, 122} Their initial findings involved the use of *n*-BuLi as a catalyst activator

and phenylsilane. Even though they obtained their lactol products with a minimal amount of diol, phenylsilane was expensive and *n*-BuLi reacts violently with water. They later optimized their method by implementing the use of polymethylhydrosiloxane (PMHS) as an activator. Their method was utilized for the large scale preparation of several sugar hemiacetals.

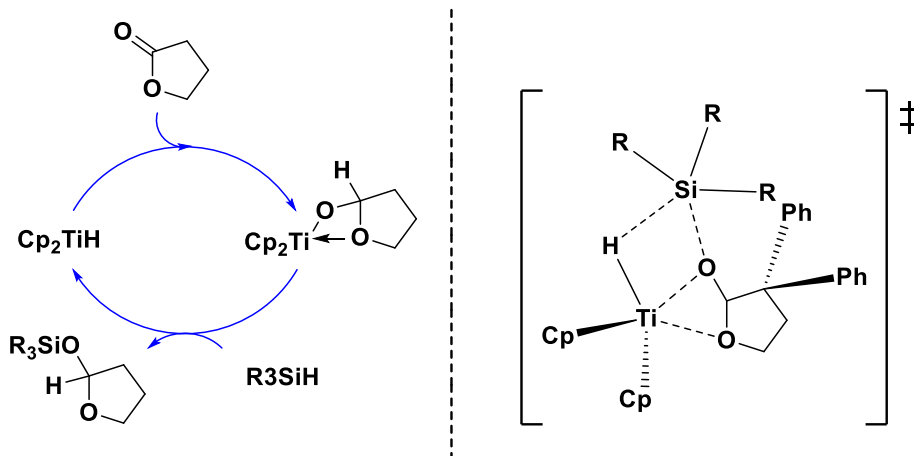
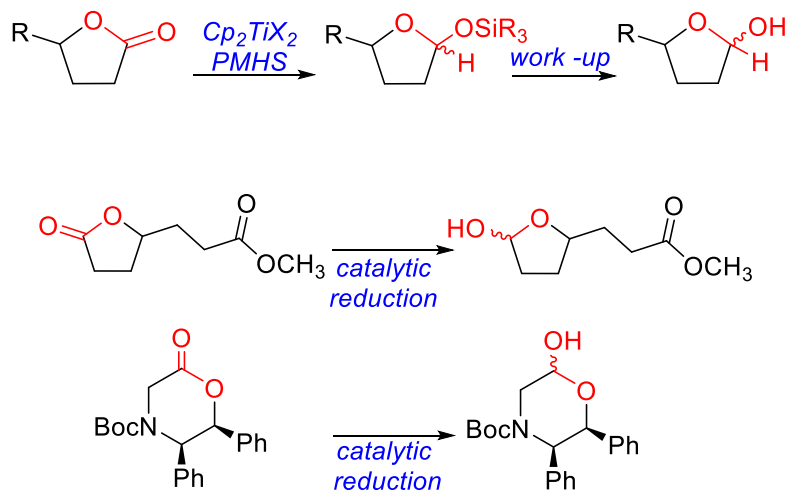


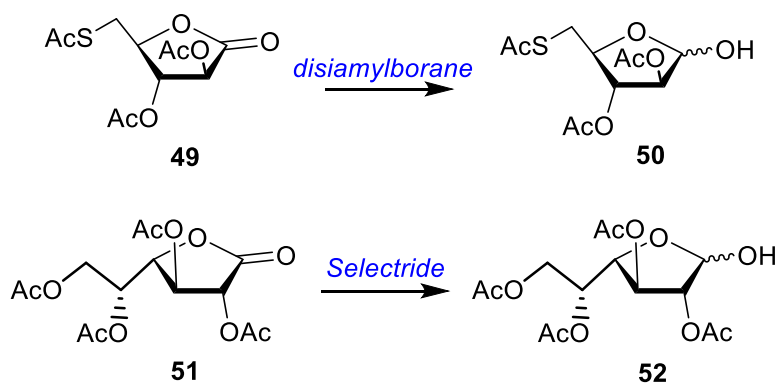
Figure 13. Catalytic cycle and transition state proposed by Buchwald *et al.*¹²¹

Limitations to this method include the size of the lactone ring, with larger rings producing the open aldehyde product that is then reduced to diols and in compounds bearing both a lactone as well as an ester group, when subjected to the hydrosilylation conditions, the ester moiety was reduced to the alcohol while the lactone moiety was reduced to the lactol (Scheme 9).^{121, 122}



Scheme 9. General and specific reduction of lactones with titanocene(III) hydride¹²²

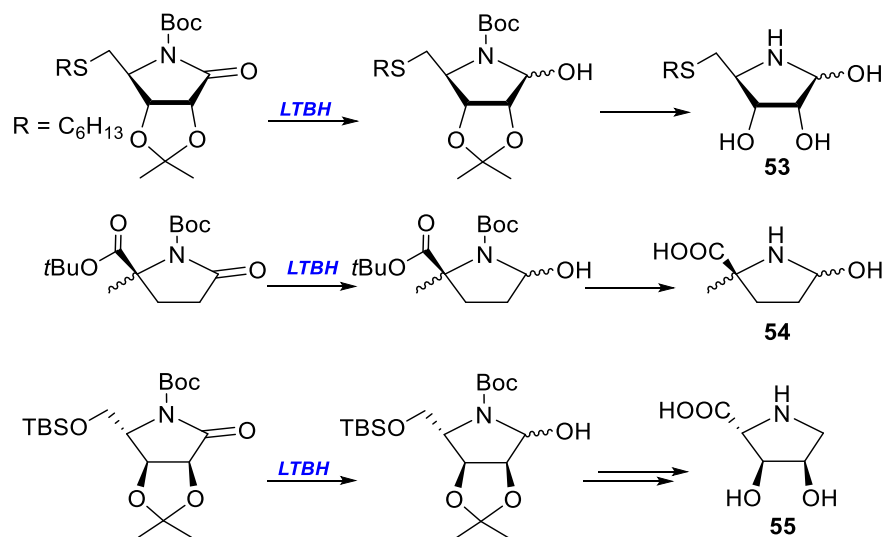
Although borane-based reagents have been used for the reduction of lactones to lactols and diols,¹¹⁴ reports of reductions of sugar lactones to lactols using borane reagents are sparse. For example, disiamylborane was used for the conversion of 2,3-di-*O*-acetyl-5-*S*-acetyl-5-thio-D-arabinono-1,4-lactone **49** to the corresponding arabinofuranose **50**,¹⁰² and Selectride was employed for the partial reduction of acetyl protected D-galactono-1,4-lactone **51** (Scheme 10).¹²³



Scheme 10. Use of borane-based reducing agents for reduction of lactones to hemiacetals

Also, application of LTBH for the reduction of lactams to cyclic hemiaminals (azahemiacetals) has been used by Casiraghi, Schofield *et al.* in the synthesis of

dihydroxyprolines **55** and functionalized prolines respectively **54** (Scheme 11).^{124, 125} To the best of my knowledge, there is no other examples in sugar lactones being reduced to hemiacetals with the use of LTBH.



Scheme 11. Synthesis of cyclic azahemiacetals SRH analogues **53**¹¹¹, dihydroxyprolines **54** and functionalized prolines **55** through the use of LTBH^{124, 125}

2. RESEARCH OBJECTIVES

The main objective of my dissertation is the synthesis and *in vivo* and *in vitro* biological evaluation of novel 4-*N*-alkyl gemcitabine analogues with i) β keto sulfonate moieties (**A**) and ii) 4-*N*-alkanoyl and 4-*N*-alkyl gemcitabine analogues bearing silicon-fluoride acceptor building blocks (**B & C**) suitable for ^{18}F labeling (Figure 14).

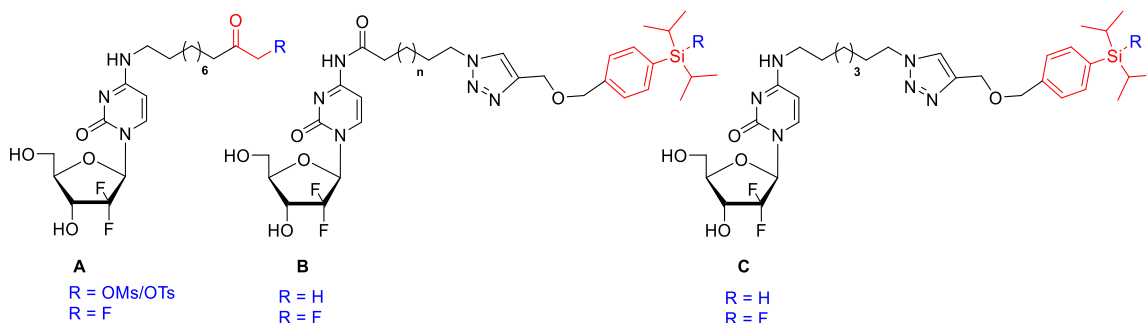


Figure 14. Proposed structures of 4-*N*-alkanoyl and 4-*N*-alkyl gemcitabine analogues

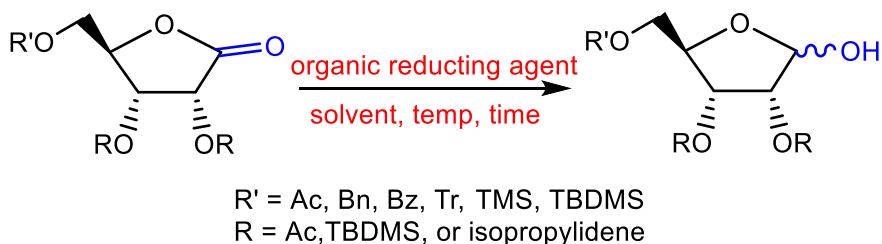
The design and synthesis of 4-*N*-alkanoyl gemcitabine analogues, through a number of strategies, have shown to decrease the release of the parent drug, increasing its bioavailability and used in theranostics. In the case of 4-*N*-alkyl gemcitabine analogues, the Wnuk's group has shown that these type of analogues have increased stability as they are enzymatically resistant to cleavage and intracellular deamination by CDA at 4-*N*-position. Their stability provides an alternative strategy for PET imaging.

The synthesis of the 4-*N*-alkyl gemcitabine analogues with β keto sulfonate moieties **A** involves 4-*N*-alkylation of gemcitabine followed by a series of oxidation steps in the side chain of the gemcitabine analogue to provide the β keto sulfonate. The latter are anticipated to be good substrates for an efficient fluorination, including fluorination protocols with ^{18}F labeling. Moreover, the β keto moiety is expected to prevent chemical elimination of HF of fluoride anion during cell assays because of its lack of β -hydrogens. In my second

approach for the synthesis of gemcitabine-derived PET imaging precursors I was planning to investigate the use of silicon-fluoride acceptors for an alternative mode of fluorination. The synthesis of such gemcitabine analogues with silicon-fluoride acceptors would involve the preparation of 4-*N*-alkyl or 4-*N*-alkanoyl derivatives of gemcitabine with a terminal azido or terminal alkyne group for efficient click chemistry with silane counterparts.

These analogues are expected to have greater bioavailability than gemcitabine by providing an increase in lipophilicity and in the case of the 4-*N*-alkyl analogues, increased chemical and fluoride stability. Therefore, the next objective was to study the cytotoxicity of these 4-*N*-gemcitabine as well as study their capability as radioligands for positron emission tomography imaging with ^{18}F .

The synthesis of modified nucleosides and sugars, including SRH analogues, often require the reduction of sugar lactones to the corresponding hemiacetals in the final steps of their synthetic pathways. Therefore, in my last objective, I envisioned optimizing conditions for the partial reduction of lactones to hemiacetals. The goal of the objective was to study reduction conditions of different protected and unprotected sugar lactone derivatives with common organic-based reducing reagents, with a special focus on lithium triethylborohydride (LTBH), that are usually used in carbohydrate chemistry for their conversion to lactols and/or hemiacetals (Scheme 12).



Scheme 12. Reduction of sugar lactones to hemiacetals under various conditions

3. RESULTS AND DISCUSSION

3.1. Design and synthesis of 4-*N*-alkanoyl and 4-*N*-alkyl gemcitabine analogues

3.1.1. 4-*N*-Alkyl β -keto sulfonate gemcitabine analogue

3.1.1.1. 4-*N*-Alkyl β -keto sulfonate gemcitabine analogue: Rationale

The goal of my objective was the synthesis of 4-*N*-modified gemcitabine analogue with a β -hydroxyl keto moiety suitable for ^{18}F radiolabeling (**A**). The addition of an aliphatic chain should affect cellular uptake of the drug by its increased lipophilicity, while the 4-*N*-alkyl modification, bearing β -hydroxy-keto moiety, with the ability of conversion of hydroxyl group to a leaving group, provides opportunity for the incorporation of the fluorine atom suitable for ^{18}F PET imaging. The modification at 4-*N*-alkyl of nucleosides containing cytosine such as gemcitabine has been reported by our group to have less cytotoxic strength as compared to their 4-*N*-alkanoyl counterparts.²⁸ This cytotoxicity is hypothesized to be a result of their lack of hydrolysis back to the parent molecule, gemcitabine. There is minimal phosphorylation and DNA incorporation, but it also means that there is an increased stability, with the compound entering and staying in the cell. The increased stability is a positive effect for its role in ^{18}F PET imaging of cancerous tumors. The stability of the 18-fluorine labeled gemcitabine in biological conditions is an issue observed-previously by Pulido *et al.* They showed that their 4-*N*-fluoroalkylgemcitabine [^{18}F]-radioligand (**10**) underwent *in vivo* defluorination when introduced to non-tumor bearing and tumor bearing mice. The defluorination was apparent by the accumulation of ^{18}F - signal in the bones over time³⁸ and was most likely the result of elimination reactions that can occur with β -hydrogens to the fluorine available in the side chain. The presence of a β -carbon that lacks hydrogens can evade this issue. With that in mind, a β -hydroxyketo

gemcitabine analogue, which lacks β hydrogens can provide the necessary stability for the fluorine labelled probes (Figure 15).

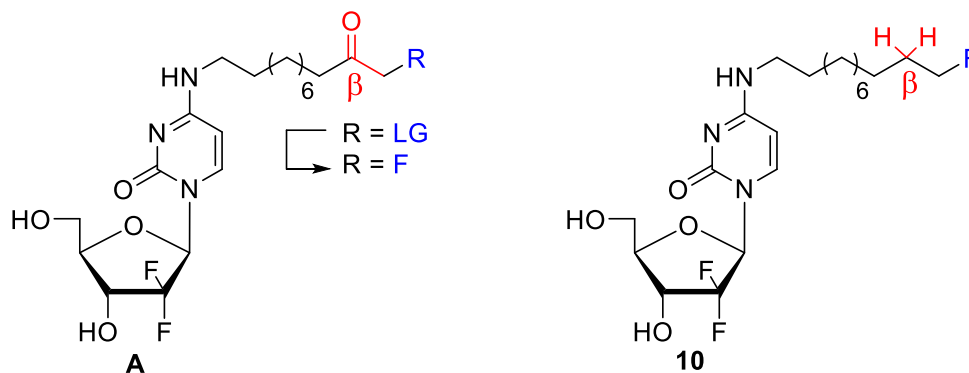


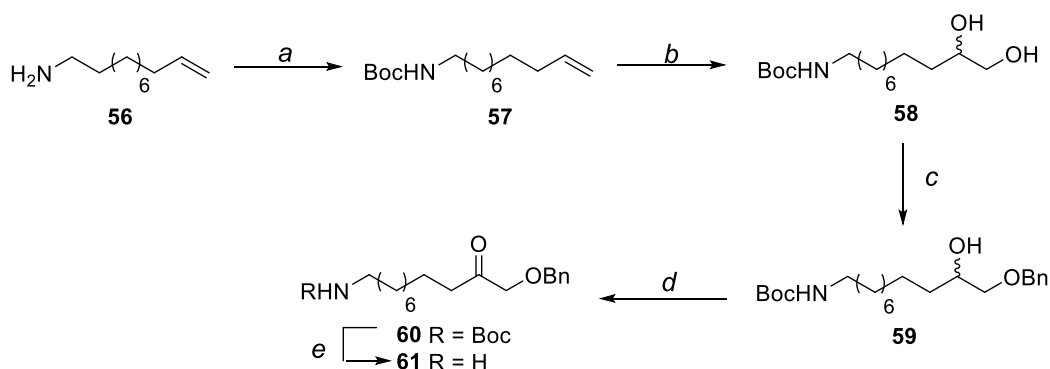
Figure 15. Key structural differences between β -keto **A** and 4-*N*-alkyl **10** gemcitabine analogues

3.1.1.2. 4-*N*-Alkyl β -keto sulfonate gemcitabine analogue: Synthesis

The synthesis of 4-*N*-alkylgemcitabine with β -keto substituent was attempted through two different pathways. The first pathway was through the synthesis of the desired alkyl amine modified sidechain bearing a terminal α -hydroxy methyl ketone, followed by its coupling with 4-*N*-tosylgemcitabine **62**. The second pathway involves coupling of the commercially available 1-amino-10-undecene with 4-*N*-Ts-gemcitabine **62**, with the chemical modifications of the sidechain done post coupling. It is important to state that in both cases, the fluorination is carried out in last step so the product can be conveniently used for PET imaging in the medical setting.

For the first pathway, treatment of 1-amino-10-undecene **56**, with di-*t*-butyl dicarbonate (Boc_2O) provided Boc-protected amine **57** (95%). Oxidation of terminal olefin of Boc-protected amine **57** was effected with a catalytic amount of osmium tetroxide (OsO_4) and *N*-methylmorpholine-*N*-Oxide (NMO) to yield vicinal diol **58** (88%). Regioselective benzylation of amino diol **58** with BnBr effected protection of the primary

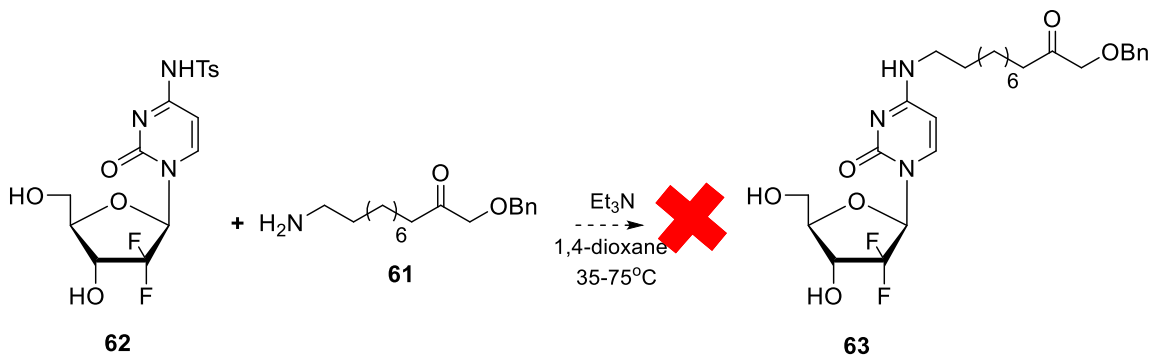
hydroxide, yielding amino alcohol **59**. The average yield in this reaction was 51%, because of benzylation of both hydroxide groups. Oxidation of benzyl protected amino alcohol **59** with Collins reagent yielded amino keto **60** (91%). This was followed by deprotection of Boc group by treatment with TFA yielding amino keto **61** (93%, Scheme 13).



^aReactions and conditions:(a) $\text{Boc}_2\text{O}/\text{MeOH}$; (b) (i) OsO_4/NMO (1.5 eq.)/acetone: H_2O (10:1); (c) BnBr (1 eq.)/ Ag_2O (1 eq.)/ CH_2Cl_2 ; (d) Collins Reag/ CH_2Cl_2 ; (e) $\text{TFA}/\text{CH}_2\text{Cl}_2$.

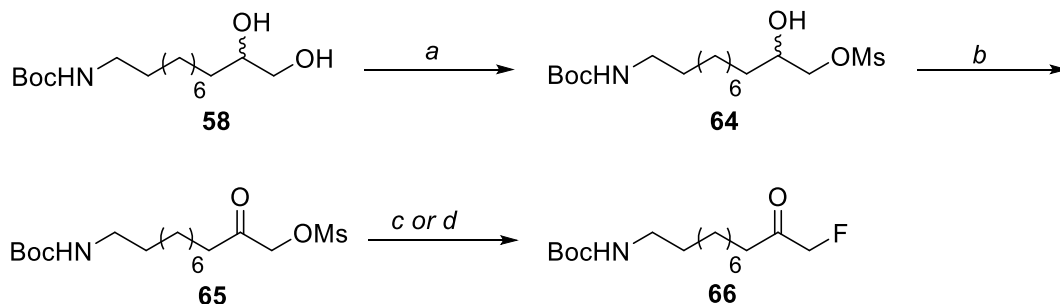
Scheme 13. Synthesis of amino with β -keto side chain

With the side chain modified, the next step was the coupling with gemcitabine. Thus, reaction of transient protected with trimethylsilyl group gemcitabine with TsCl in the presence of pyridine followed by deprotection with methanolic ammonia afforded 4-*N*-tosylgemcitabine **62** (90%).²⁸ Tosylate **62** was then treated with Et_3N (TEA)/1,4-dioxane and amino side chain **61** for the expected β -keto-4-*N*-alkylgemcitabine **63**. The coupling reaction was attempted three times with varying temperature (from 35°C to 75°C) with no desired coupled product observed (Scheme 14) with tosylated gemcitabine and modified side chain recovered in all case. Additionally, the purity of the amine appears to be key for a successful transamination reaction.



Scheme 14. Unsuccessful attempted 4-*N*-tosylgemcitabine **62** and **61** coupling reaction

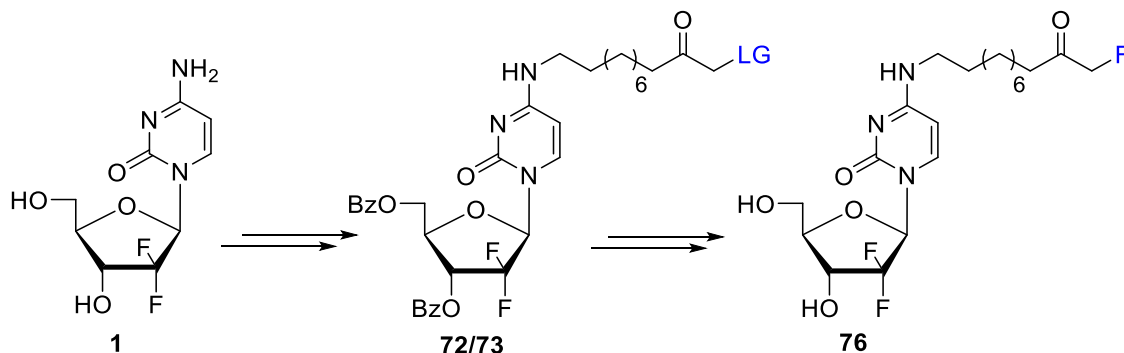
To check the validity of my approach, I took advantage that amino diol **58** was synthesized in great quantity. The modification of the side chain provided an opportunity to test fluorination reactions. Thus, vicinal diol **58** was regioselectively mesylated with 1.1 eq. MsCl at low temperature at the terminal primary hydroxyl to give mono-mesylate **64** (55%). Subsequently, oxidation of **64** with DMP gave β -keto mesylate **65** (92%). Appearance of α -hydrogens to the newly formed keto at 2.5 and 4.8 ppm on ¹H NMR and peak at 205 ppm on ¹³C NMR demonstrated oxidation of secondary alcohol to ketone. Next, fluorination was explored by displacement of mesylate with fluoride. Initially, fluorination was attempted using conventional radiosynthetic protocol. Treatment of **65** with KF in the presence of K₂CO₃ and Kryptofix 222, carried out in CH₃CN at 80°C for 25 min gave **66** (55%). Interestingly, better yields of **66** were obtained when **65** was treated with TBAF as fluorinating agent (80%, Scheme 15). In both cases, ¹⁹F NMR showed formation of the expected triplet at -227.5 ppm.



^aReagents and Conditions: (a) MsCl (1.1 eq.)/Et₃N/CH₂Cl₂/-20°C;
 (b) DMP/ CH₂Cl₂; (c) KF/Kryptofix 2.2.2/CH₃CN/80°C/25 min; (d) TBAF/THF/60°C.

Scheme 15. Synthesis of fluoro β-keto side chain

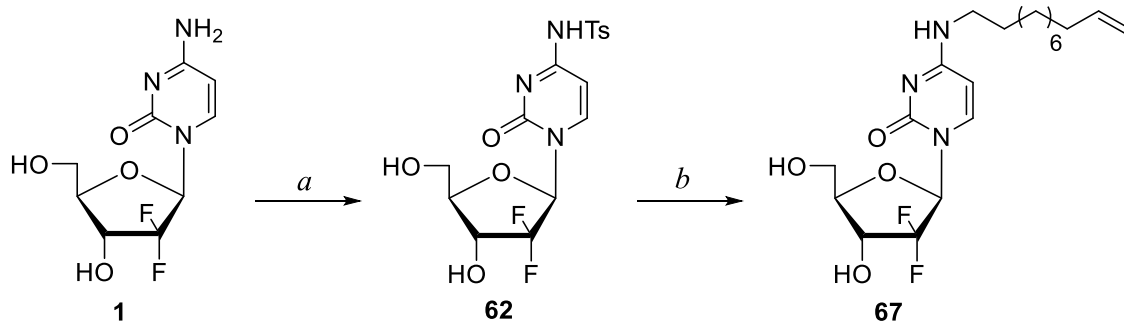
The fluorination of the side chain provided the foundation for the continuation of the project by using the second approach. The synthesis of the targeted gemcitabine analogue was accomplished through three main critical transformations: (i) displacement of 4-*N*-tosylamine group with commercially available 1-amino-10-undecene, (ii) modification of terminal olefin to β-keto sulfonate moiety, and (iii) displacement of sulfonate leaving group with fluoride followed by deprotection (Scheme 16).



Scheme 16. Overall synthesis of 4-*N*-modified β-keto fluoro gemcitabine analogue

The alkylation of the 4-exocyclic amine group in gemcitabine was achieved by displacement of a 4-*N*-tosylamine group with 1-amino-10-undecene. Treatment of **62** with 1-amino-10-undecene effected displacement of the *p*-toluenesulfonamido group from the

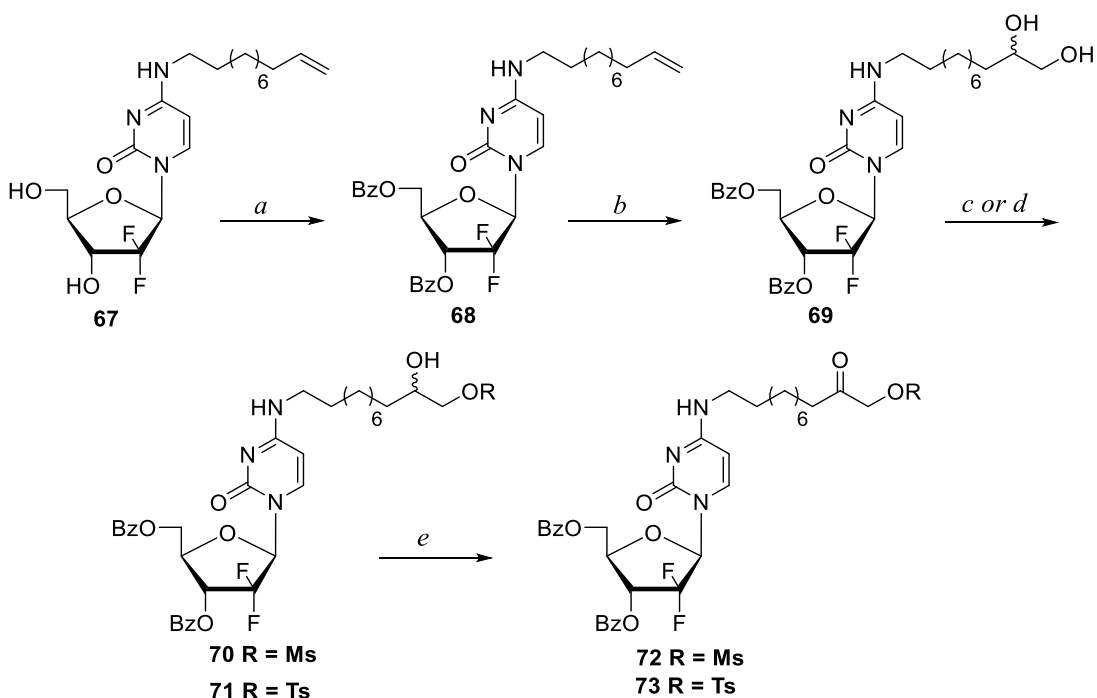
C4 position of the cytosine ring to give 4-*N*-(10-undecene) derivative **67** (85%, scheme 17).



^aReagents and Conditions:(a) (i) TMSCl/Pyr, (ii) TsCl, (iii) MeOH/NH₃;
(b) 1-amino-10-undecene/Et₃N/1,4-dioxane

Scheme 17. Synthesis of 4-*N*-(10-undecene) gemcitabine analogue

Benzoylation of 4-*N*-alkene-gemcitabine **67** with BzCl in the presence of DMAP and 2,6-lutidine yielded 3' and 5' protected nucleoside **68** (77%). Oxidation of the benzoyl protected 4-*N*-alkyl-gemcitabine **68** with NMO in the presence of catalytic OsO₄ gave terminal vicinal diol **69** (96%). Subsequent regioselective mesylation of the terminal primary hydroxyl (MsCl/Et₃N/-20°C) gave mono-mesylated compound **70** (55%). Analogously, terminal vicinal diol **69** was treated with tosyl chloride in the presence of Et₃N to make regioselectively mono-tosylated compound **71** (62%). Subsequently, oxidation of **70** or **71** with Collins reagent (CrO₃, pyridine and Ac₂O) gave mesyl β-keto derivative **72** (93%) or tosyl β-keto derivative **73** (94%, Scheme 18).



^aReagents and Conditions: (a) BzCl/DMAP/2,6-lutidine/DCM; (b) OsO₄/NMO/Acetone/H₂O (10:1); (c) MsCl (1.1 eq.)/Et₃N/DCM; (d) TsCl/DMAP/Pyr (e) CrO₃/pyr/Ac₂O/DCM

Scheme 18. Overall synthesis of β -keto gemcitabine sulfonate analogue

3.1.1.3. 4-N-Alkyl β -keto sulfonate gemcitabine analogue: Fluorination studies

The β -keto sulfonates **72** and **73** were subjected to the same fluorination conditions (18-crown-6, KF) at different temperatures with the ultimate goal of finding the optimal fluorination conditions. Table 2 shows a summary of the reactions that were attempted. Briefly, temperature was found to be critical for this reaction. As the temperature was increased, the yield also increased. Reactions at room temperature did not yield any product (entry 1 and 5) with substrate recovered back in both cases. When comparing the two different leaving groups, tosyl showed to be the better option for its displacement with KF (entry 6) than mesyl (entry 3). Aside from yield, tosylate **73** provided the cleaner fluorinated product with no formation of side products. On the other hand, the fluorination

of the mesylated β -keto **72** formed several biproducts in addition to the targeted **74**. The three set of signals in ^{19}F NMR were diagnostic for the presence of three fluorine atoms in **74** [-119.41 (d, $J = 245.1$ Hz, 1F) and -120.17 ppm (br d, $J = 245.1$ Hz, 1F) for the C2' *gem*-difluoro unit and triplet at -227.42 ($J = 47.7$) for the terminal CH_2F].

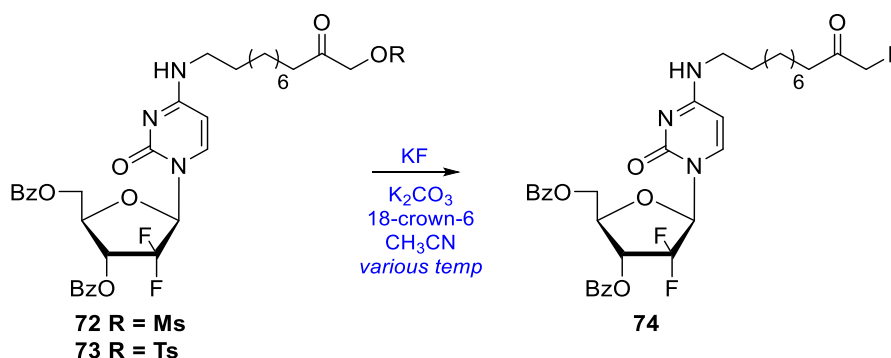


Table 2. Fluorination reactions with different conditions^a

Entry	Sulfonate	F- source	Solvent	Temperature (°C)	Yield (%)
1	Mesyl	KF	CH ₃ CN	20	0
2	Mesyl	KF	CH ₃ CN	30	10
3	Mesyl	KF	CH ₃ CN	60	40
4	Mesyl	KF	CHCl ₃	60	30
5	Tosyl	KF	CH ₃ CN	20	0
6	Tosyl	KF	CH ₃ CN	60	60

^a 0.1 mmol reaction scale, KF (4 eq.), K₂CO₃ (4 eq.), 18-Crown-6 (4 eq.)

After fluorination conditions were optimized, the final step was the removal of the benzoyl protection. The conditions for deprotection require fast and effective removal of the benzoyl groups, but also should be mild enough not to cause any unwanted side reactions on the fluorinated side chain. A series of reactions with model fluoro keto derivative **75** (synthesized similarly to **66**; see experimental section 4.2. for detailed procedure) were performed using common debenzoylation methods (e.g., methanolic ammonia or sodium methoxide) in order to study the stability of the fluoro β -keto compounds (Table 3). Briefly, varying both the temperature and the base did not yield any

significant decomposition in the model compound, to showing us that these bases are compatible with the required deprotection. Methanolic ammonia is a milder base than sodium methoxide (entries 1-3), but it has been shown to remove benzoyl groups from nucleosides requiring longer reaction times. The reaction time is a drawback when time sensitive radiochemical protocols need to be followed. Deprotection with sodium methoxide takes less time and also does not affect the fluorine atom of the fluoro β -keto model compound **75** (entries 4-6). It is also noteworthy that, even though model **75** bears the benzoyl protection, it is an amide moiety, not an ester, therefore it is less reactive and requires harsher conditions (strong acid/base) for its hydrolysis.

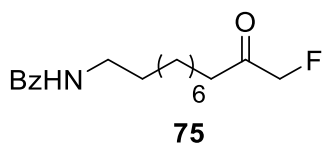
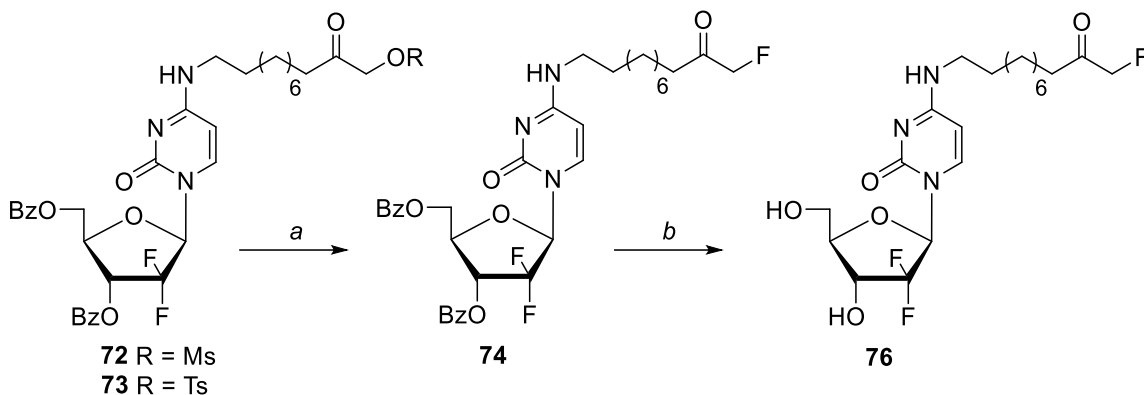


Table 3. Stability studies of fluoro β -keto model compound **75**

Entry	Base	Temperature ($^{\circ}$ C)	Time (min)	Result
1	NH ₃ /MeOH	0	30	No change
2	NH ₃ /MeOH	25	30	No change
3	NH ₃ /MeOH	80	120	Minimal decomposition
4	NaOCH ₃ ^a	0	30	No change
5	NaOCH ₃ ^a	25	30	No change
6	NaOCH ₃ ^a	80	120	Minimal decomposition

^a 0.5 M NaOCH₃ in methanol

With these model studies in hand, I found that deprotection of gemcitabine analogue **74** with MeOH/NH₃ gave β -keto fluorine **76** (55%, Scheme 19). The next step was simulating conventional radiosynthetic conditions with both of these substrates to prepare the deprotected fluorinated product in a short amount of time and in suitable purity.



^aReagents and Conditions: a) KF/Kryptofix₂₂₂/CH₃CN, 75°C, 1h; b) MeOH/NH₃, 0°C, 30 min.

Scheme 19. Fluorination of β -keto sulfonate gemcitabine analogues and subsequent deprotection under conditions compatible with ¹⁸F-radiolabeling protocols^a

Using both β -keto sulfonate analogues **72** and **73**, attempts were made to use common ¹⁸F-radiolabeling protocols. Treatment of **72** or **73** with Kryptofix 2.2.2 and KF (75°C, 30 min), followed immediately by deprotection with MeOH/NH₃ or NaOMe yielded compound **76**, but at a low yield (~25%). Additionally, separation of the targeted compound from side products required extensive HPLC purification as a consequence of the proximities of the peaks. Also, when these steps were analyzed further, the use of Kryptofix 222 instead of 18-crown-6, another cryptand, for the fluorination step using both substrates proved to be intricate by giving several byproducts in addition to the target **76**. Through TLC (not shown) and HPLC analysis, the fluorination of tosylated substrate **73** (Figure 16) was shown to be cleaner than for the mesylated substrate **72** (Figure 17). It is expected that radiochemical yields would be even lower than those experienced in cold conditions. The RP-HPLC analysis of these reactions suggests that isolation of the desired product would be difficult. Synthesis of this 4-*N*-alkyl fluoro β -keto gemcitabine analogue

was successful, but the require fluorination and deprotection conditions coupled with the necessary extensive purification make this method impractical for medical radiolabeling.

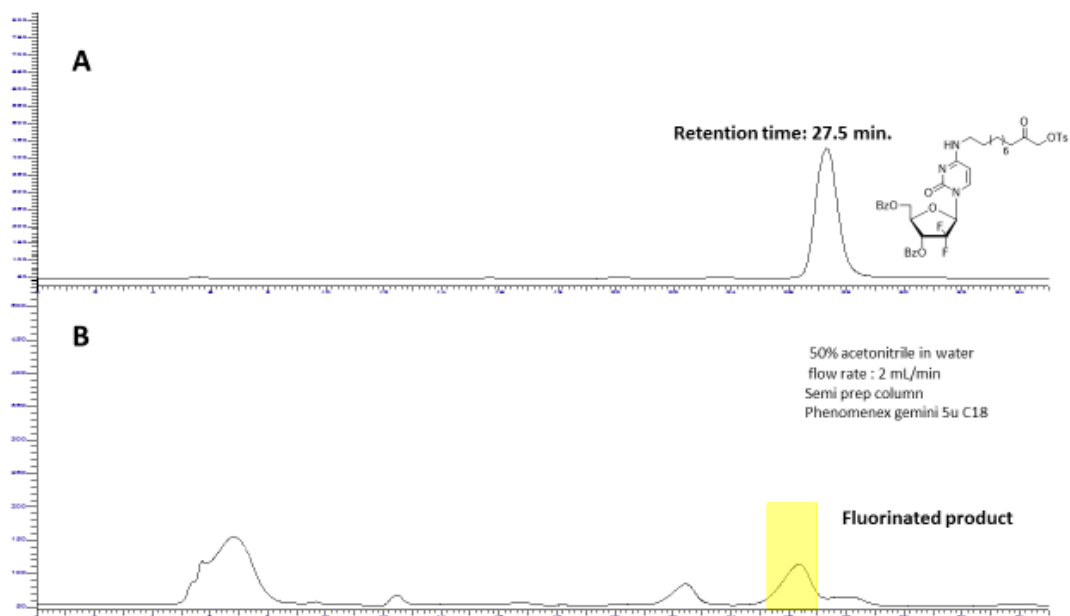


Figure 16. Fluorination of 4-*N*-alkyl **73** (chromatogram A: **73** standard, chromatogram B: Crude fluorination reaction) in 50% CH₃CN/H₂O.

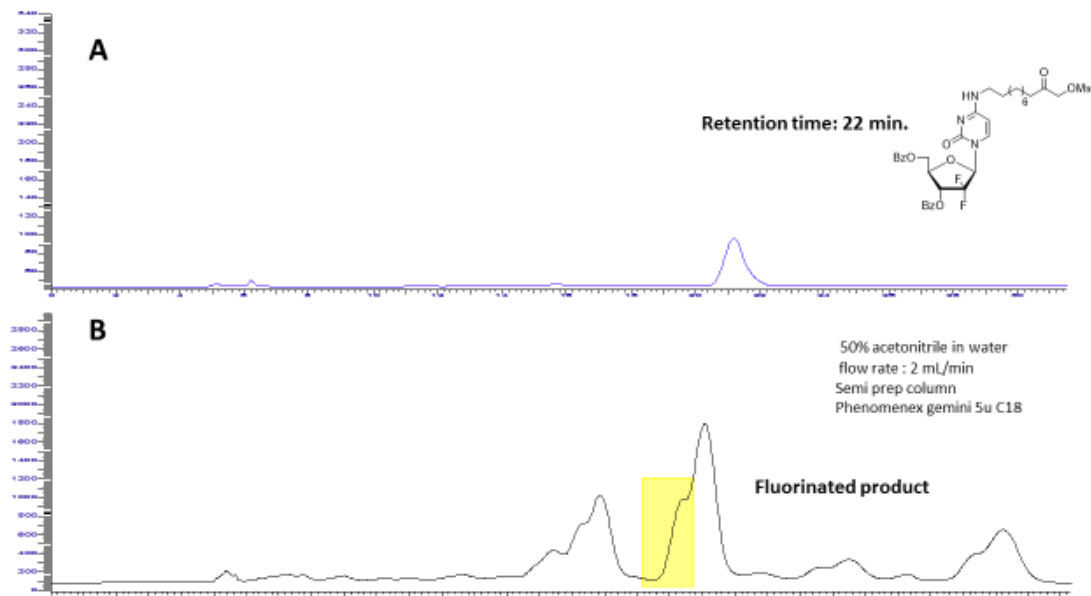


Figure 17. Fluorination of 4-*N*-alkyl **72** (chromatogram A: **72** standard, chromatogram B: Crude fluorination reaction) in 50% CH₃CN/H₂O.

3.1.2. 4-*N*-Alkyl and alkanoyl gemcitabine analogues with silicon-fluoride acceptors

3.1.2.1. Silicon-fluoride acceptors gemcitabine analogues: Rationale

In continuation of syntheses of stable gemcitabine analogues with fluorine atom compatible for PET imaging, my next goal was the synthesis of 4-*N*-modified gemcitabine analogues with silicon-fluoride-acceptor building blocks suitable for ^{18}F radiolabeling. As it has been previously discussed, the addition of an aliphatic chain should affect pharmacodynamics and cellular uptake of the parent drug. More importantly, the use of silicon-fluoride-acceptor building block will provide another option for to study PET imaging through the “Si-F” bond which is stronger than “C-F” bond.⁸⁷ Also, the “Si-F” bond, in the presence of bulky groups, is hydrolytically stable in physiological conditions (discussed in section 1.2.3.). The strategy for the synthesis of gemcitabine analogues bearing silicon fluoride acceptors attached to an exo-amino group of cytosine ring involve: (a) synthesis of gemcitabine analogues having terminal azido or alkyne group at an alkyl chain attached to 4-amino group, and (b) copper(I) catalyzed click reaction with the corresponding silane reagent having terminal alkyne or azido group, followed by its fluorination. This synthesis provide two clear advantages: *i*) it does not require the sugar protection of nucleoside and *ii*) it utilizes high-yielding copper(I)-catalyzed click chemistry. Both of these synthetic approaches lower the number of steps, have increased reaction yields and low reaction times. (Figure 18).

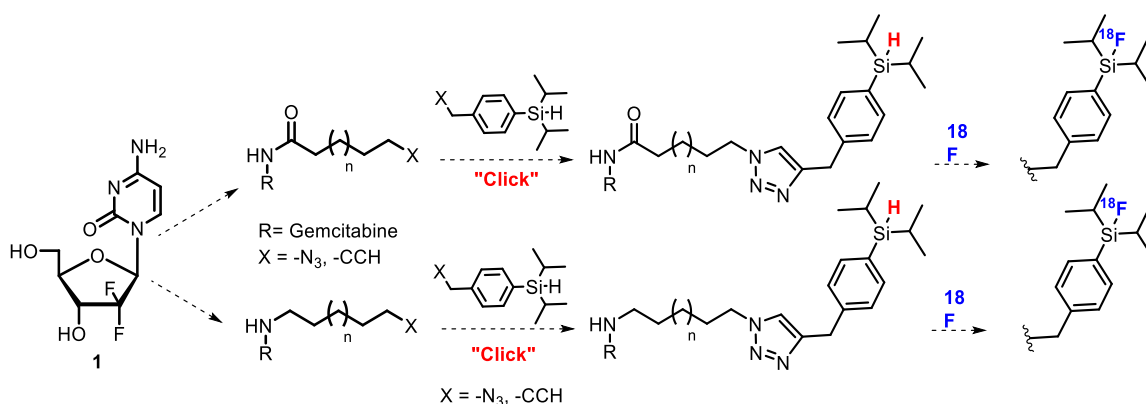
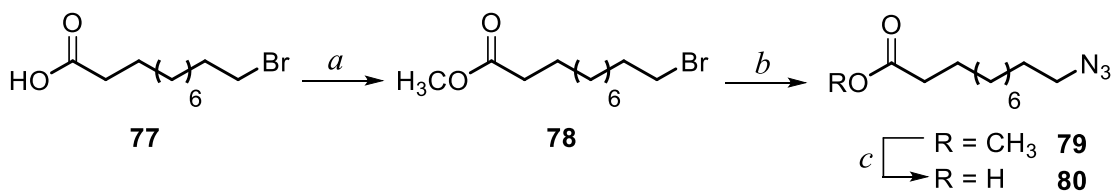


Figure 18. General synthetic goal of gemcitabine silicon-fluoride acceptors analogues

3.1.2.2. Silicon-fluoride acceptors gemcitabine analogues: Synthesis

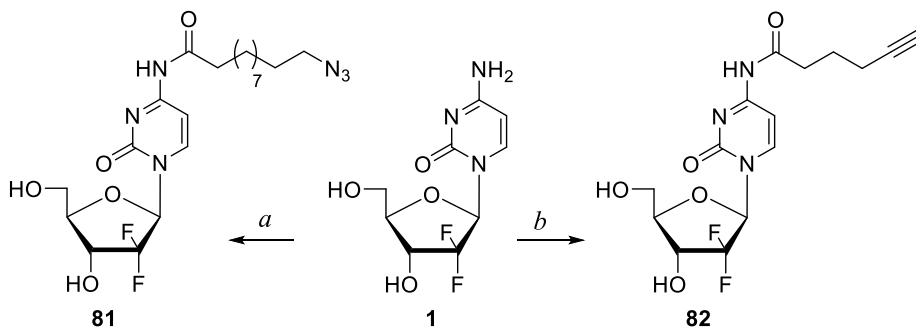
The condensation of gemcitabine **1** with 11-azidoundecanoic acid **80** under peptide coupling conditions [(*N*-dimethylaminopropyl)-*N'*-ethyl-carbodiimide (EDC)/1-hydroxybenzotriazole (HOBT)/ *N,N*-Diisopropylethylamine (DIPEA)] in DMF at 65°C afforded 4-*N*-(11-azidoundecanoyl)gemcitabine **81** (70%; Scheme 21). The 11-azidoundecanoic acid **80** was prepared by esterification of the commercially available 11-bromoundecanoic acid and subsequent azidation (NaN₃/DMF) followed by saponification with the overall 81% yield (Scheme 20).



^aReagents and Conditions:(a) 2,2-Dimethoxypropane/MeOH; (b) NaN₃/DMF; (c) NaOH/MeOH.

Scheme 20. Synthesis of 11-azidoundecanoic acid^a

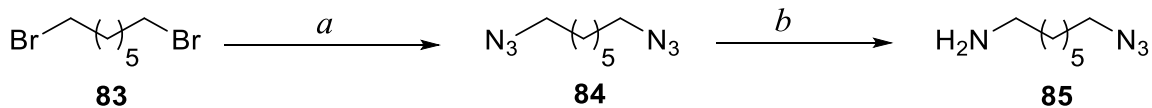
Condensation of **1** with 5-hexynoic acid under similar conditions gave 4-*N*-(hexynoyl)gemcitabine **82** but with lower yield and contaminated with mono and/or di sugar 5-hexynoate esters. However, transient protection⁴⁵ of **1** with trimethylsilyl group followed by condensation with 5-hexynoic acid in the presence of EDC provided **82**⁴⁵ (63%; Scheme 21).



^aReactions and conditions: (a) $\text{N}_3(\text{CH}_2)_{10}\text{COOH}/\text{HOBt}/\text{DIPEA}/\text{EDC}/\text{DMF}/60^\circ\text{C}/\text{overnight}$; (b) (i) $\text{TMSCl}/\text{Pyr}/\text{CH}_3\text{CN}$, 3 h, (ii) $\text{CHC}(\text{CH}_2)_3\text{COOH}/\text{EDC}/\text{CH}_3\text{CN}/65^\circ\text{C}/\text{overnight}$; (iii) EtOH , 45°C , 5 h

Scheme 21. Synthesis of 4-*N*-alkanoyl gemcitabine substrates for click reactions^a

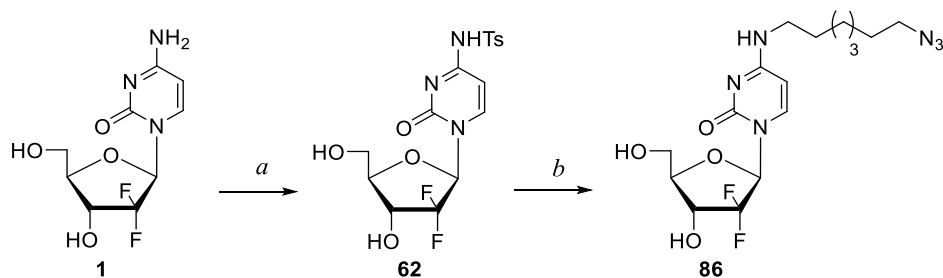
The synthesis of the 4-*N*-alkyl gemcitabine analogues with silicon-fluoride acceptor started from displacement of a 4-*N*-tosylamine group from **62** with freshly prepared 7-azidoheptylamine **85**. Thus, reaction of transient protected with trimethylsilyl group gemcitabine with TsCl in the presence of pyridine followed by deprotection with methanolic ammonia afforded protected 4-*N*-tosylgemcitabine²⁸ **62** (90%, Scheme 23). Treatment of **62** with 7-azidoheptylamine **85** effected displacement of the *p*-toluenesulfonamido group from the C4 position of the cytosine ring to give 4-*N*-(7-azidoheptyl) gemcitabine **86** (82%).



^aReagents and Conditions:(a) (i) NaN₃/DMF; (b) PPh₃/EtOAc/5% HCl (aq)

Scheme 22. Synthesis of 7-azido-1-aminoheptane^a

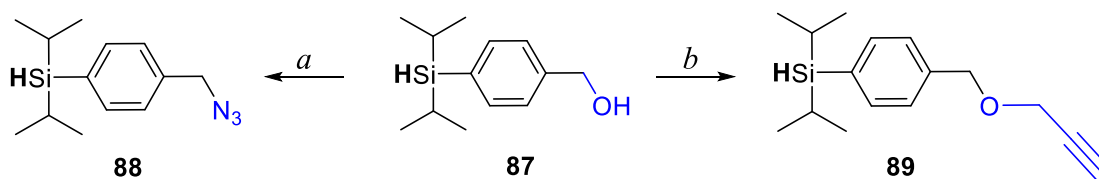
The 7-azidoheptylamine **85** was prepared from 1,7-dibromoheptane by treatment with 2 eq. of NaN₃, followed by selective Staudinger reduction of one of the azido group in intermediary 1,7-diazidoheptane **84** with triphenylphosphine in 83% overall yield (Scheme 22).



^aReagents and Conditions:(a) (i) TMSCl/Pyr, (ii) TsCl, (iii) MeOH/NH₃; (b) N₃(CH₂)₇NH₂/Et₃N/1,4-dioxane

Scheme 23. Synthesis of 4-*N*-alkyl gemcitabine derivatives for click reactions^a

Two bifunctional silicon building blocks **88** and **89** (Scheme 24) were synthesized from commercially available 4-di-isopropylsilyl-benzylalcohol **87**. Benzyl alcohol **87** was successively treated with mesyl chloride and NaN₃ to give **88** (95%). Benzyl alcohol **87** was treated with propargyl bromide in the presence of sodium hydride to give **89** (82%).



^aReagents and Conditions: a) (i) MsCl/Et₃N/CH₂Cl₂ (ii) NaN₃/DMF;
b) Propargyl Bromide/NaH/THF

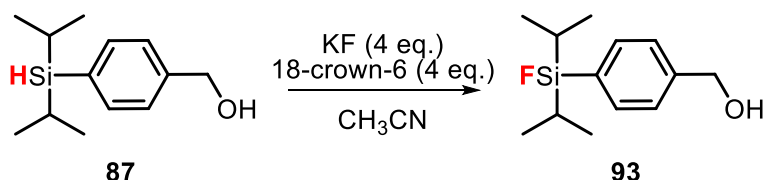
Scheme 24. Synthesis of silane building blocks for click reactions^a

The 4-*N*-alkanoyl and 4-*N*-alkyl gemcitabine analogues were then reacted with these two different bifunctional silicon-fluoride-acceptor building blocks (Scheme 25) using copper-catalyzed click reaction conditions (sodium ascorbate and copper(I) sulfate) to give **90** (92%), **91** (87%), and **92** (90%).

3.1.2.3. Silicon-fluoride acceptors gemcitabine analogues: Fluorination studies

Once the silane-modified 4-*N*-alkanoyl and 4-*N*-alkyl gemcitabine analogues were prepared, in the next step I investigated the fluorination of these compounds with KF, a cryptand (18-crown-6) and AcOH in CH₃CN under a time frame compatible with ¹⁸F radiochemical reaction conditions. Model studies were performed with silicon-fluoride-acceptor benzyl alcohol **87** using temperature and time as variables maintaining KF and 18-crown-6 constant (Table 4).

Table 4. Summary of model fluorination studies

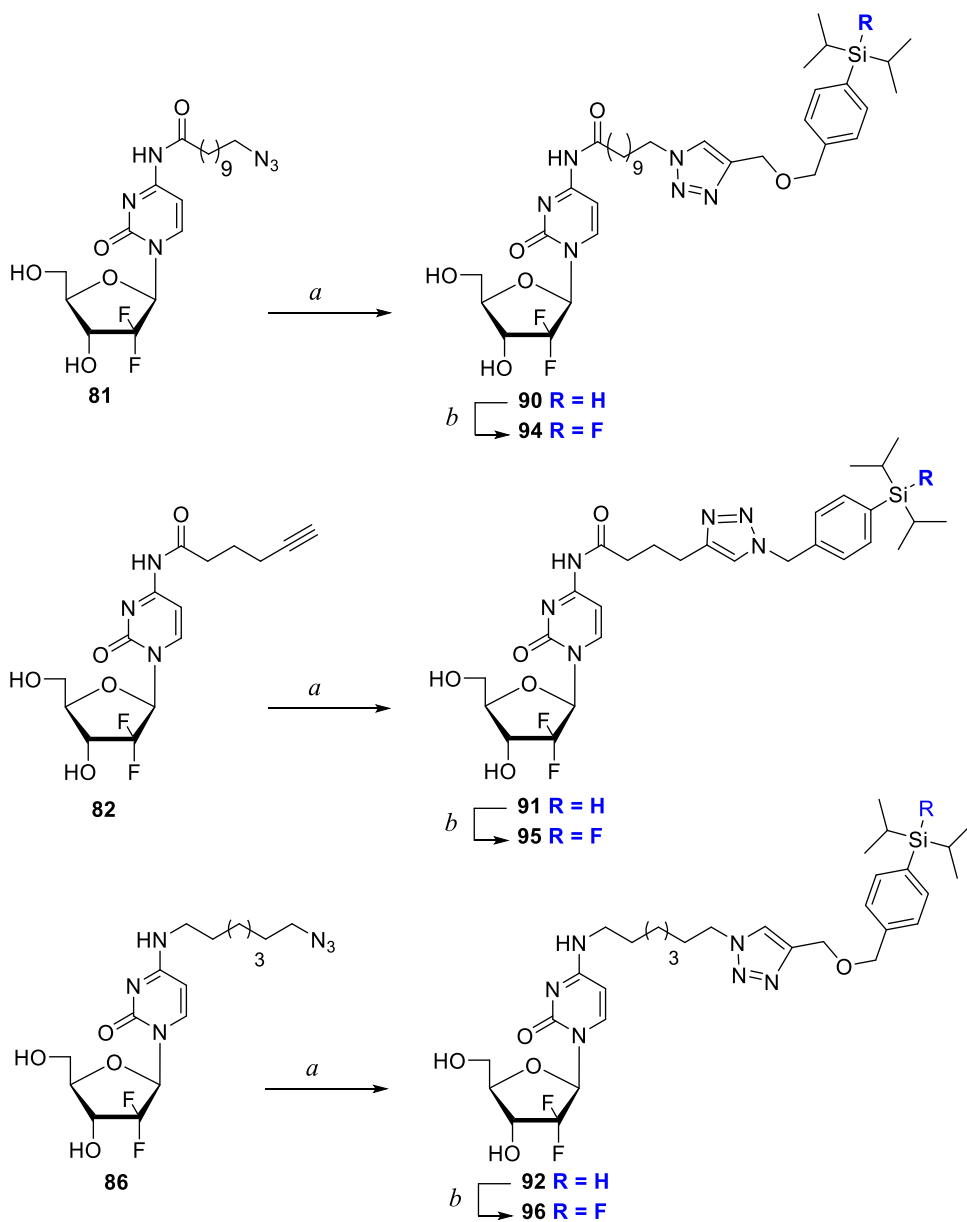


Entry	Temperature (°C)	Time (min)	Fluorination?	Yield	Comments
1	30	30	No	-	
2	40	30	No	-	
3	60	20	Yes	20%	
4	80	20	Yes	50%	
5	80	20	Yes	60%	<i>Catalytic AcOH added</i>

Briefly, when different temperatures were tested (30-80°C) it was clearly concluded that increasing temperature led to the fluorinated product **93** in an increased yield. Temperatures slightly above room temperature (30 and 40°C), did not give any product (entry 1 and 2). When the temperature was increased to 80°C, product formed in acceptable yields (entry 4) but the addition of acetic acid (AcOH) increased the yield even more (entry 5). When Silicon building blocks have been used as fluoride acceptors, many reports have shown that addition of acetic acid leads to an increased yield.^{89, 90, 94, 126} It is important to note that the time was always kept under 30 minutes in an attempt to replicate ¹⁸F radiochemical fluorination conditions.

It is critical to mention that once the reaction time was over, the crude mixture was carefully filtered and diluted to keep the pH of the reaction neutral. Any deviation from neutral pH leads to hydrolysis of the Si-F bond to the silanol (Si-OH). This was clearly seen when the reactions were followed by TLC since a more polar spot appeared. After column isolation, this lower spot was shown to be the corresponding silanol by ¹H NMR through the absence of the Si-H peak and ¹⁹F NMR through the absence of peak at 189 ppm. This issue was discussed extensively in section 1.2.3. This model study showed that

20 minutes at 80°C with the addition of acetic acid was the optimal fluorination condition and extra precautions are needed to avoid hydrolysis. This optimized fluorination condition was then applied to gemcitabine derivatives **90**, **91** and **92**.



^aReagents and Conditions: (a) **88** or **89**/Sodium ascorbate/Cu₂SO₄/tert-butanol/water (3:1), 6 h; (b) KF/18-crown-6/AcOH/CH₃CN/80°C/25 min.

Scheme 25. Synthesis of the 4-*N*-acyl/alkyl gemcitabine analogues with the silicon-fluoride-acceptors^a

Reaction of gemcitabine analogues **90**, **91** or **92** with KF in the presence of 18-Crown-6 were carried out in CH₃CN at 80 °C for 20 min followed by quick cooling and filtration, followed by column chromatography gave their respective fluorinated products **94** (63%), **95** (65%) and **96** (62%), respectively (Scheme 25). Besides desired **94-96**, the corresponding silanols resulting from the hydrolysis of Si-F to Si-OH were also isolated during the purification on column (~20-25%). The structure of the silanols were confirmed by the absence of hydrogen from of Si-H bond (e.g., in **96** at 3.92 ppm) and lack of fluorine signal (e.g., in **96** at -188.86 ppm) by ¹H or ¹⁹F NMR and additionally defined by HRMS. This hydrolysis was not observed in any other reaction that involved silicon-fluoride acceptors **87-89**.

3.1.2.4. Silicon-fluoride acceptors gemcitabine analogues: Stability studies

Stability of 4-*N*-alkanoyl **90** and 4-*N*-alkyl **92** substrates as well as their fluorinated products **94** and **96** were examined employing RP-HPLC with isocratic mobile phase of CH₃CN/water containing 0.1% of TFA which is compatible with the purification protocols for the [18F]-labeled products (*vide infra*). In the presence of 0.1% TFA, the 4-*N*-alkanoyl **90** were found to be prone to hydrolysis of the amide bond. For example gemcitabine (10-15%, 30 min) was detected after **90** was dissolved in 35% CH₃CN/0.1% TFA (Figure 19).

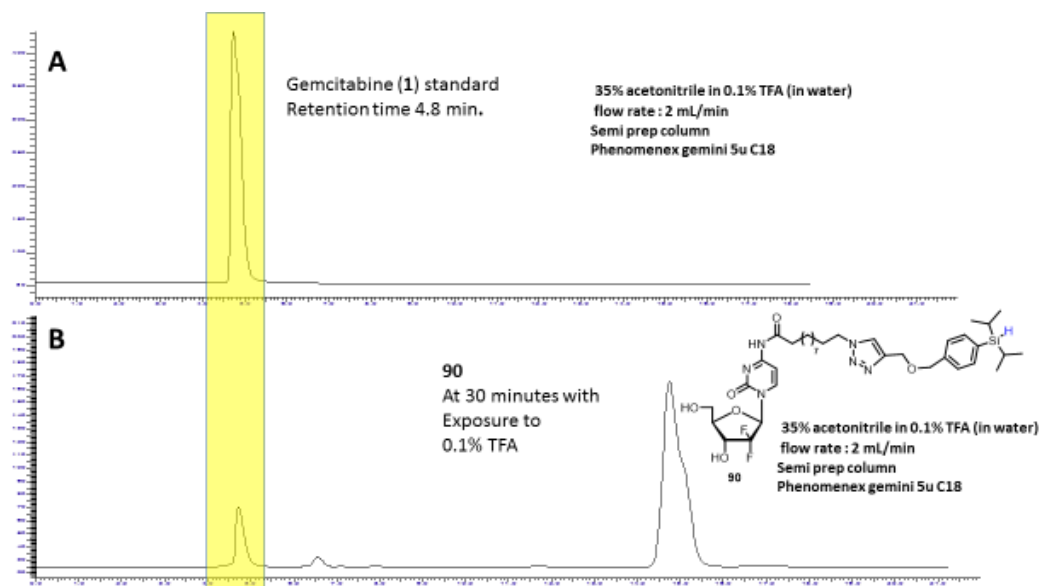


Figure 19. Stability of 4-*N*-alkanoyl **90** (chromatogram A: **1**, chromatogram B: **90** after 30 min) in 35 %CH₃CN /0.1% TFA

The RP-HPLC of the fluoro product **94** also showed hydrolysis of the acyl chain to gemcitabine (15%, 30 min) and Si-F bond to the corresponding silanol (20%, 30 min). HPLC after 2 h showed larger amounts of silanol (30%) and gemcitabine (20%; Figure 20).

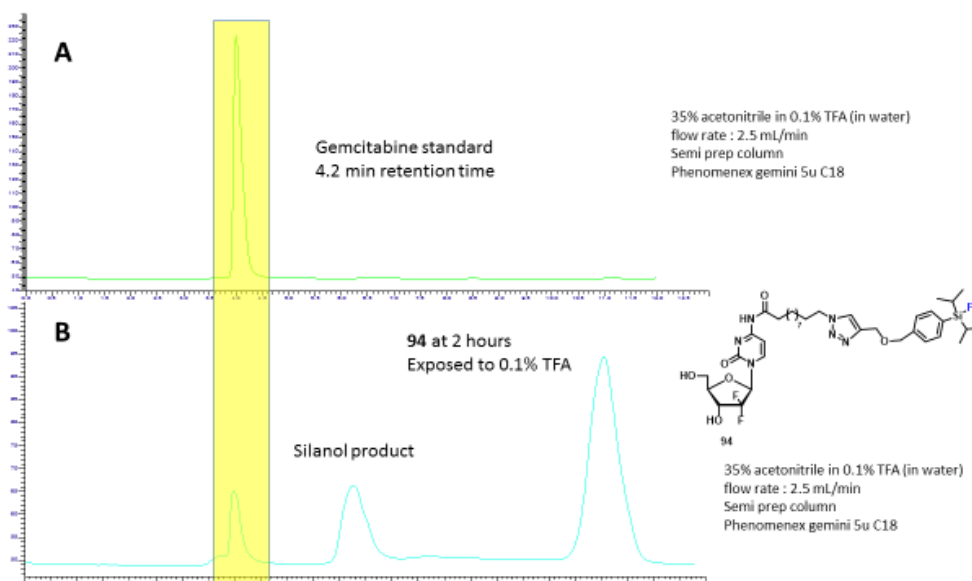


Figure 20. Stability of 4-*N*-alkanoyl **94** (chromatogram A: **1**, chromatogram B: **94** after 2 h) in 35% CH₃CN/0.1% TFA.

On the other hand, the 4-*N*-alkyl substrate **92** was found to be stable with only very minor formation of byproduct peak(s) (e.g., gemcitabine) observed after long exposure (8 h) to 35% CH₃CN/0.1% TFA (Figure 21).

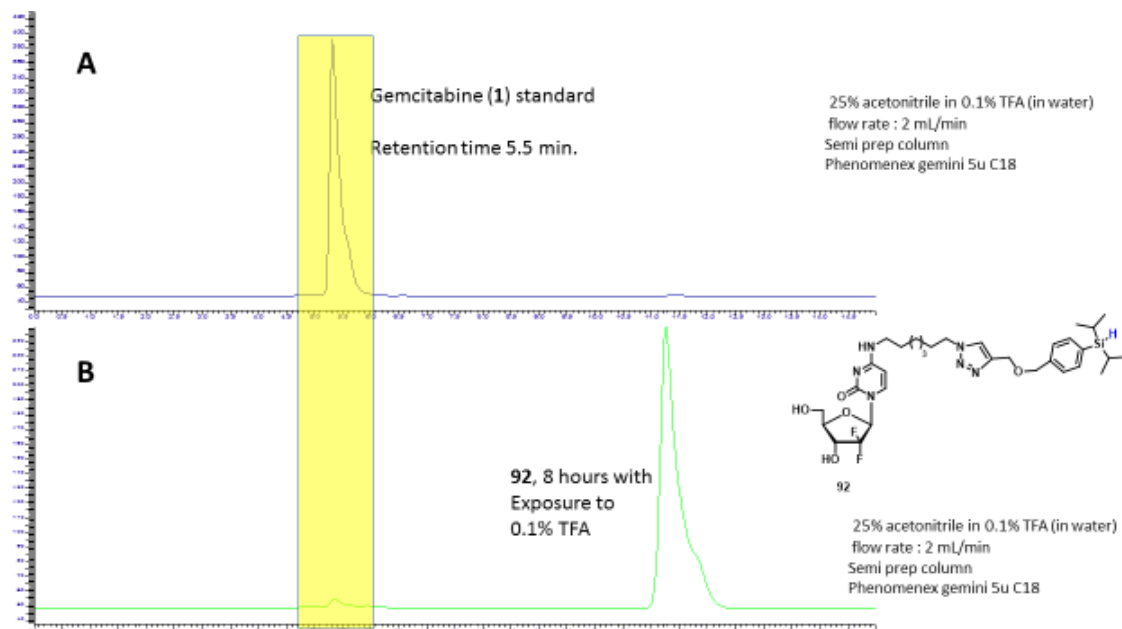


Figure 21. Stability of 4-*N*-alkyl **92** (chromatogram A: **1**, chromatogram B: **92** after 8 h) in 25% CH₃CN/0.1% TFA.

The fluorinated product **96** in the 25% CH₃CN/0.1% TFA in water hydrolyzes to silanol (25%, 1 h, 55%, 3 h; Figure 22). However, hydrolysis of **96** in TFA-free system (25% CH₃CN/water) occurred to a lesser extent (25%, 1 h, 30%, 3 h; Figure 23). These studies show that the 4-*N*-alkyl silanes and fluorosilanes are more stable under acidic conditions, indicating an advantage when discussing their potential as PET imaging agents. Moreover, the 4-*N*-alkyl derivatives have a lower chance to decompose/break down as they travel through the different environments for biological testing (cell/mice/human).

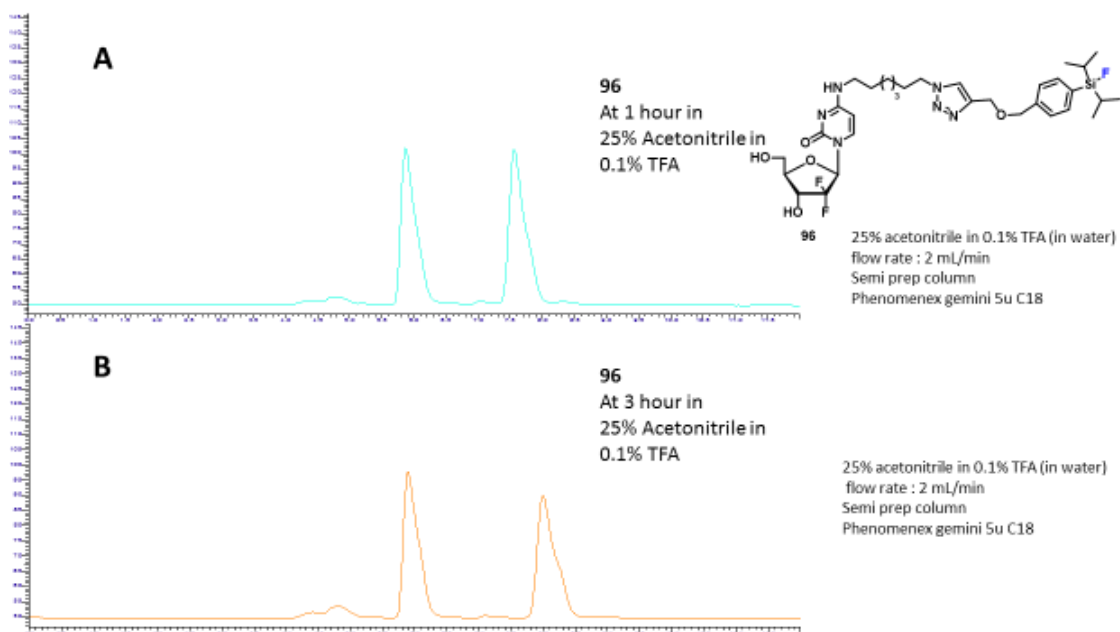


Figure 22. Analysis of stability of 4-*N*-alkyl **96** (chromatogram A: **96** after 1 h, chromatogram B: **96** after 3 h) in 25%CH₃CN/0.1% TFA.

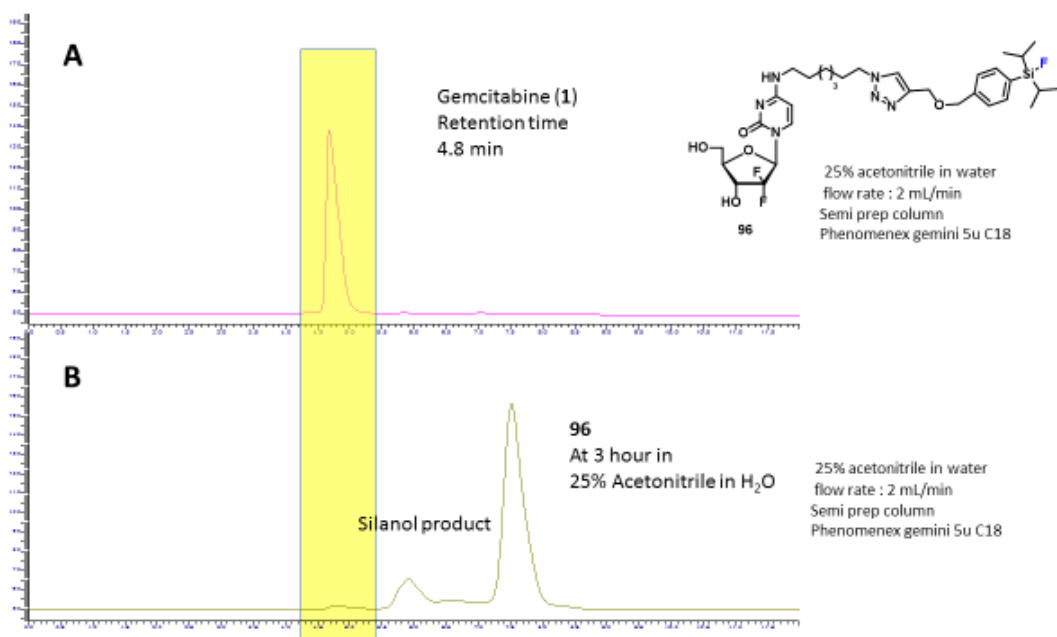


Figure 23. Analysis of stability of 4-*N*-alkyl **96** (chromatogram A: **1**, chromatogram B: **96** after 3 h) in 25%CH₃CN/H₂O (NO TFA).

3.1.2.5. Biological evaluation of the 4-*N*-alkyl & alkanoyl gemcitabine analogues

The biological aspect of the 4-*N*-alkanoyl and 4-*N*-alkyl gemcitabine analogues was 1) assess their cytotoxic activity through preliminary biological evaluations in cancer cell lines; 2) to assess their cell permeability, due to their lipophilic nature; 3) to examine their resistance to deamination from cytosine to uracil base; and 4) to study their rate of hydrolysis to the parent gemcitabine. All of these points would reflect a change in the pharmacokinetics and more importantly, the anti-cancer potency of the designed analogues compared to the parent drug. Some of these pharmacokinetics deviations have been observed and reported in 4-*N*-alkanoyl derivatives^{21, 24} and to a much lesser extent with 4-*N*-alkyl analogues.²⁸ Most of the examples in literature are lipophilic 4-*N*-alkanoyl gemcitabine analogues, with focus on their resistance to deamination as well as slow hydrolysis for a slow release to the parent drug.^{19, 21, 24} 4-*N*-alkyl modifications have shown to be chemically and enzymatically resistant to cleavage, therefore having little to no release of gemcitabine, showing very little biological effect on cells.²⁸

Cytostatic evaluation of 4-*N*-modified gemcitabine analogues

In collaboration with the Ramachandran's group at Nicklaus Children Hospital, Miami Children's Health System cytostatic activities of the 4-*N*-modified gemcitabine analogues **81**, **86**, **90**, **91**, **92** and **94** were analyzed in L1210 mouse lymphocytic leukemia cell line. All compounds were directly tested in free-base form, and were found to have different levels of inhibition in a dose-dependent manner. This is demonstrated by the cytostatic activity curves in Figure 24 and Table 5. The 4-*N*-alkylgemcitabines **86** and **92**, with both IC₅₀ >200 μM, demonstrated no cytostatic activities in L1210 cells (after 72 h incubation) in comparison to the 4-*N*-alkanoylgemcitabine analogues **81**, **90**, **91** and **94** with IC₅₀ =

7.99 μM , $\text{IC}_{50} = 7.47 \mu\text{M}$, $\text{IC}_{50} = 65.3 \mu\text{M}$ and $\text{IC}_{50} = 39.96 \mu\text{M}$ respectively. These results confirmed what previous studies have shown, that the 4-*N*-alkanoylgemcitabine analogues do undergo slow hydrolysis and release the parent gemcitabine for DNA incorporation and apoptosis. In the case of the 4-*N*-alkylgemcitabine analogues, there appears to be no such release of the parent drug, leading to the small biological effect on the L1210 cells studied. These results also in conformity with our group's previous studies in other 4-*N*-alkyl gemcitabine analogues.^{28, 38} With these results in hand, we were intrigued in the outcome of the 4-*N*-alkyl analogues.

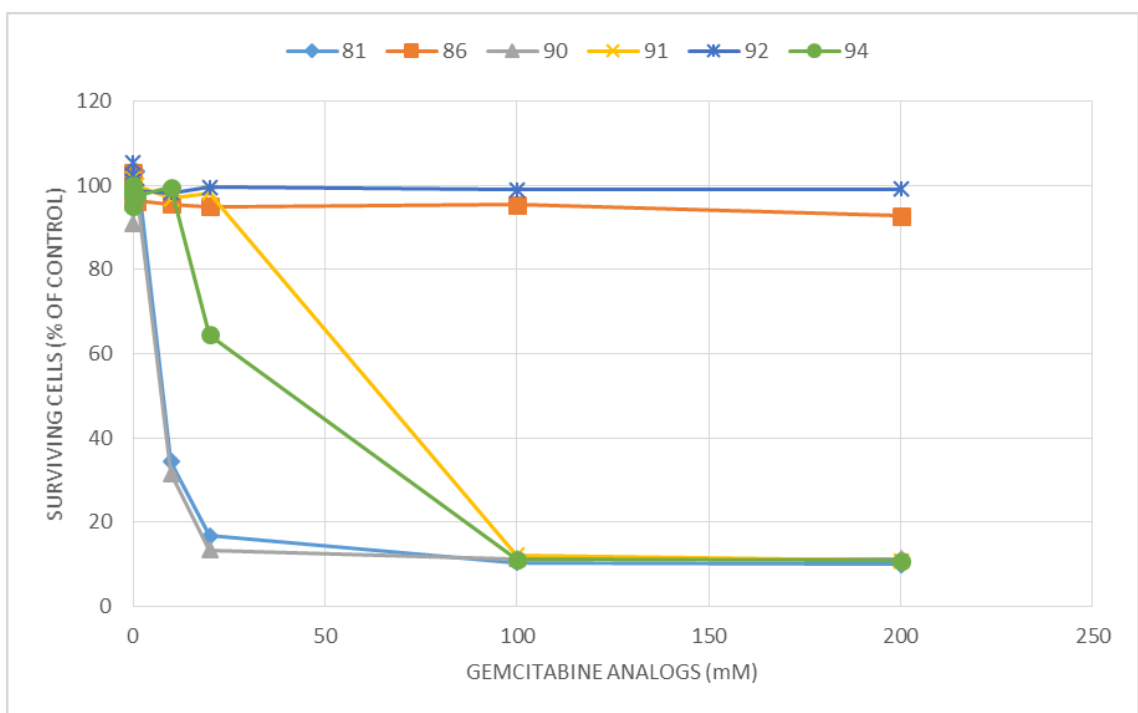


Figure 24. *In vitro* cytotoxicity curve of 4-*N*-alkanoyl and 4-*N*-alkyl gemcitabine analogues on L1210 mouse leukemic cell lines. Cells were treated with analogues for 72 h before the viability of treated cells was determined by MTT assay. Results represent the mean of triplicates with error bars indicating standard deviation.

Table 5. *In vitro* cytostatic activity of 4-*N*-modified gemcitabine analogues on L1210 cell line

Analogs	IC₅₀ (μM)	IC₇₅ (μM)
81	7.99±0.41	14.87± 2.40
86	>200	>200
90	7.47±0.41	13.33±1.14
91	65.3±0.61	88.33±1.15
92	>200	>200
94	39.96±1.95	78.33±5.51

Additionally, in collaboration with Dr. Barbieri from FIU Department of Biological Sciences, we tested cell proliferation of gemcitabine **1** as well as the 4-*N*-alkyl modified gemcitabine analogues **86** and **92**, and 4-*N*-alkanoyl **81** and **92** in HEK 293 cell line (48h). Again, all compounds were directly tested in free-base form, and were found to have different levels of inhibition in a dose dependent manner. As with the L1210 cell line, as the concentration of the nucleosides was increased (50 to 100 μM), cell proliferation decreased. Furthermore, all of the 4-*N*-modified gemcitabine analogues showed lower proliferation than the parent drug (57-21% in 50 μM versus 64% in 50 μM gemcitabine; Figure 25). This evidently shows that the addition of the lipophilic chain, either in the alkanoyl or alkyl analogues, affords a greater incorporation of the drug into cells. Also, these results might be due to HEK 293 cells having higher specific activity of CDA, than that reported for many other cells and organs, than that reported for many other cells and organs. In many tumoral tissues/cells, the CDA activity is lower than 0.1 mU/mg.^{127, 128} Additionally, CDA activity is present at higher levels in human cell lines than in rodents (L1210 cell line).^{129, 130} This increase in CDA activity might explain the relatively low gemcitabine cytotoxicity but it does not explain the higher cytotoxicity of the 4-*N*-

gemcitabine analogues, other than show their lack of potential as CDA substrates. At this moment, no further conclusion can be made about these results, and future studies in this cell line as well as other cancer cell lines is required.

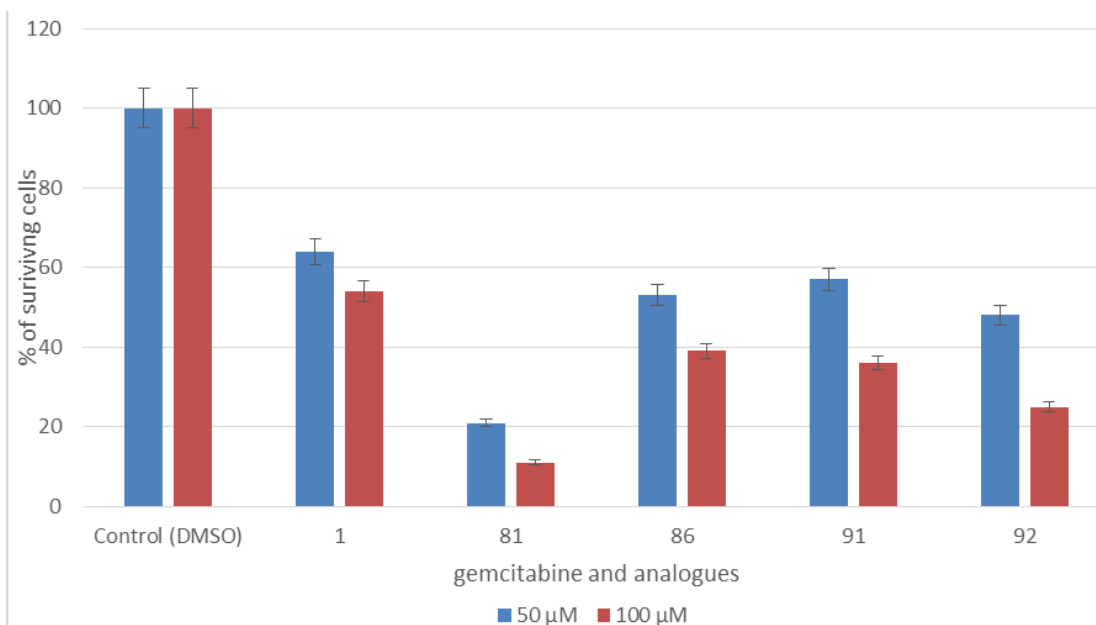


Figure 25. *In vitro* cytotoxicity graph of 4-*N*-alkanoyl (**81** & **91**) and 4-*N*-alkyl (**86** & **92**) gemcitabine analogues on HEK 293 cell lines. Cells were treated for 48 h before the viability of treated cells was determined by MTT assay. Results represent the mean of triplicates

4-*N*-Alkylgemcitabine analogues membrane permeability studies

As previously discussed, studies done by Pulido *et al.* showed 4-*N*-alkylgemcitabines **9** and **10** showed relatively weak to modest cytostatic activity in a number of cancer cell lines due to a lack of conversion to gemcitabine.²⁸ These outcome with this type of analogue was not clear, and it was assumed that 4-*N*-alkylgemcitabines either undergo a different metabolic process or a cellular uptake was poor. In collaboration with Dr. Barbieri, we studied a series of biological experiments to better understand the outcome/effect of 4-*N*-alkylgemcitabine analogues in cells.

Cell Permeability: 4-N-Alkylgemcitabine analogue 86 HPLC studies

We decided to monitor the outcome of the analogue **86** after 24 h incubation period in HEK 293 human embryonic kidney cell line. The initial goal of this experiment was to investigate if 4-*N*-alkylgemcitabine analogues enter the cells, and if so, are they being hydrolyzed to the parent molecule, leading to incorporation in DNA or were they trapped in the cell and/or nucleus. Analogue **86** was used as a model and HPLC analysis was performed to examine if the analogue is incorporated into the cell.

After 24 h incubation of HEK 293 cells with **86**, the culture medium, which contained the gemcitabine analogue and the cells adhered to the flask were separated. The cells were then lysed. With the two samples in hand, each was then extracted with an organic solvent to recover the analogue and analyzed using reversed-phased HPLC by comparing each sample to the retention time of standard **86** (25 min, Figure 26).

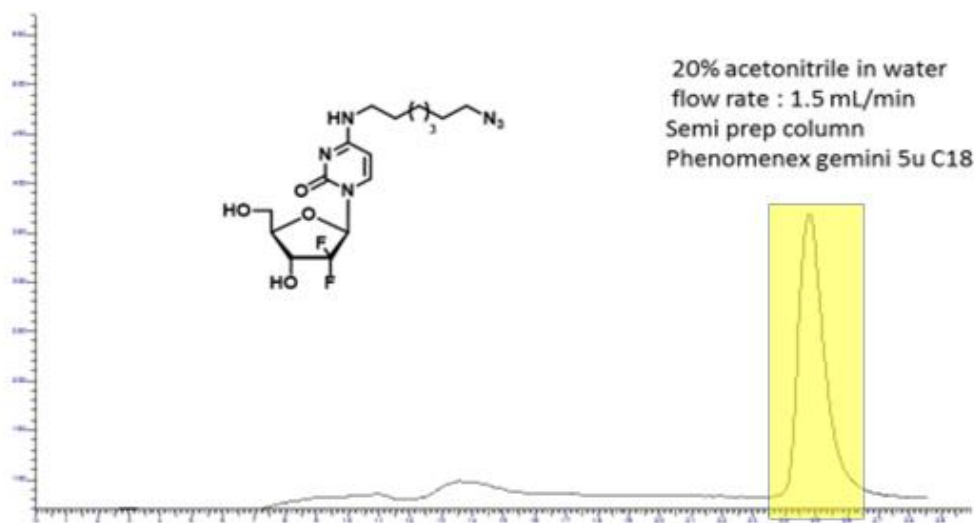


Figure 26. HPLC chromatograph of **86** in 20% CH₃CN/H₂O

HPLC analysis was done of three samples: the blank cell sample that did not contain **86**, the cell culture and cell sample of HEK 293 cells after they were incubated with **86** for

24 hours. The results clearly confirm that in both the cell culture sample, and the cell sample contained **86**. These results evidently demonstrate that **86** passes through the cell and even after 24 h of incubation, does not undergo hydrolysis (Figure 27).

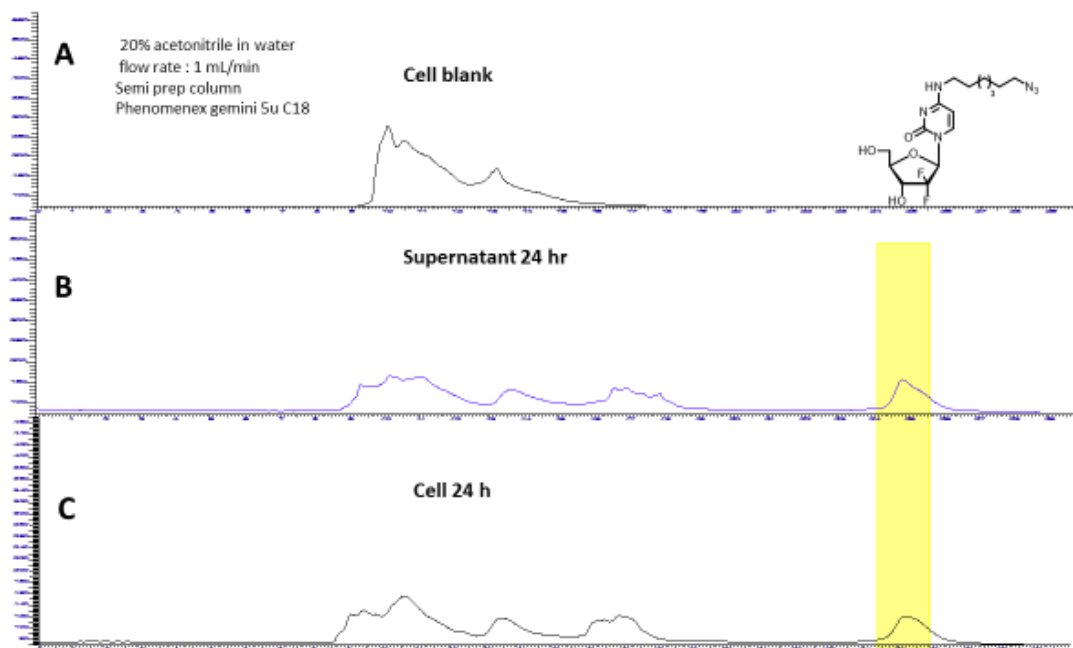


Figure 27. HPLC analysis of **86** in CH₃CN/H₂O after incubation in HEK 293 cell line (chromatogram A: cell blank, chromatogram B: supernatant after 24 h, chromatogram C: cell sample after 24 h) in 20% CH₃CN/H₂O.

Cell Permeability: Fluorescence microscopy studies with 4-N-Alkylgemcitabine analogue 86

In addition to the HPLC analysis of incorporation of **86** into the cell, we decided to use confocal fluorescence microscopy in order to visualize where in the cell **86** is incorporated. Specifically, we wanted to evaluate the ability of **86** to be metabolically incorporated into the cell by exploring its ability to be used for click chemistry.

Visualization of cells, its components and its interaction with small and large biomolecules such as proteins, peptides and nucleosides have been done through the use of highly fluorescent probes.¹³¹⁻¹³⁵ These probes or dyes, which are fluorophores, are typically

designed to react within a specific region of the sample, such as a specific functional group like amines or thiols, or in my case, an azido group for a copper catalyzed click reaction (CuAAC) with a fluorescent dye that contains a terminal alkyne.^{136, 137}

HEK 293 cells were treated with 100 μm of **86** for 24 h, fixed, and stained with Fluor 488 alkyne in the presence of copper(I) in order to perform a click reaction with the azido bearing **86**. If the click reaction occurs in the cell, we would then observe fluorescence, which would then demonstrate that **86** crosses the cell membrane but also show where in the cell **86** is incorporated and trapped (Figure 28).

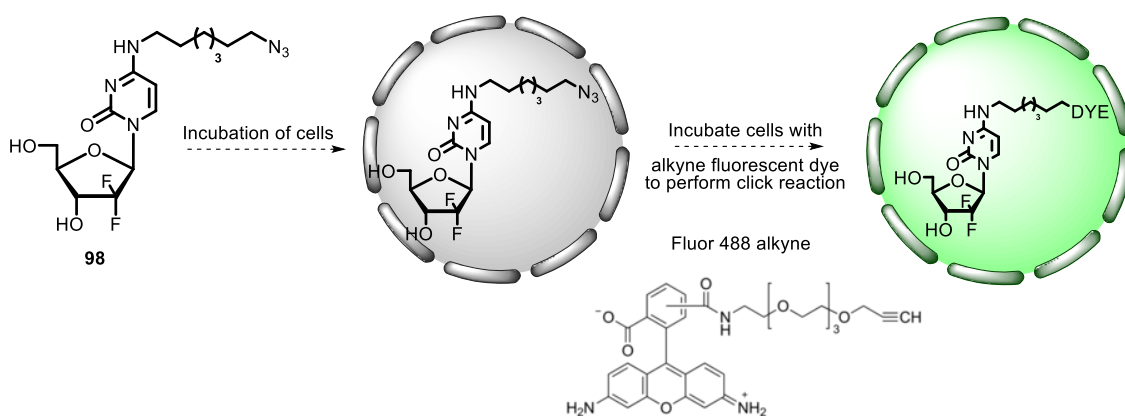


Figure 28. General outline for fluorescence labeling experiment

Incubation of HEK 293 cells with 4-*N*-alkylgemcitabine **86** followed by treatment with Fluor 488 alkyne was successful after 1 hour and exhibited strong CuAAC staining (seen in green) that colocalized with the strong nuclear noncovalent stain DAPI (seen in blue, Figure 29). This shows that **86** is incorporated into the cell but also trapped in the nucleus (seen through DAPI staining). Additionally, it appears that it does not undergo hydrolysis compared to 4-*N*-alkanoylgemcitabine analogues. In their design, it appears that 4-*N*-alkyl analogues are not substrates for dCK, as the cytotoxicity activity in L1210 cells are low,

but chemical stability is gained. In accordance with the HPLC stability studies, our imaging studies show that 4-*N*-alkyl are stable and that they are trapped inside the cell/nucleus. Based on the activity of 4-*N*-alkanoyl analogues of gemcitabine, whose lipophilicity are similar to our 4-*N*-alkyl analogues, we can expect that the 4-*N*-alkyl analogues would be up taken by variety types of cells but have a lower chance to decompose/break down as they travel through the different environments for biological testing (cell/mice/human), including PET imaging.

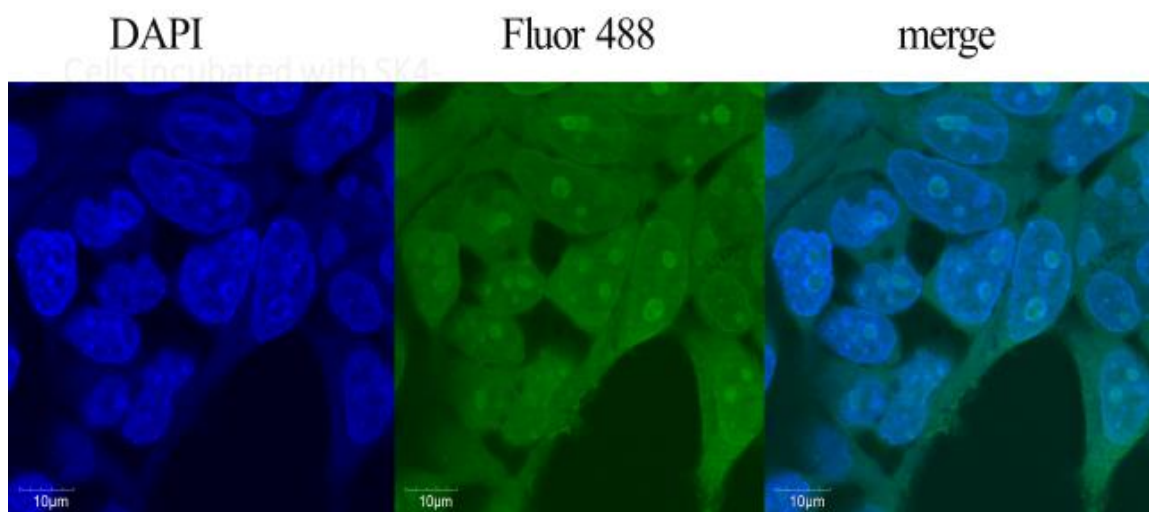


Figure 29. Labeling of **86** in HEK 293 cells for 24 h, followed by fixation and addition of Fluor 488 alkyne and copper(I).

3.1.2.6. [¹⁸F]-Labeling of 4-*N*-alkanoyl and alkyl gemcitabine radioligands

Following cold fluorination studies, radiosynthesis of [¹⁸F]-4-*N*-alkanoyl and alkylgemcitabine radioligands **94** and **96** were performed in the laboratory of Dr. Michael van Dam from the Crump Institute for Molecular Imaging using macroscale and microscale in simple microfluidic chip protocols.

Macroscale radiosyntheses of 4-*N*-alkanoyl [¹⁸F]**94** and 4-*N*-alkyl [¹⁸F]**96**

The one-pot syntheses of 4-*N*-alkanoyl [¹⁸F]**94** and 4-*N*-alkyl [¹⁸F]**96** were performed on the ELIXYS FLEX/CHEM radiosynthesizer and adapted from literature.⁹⁹ Thus, by adding silane precursor **90** in DMSO with 1% v/v AcOH to the previously dried [¹⁸F]KF/K₂₂₂ complex and reacting at 100°C for 25 min, followed by HPLC purification, 4-*N*-alkanoyl [¹⁸F]**94** in ~0.5% (n = 1) decayed-corrected crude radiochemical yield (Table 6, Figure 30). Analogously, the [¹⁸F] fluorination of precursor **92** gave 4-*N*-alkyl [¹⁸F]**96** with 6.6 ± 3.2% (n = 5) decayed-corrected isolated yield and >99% radiochemical purity. (Figure 31, see experimental section for more detailed protocol).

Scheme 26. Radiosynthesis of [¹⁸F] 4-*N*-alkanoyl and alkyl gemcitabine analogues with silicon-fluoride acceptors

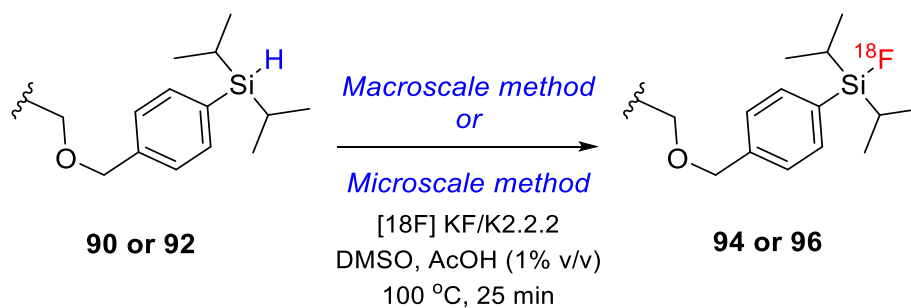


Table 6. ¹⁸F radiosynthetic yields of 4-*N*-modified gemcitabine analogues **94** and **96**

Entry	Analogue	Macroscale	Microscale
		radiosynthesis ^a	radiosynthesis ^b
		Average decay-corrected isolated RCY (%)	Decayed corrected crude RCY (%)
1	94	0.5	10
2	96	6.6 ± 3.2 (n = 5)	24.4 ± 4.1 (n = 5)

a 2-3 mg scale reactions

b 0.2 mg scale reactions

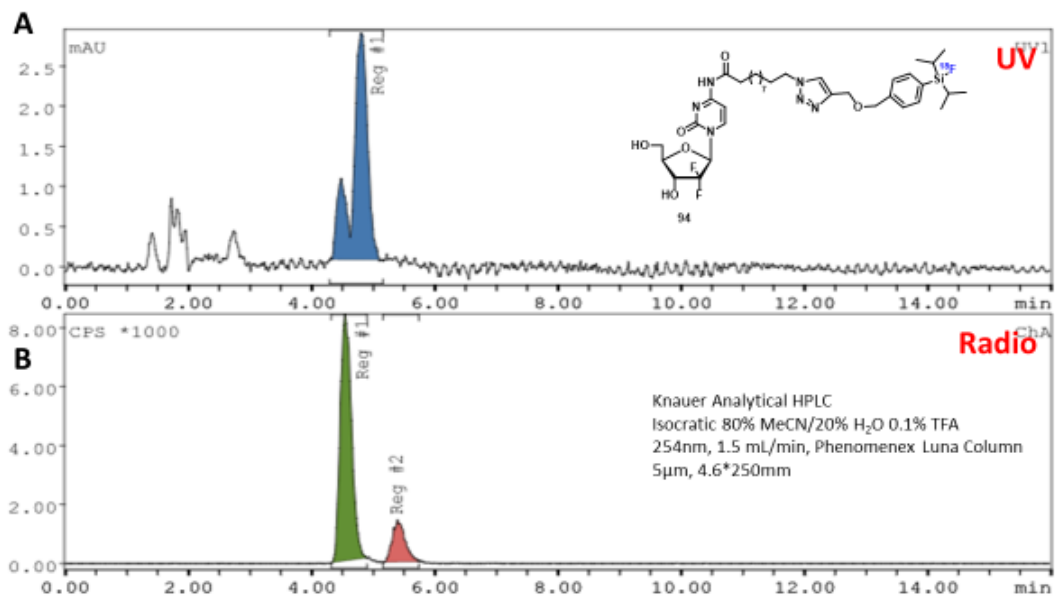


Figure 30. Macroscale radiosynthesis of 4-*N*-alkanoyl [^{18}F]**94** (chromatogram A: UV detector, chromatogram B: gamma detector, radiolabeled product in green) in 80% $\text{CH}_3\text{CN}/0.1\%$ TFA

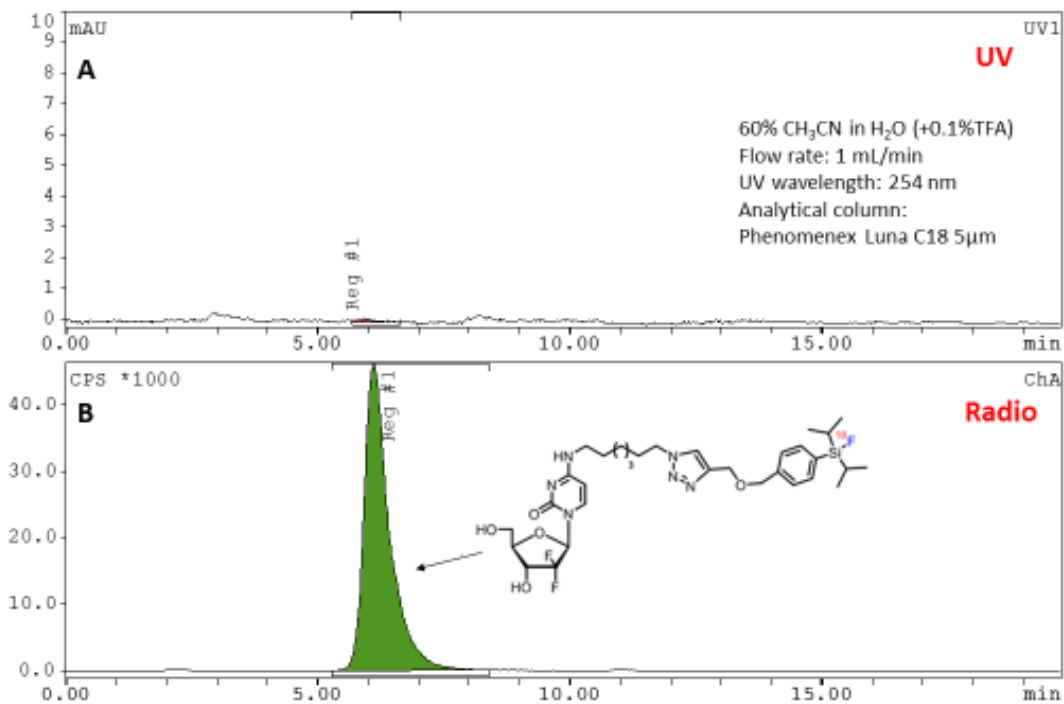


Figure 31. Macroscale radiosynthesis of 4-*N*-alkyl [^{18}F]**96** (chromatogram A: UV detector, chromatogram B: gamma detector, radiolabeled product in green) in 60% $\text{CH}_3\text{CN}/\text{H}_2\text{O}$

Microscale radiosyntheses of 4-*N*-alkanoyl [¹⁸F]94 and 4-*N*-alkyl [¹⁸F]96

The microscale synthesis of [¹⁸F]94 and 96 was performed in microdroplets on simple microfluidic chips.^{138, 139} By adding silane precursor 90 or 92 in DMSO with 1% v/v AcOH to the previously dried [¹⁸F]KF/K₂₂₂ residue on one chip, covering with a second chip, and heating at 100°C for 20 min, a decay-corrected crude radiochemical yield (without purification) for 4-*N*-alkanoyl [¹⁸F]94 was 10% (n = 1) (Figure 32) and for 4-*N*-alkyl [¹⁸F]96 was 24.4 ± 4.1% (n = 5) (Figure 33; for more detailed protocol see experimental section).

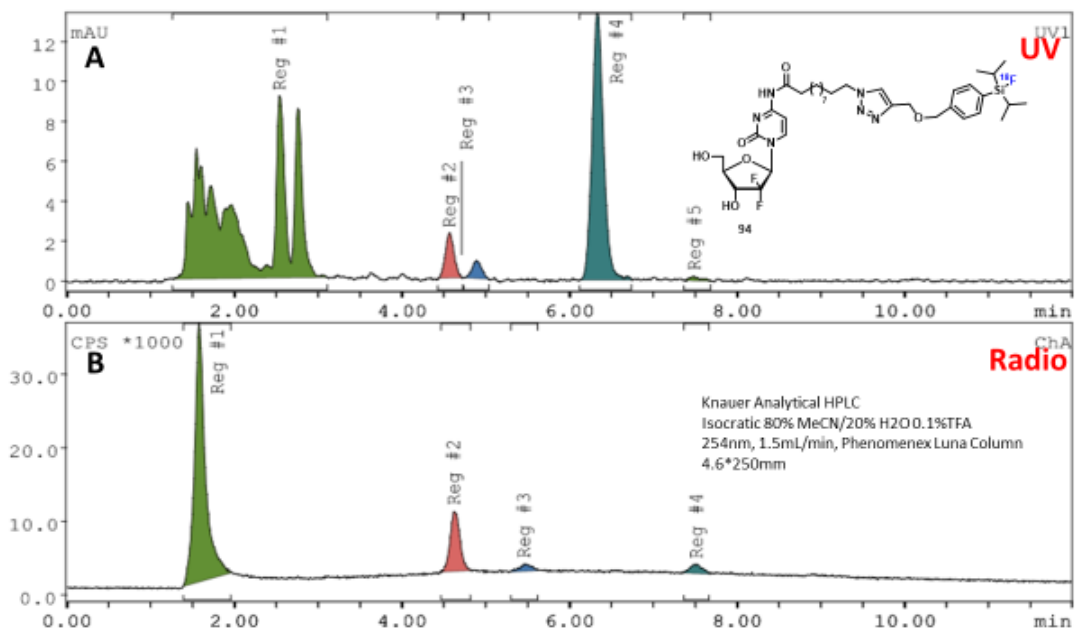


Figure 32. Microscale radiosynthesis of 4-*N*-alkanoyl [¹⁸F]94 (chromatogram A: UV detector, chromatogram B: gamma detector, radiolabeled product in red) in 80% CH₃CN/0.1% TFA

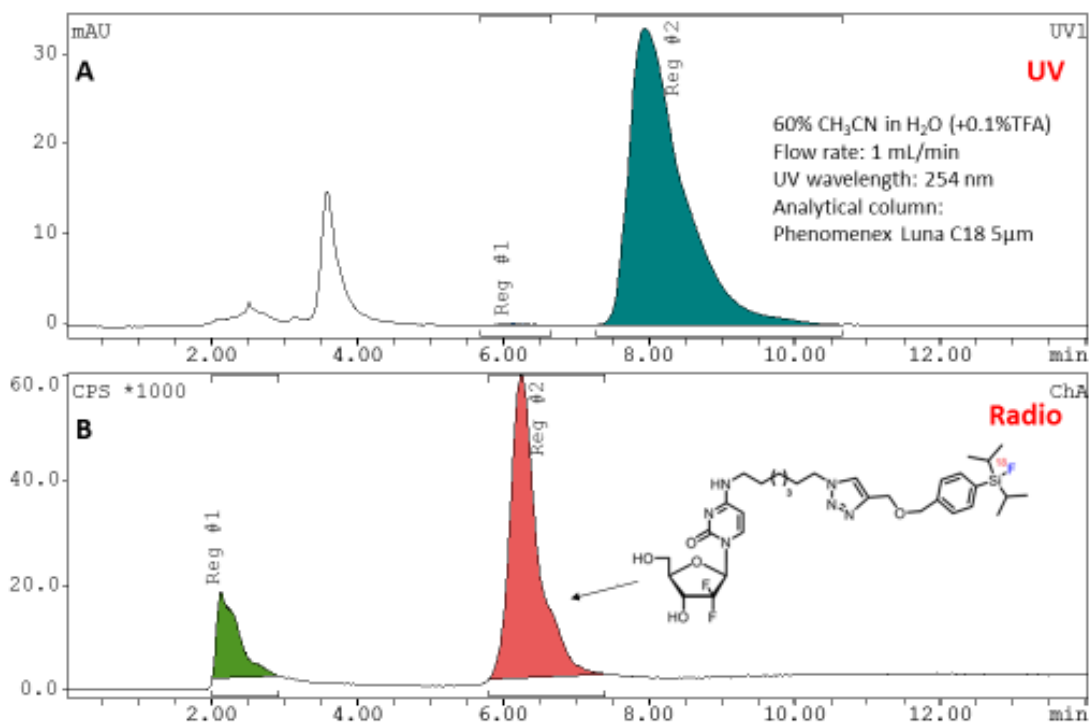


Figure 33. Microscale radiosynthesis of 4-*N*-alkyl [^{18}F]96 (chromatogram A: UV detector, chromatogram B: gamma detector) in 70% $\text{CH}_3\text{CN}/\text{H}_2\text{O}$

3.1.2.7. Biological and PET evaluation of [^{18}F]-4-*N*-alkyl gemcitabine radioligand 96

In continuing collaboration with Dr. Michael van Dam from the Crump Institute for Molecular Imaging, a series of preliminary biological evaluations were performed with [^{18}F]-4-*N*-alkyl gemcitabine radioligand **96**. These studies included formulation stability analysis, *in vivo* imaging and metabolite analysis.

Saline Formulation stability studies of [^{18}F]-4-*N*-alkyl gemcitabine radioligand 96

In order to understand the stability of radioligand **96**, the radioligand was dissolved in saline solution and passed through a sterilization filter to obtain its final formulation. The sample was then analyzed via radio-HPLC in 1 h intervals for a total of 4 h. The majority of the tracer remains intact (100% to ~90%, purity >95%) for at least 4 h ($n = 2$). More

studies need to be performed in order to have a real conclusion of the stability of radioligand **96**.

In vivo* imaging of [¹⁸F]-4-*N*-alkyl gemcitabine radioligand **96*

The distribution of [¹⁸F]**96** *in vivo* was studied using static and dynamic PET, immediately followed by computed tomography (CT) acquisition of non-tumor bearing mice (WT C57B/6). For static PET scans, a WT C57BL/6 mouse was injected with approximately 75 μCi [¹⁸F]**96** via tail vein and imaged after 1 h. For dynamic PET scans, dynamic microPET imaging was started concurrently at the beginning of a 10 sec infusion via a catheter with approximately 75 μCi of [¹⁸F]**96**. All images were corrected for CT-based photon attenuation, detector normalization and radioisotope decay (scatter correction was not applied) and converted to units of percent injected dose per gram (%ID/g).

The dynamic uptake of [¹⁸F]**96** is shown as a series of frames (0 h to 1 h; Figures 34 and 35). Figure 36 shows the time course of uptake in various organs. Note that the higher %ID/g in the latter figure, especially in the bladder may indicate a poor injection for the dynamic scan (i.e. much of the tracer did not get into the circulation). In the dynamic PET experiment, we observe the tracer first in the GI tract, gallbladder and liver but significant bone uptake is evident after 15-20 min post-injection (Figure 34, 35 and 36). One cause of bone uptake is defluorination of the PET tracer, releasing [¹⁸F]fluoride, which is strongly taken up by bone. Biodistribution from the 10 min static scan (Figure 37) also shows significant bone uptake. More detailed analysis of tracer metabolites *in vivo* is needed to determine whether defluorination is occurring or some other effect is leading to high bone uptake.

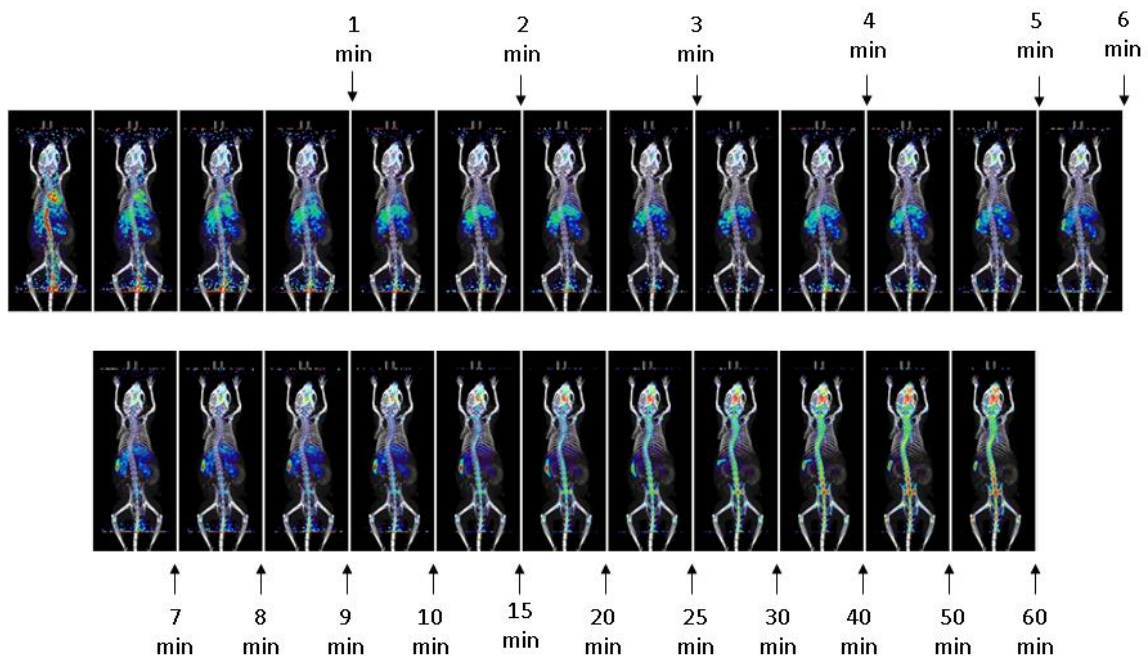


Figure 34. Series of frames from dynamic PET scan of WT C57BL/6 mouse injected with [^{18}F]96 (up to 1 h). Images are coronal maximum intensity projections.

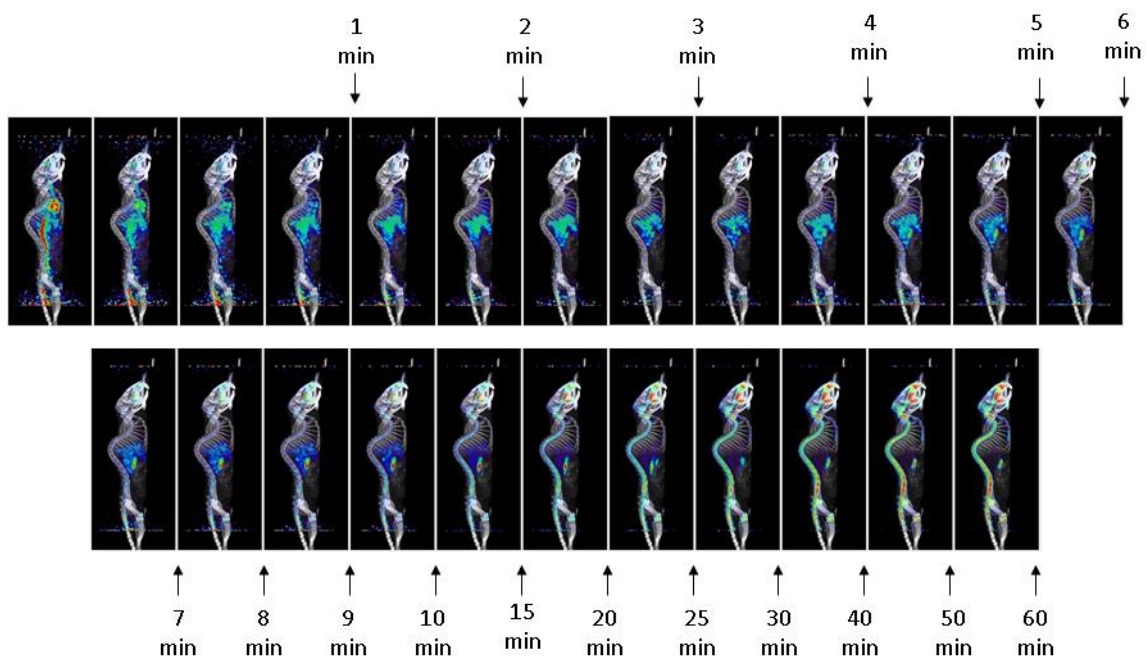


Figure 35. Series of frames from dynamic PET scan of WT C57BL/6 mouse injected with [^{18}F]96 (up to 1 h). Images are sagittal maximum intensity projections.

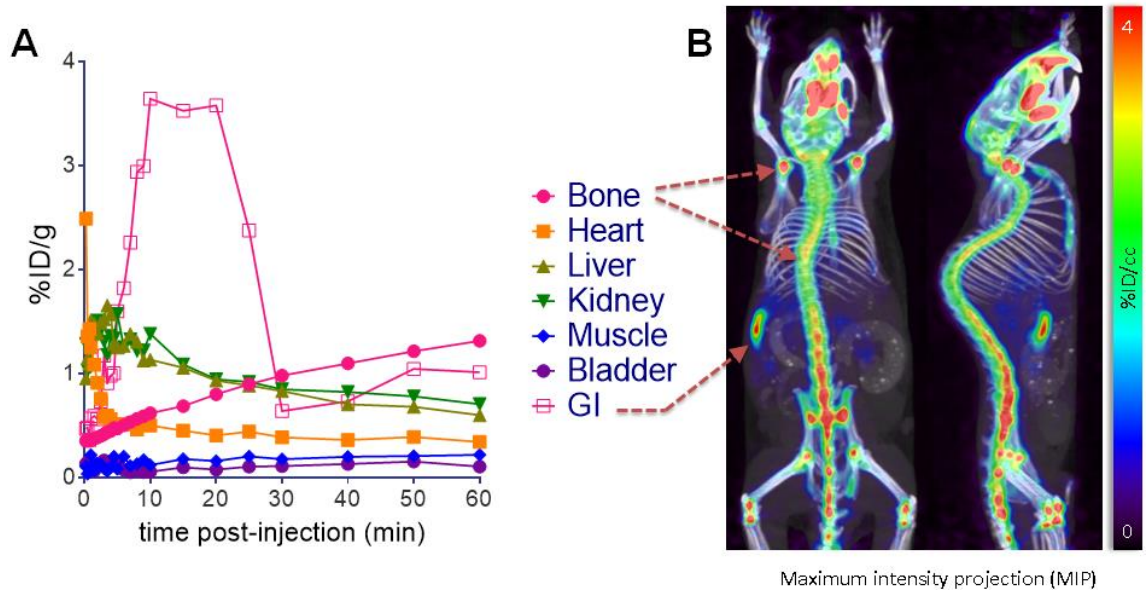


Figure 36. (Left) Dynamic biodistribution of [^{18}F]96 in WT C57BL/6 mouse. (Right) Maximum intensity projection at 1 h post-injection (left: coronal; right: sagittal).

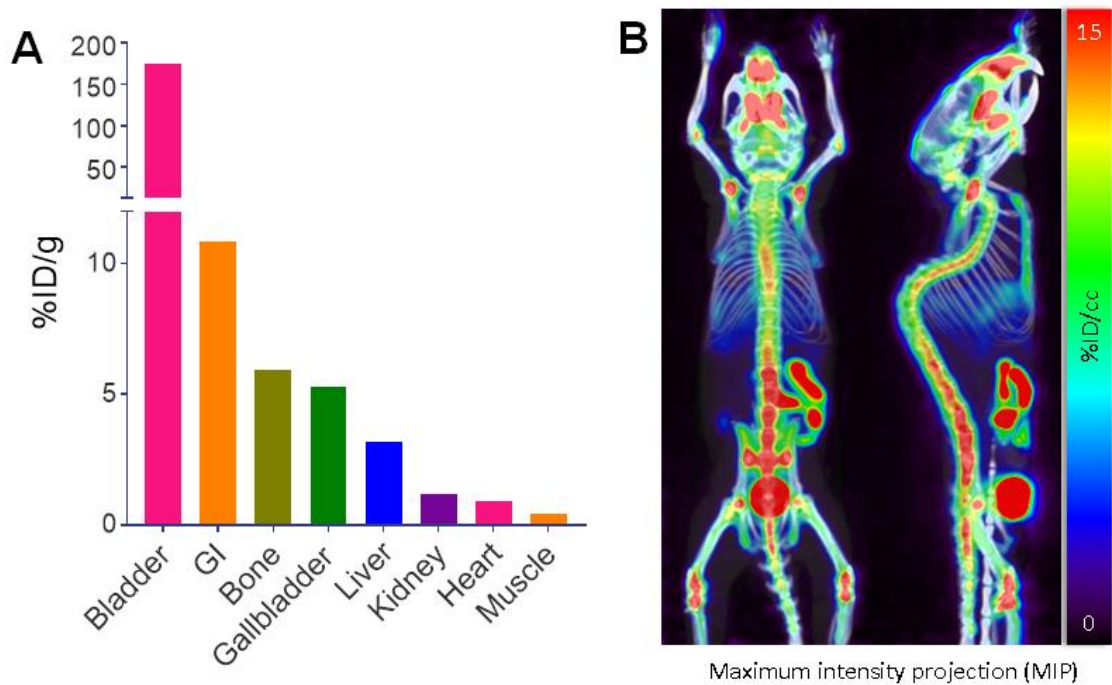


Figure 37. (Left) Biodistribution of [^{18}F]96 from 10 min static scan in WT C57BL/6 mouse at 1 h post-injection. (Right) Maximum intensity projection of 10 min static scan at 1 h post-injection (left: coronal; right: sagittal).

Metabolite analysis of [¹⁸F]-4-*N*-alkyl gemcitabine radioligand 96

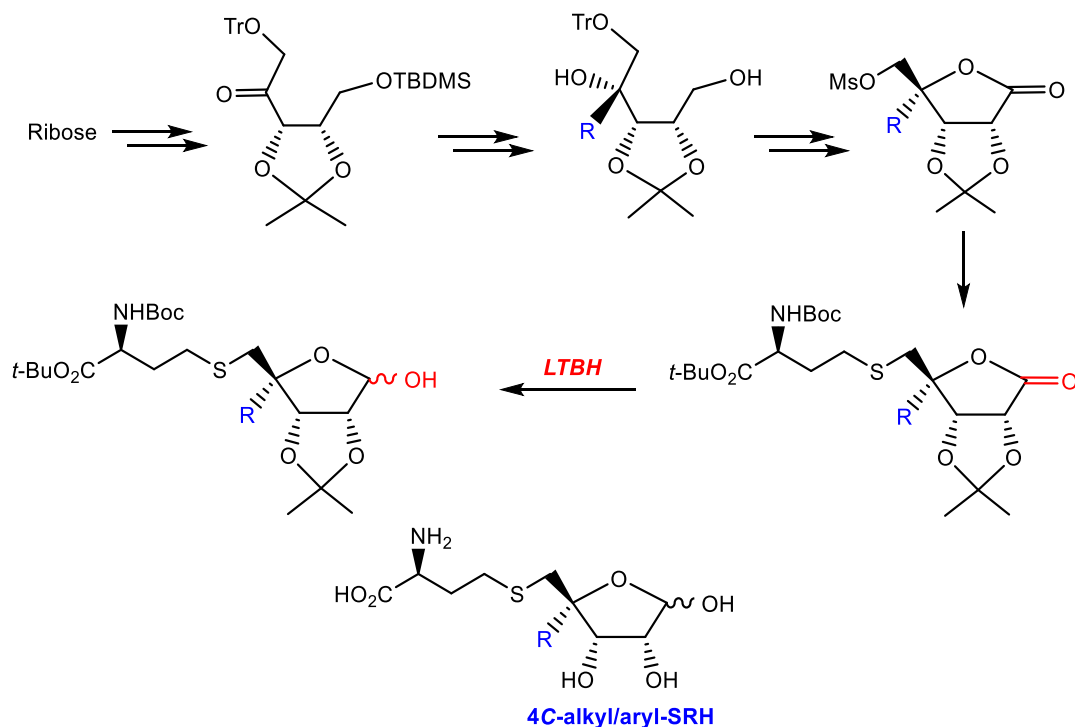
In order to study the uptake of radioligand **96** by red blood cells, *ex vivo* and *in vivo* experiments were performed with mouse blood. *Ex vivo* incubation of 0.5 mCi of [¹⁸F]**96** for 30 min at 37°C shows that 2.5% of radioactivity is in the cells, while 97.5% is found in the plasma. In the *in vivo* experiment, a mouse was injected via tail vein with 1 mCi of [¹⁸F]**96**. After 30 min, 800 μL was collected. Analysis shows 3.2% of radioactivity in the cells and 96.8% is found in the plasma. These results show that after 30 incubations, most of [¹⁸F]**96** is available to the tissues, but the samples need to be analyzed via radio-HPLC in order to check that this radioactivity is due to intact [¹⁸F]**96**.

3.2. Reduction of sugar lactones to hemiacetals using lithium triethylborohydride

3.2.1. Reduction with LTBH: Rationale

The goal of this project was to explore the use of lithium triethylborohydride (LTBH) as a reducing agent for the conversion of sugar lactones to hemiacetals without the over reduction to their diol products. As it was discussed in the introduction, there are several reducing agents that have been utilized for the transformation of lactones to hemiacetals. These reducing agents range from the common NaBH₄ and DIBAL-H, to more sophisticated methods such as catalytic reduction with generated *in situ* titanocene(III) hydride.^{121, 122} Although the application of LTBH in organic synthesis is well documented,¹⁴⁰⁻¹⁴³ including the reduction of lactams to cyclic hemiaminals (azahemiacetals), including in sugar lactams,¹¹⁰ the reduction of lactones to the lactols with LTBH is underdeveloped. In the synthesis of 4-C-alkyl/aryl-substituted *S*-ribosylhomocysteine (SRH) analogues,¹¹² which were prepared by coupling of homocysteine with 4-substituted ribonolactone derivatives, a project that I was involved

in, LTBH was used to reduce a series 4-C-alkyl/aryl-modified lactones to their corresponding hemiacetals (Scheme 27). These hemiacetals were then coupled to homocysteine to yield 4C-SRH analogues.



Scheme 27. Synthesis of 4C-SRH analogues involving reduction of ribonolactones with LTBH¹¹²

In a series of selective reduction papers from 1980, Brown reported that LTBH, when used in excess (2 equiv.), efficiently reduced esters to alcohols and lactones (γ -butyrolactone) to diols.¹⁴⁴ This protocol has been extensively used in organic synthesis, but reduction to hemiacetals has not been explored. This led to this intensive study on LTBH to better understand its use for sugar lactones.

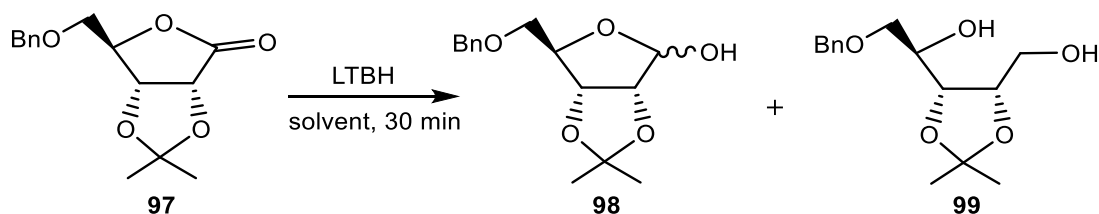
3.2.2. Reduction optimization and study of parameters

Initially, I wanted to test the reduction of lactones to hemiacetals with LTBH with a readily available sugar lactone. We chose 5-*O*-benzyl-2,3-*O*-isopropylidene-D-ribo-1,4-

lactone **97** (Scheme 28). In a previous project done by our group, reduction of protected sugar lactams was done with CH_2Cl_2 at $0\text{ }^\circ\text{C}$ in 30 min-1 h. Because of this, we decided to start with similar conditions.

Thus, treatment of **97** with 1.0 equiv. or 1.1 equiv. of LTBH ($\text{CH}_2\text{Cl}_2/0\text{ }^\circ\text{C}/30\text{ min}$) showed about 90-95% conversion to the ribofuranose **98** with ~5-10% of substrate **97** remaining unchanged ($^1\text{H NMR}$; Table 7, entries 1 and 2). However, treatment of **97** with 1.2 equiv. of LTBH gave a complete conversion to hemiacetal **98** (α/β , 1:4) after 30 min without noticeable detection of the peaks for the lactone **97** and diol **99** on the $^1\text{H NMR}$ spectra of the crude reaction mixture (entry 3). Effect of different ratios of LTBH to lactone **97** as well as temperature, reaction time and solvent are summarized in Table 7.

Briefly, increasing the ratio of LTBH to 1.5 equiv. still gives hemiacetal **98** as a single product (entry 4). However, the increase to 2.5 equiv. of LTBH led to substantial formation of diol **99** (entry 5). Yet, even when the reduction was carried out for longer time (up to 22 h) hemiacetal **98** was still isolated although in lower yields. Interestingly, temperature did not have a significant effect on the reduction of lactone **98** to hemiacetal **99** and similar results were obtained at $-78\text{ }^\circ\text{C}$, $0\text{ }^\circ\text{C}$, or r.t. (entries 4, 6 and 7). Additionally, reduction of **97** in toluene or chloroform did not affect the reduction (entries 8 and 9) but interestingly, reduction in THF gave substantially lower yield (entry 10).



Scheme 28. Reduction of the protected ribono-1,4-lactone **97** with LTBH

Table 7. Effect of various reaction parameters on reduction of **97** with LTBH^a

Entry	Solvent	LTBH (equiv.)	Temperature (°C)	Yield ^b 98 (%)	Yield ^b 99 (%)	Ratio ^b 97:98:99
1	CH ₂ Cl ₂	1.0	0	90	-	1:9:0
2	CH ₂ Cl ₂	1.1	0	95	-	1:19:0
3	CH ₂ Cl ₂	1.2	0	99 (95) ^c	-	0:1:0
4	CH ₂ Cl ₂	1.5	0	99	-	0:1:0
5	CH ₂ Cl ₂	2.5	0	40 (34) ^c	60 (55) ^c	0:4:6
6	CH ₂ Cl ₂	1.5	20	94	-	0:1:0
7	CH ₂ Cl ₂	1.5	-78	95	-	0:1:0
8	Toluene	1.5	0	93	-	0:1:0
9	CHCl ₃	1.5	0	95	-	1:19:0
10	THF	1.5	0	30	-	7:3:0

^a Reduction was performed on 0.15 mmol scale of **97** with 1 M solution of LTBH in THF.

^b Determined by ¹H NMR of the crude reaction mixture.

^c Isolated yield.

3.2.3. Reaction profile of reduction of lactone **97** to hemiacetal **98**

The reaction profile for the conversion of lactone **97** to hemiacetal **98** and diol **99**, was studied using ¹H NMR using 1.2 equiv. and 2.5 equiv. of LTBH. In both cases (1.2 and 2.5 equiv.), complete conversion of lactone **97** to lactol **98** was observed in less than 5 min, making it important to further investigate how quickly the reaction actually is and how it is affected by time.

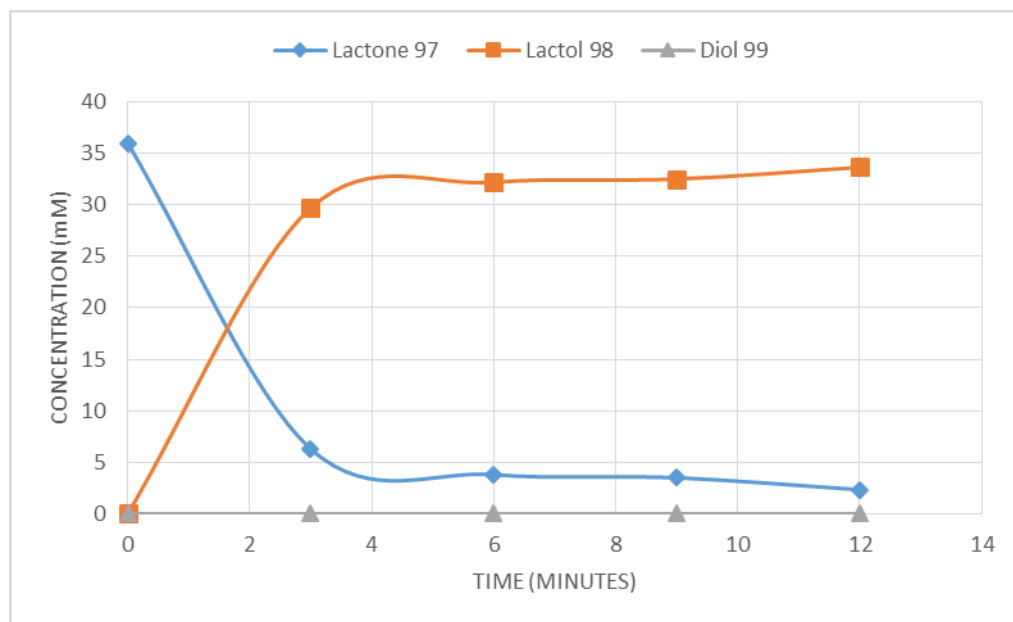


Figure 38. Reduction of lactone **97** (36 mM) with 1.2 equiv. of LTBH (0 °C/CH₂Cl₂). The profile for the reactions was measured by integrating the peaks of the ¹H NMR spectra (e.g., disappearance of the H4 peak at 4.65 ppm for **98** and appearance of the H1 peak at 5.28 ppm for **99**).

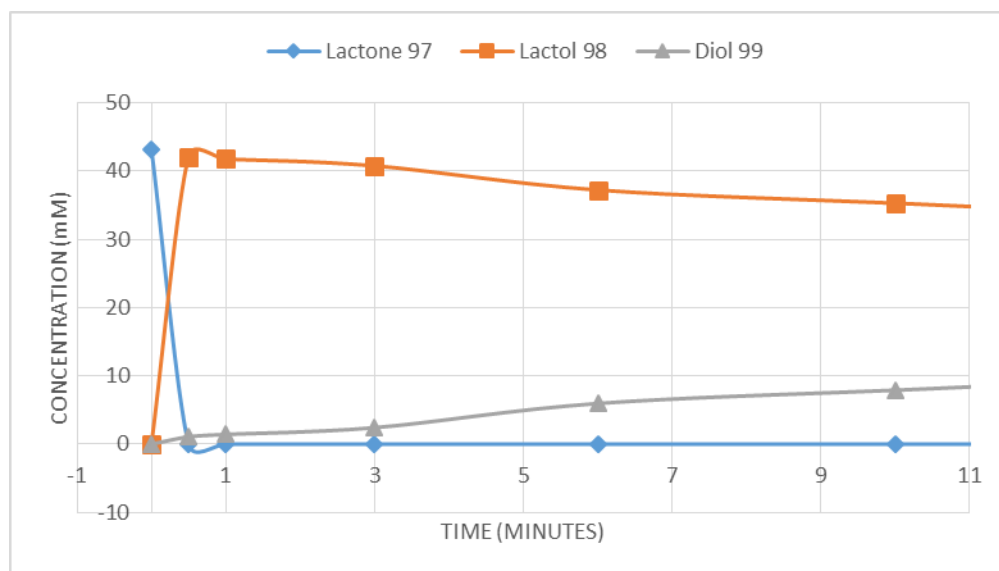


Figure 39. Reduction of lactone **97** (42 mM) with 2.5 equiv. of LTBH (0 °C/CH₂Cl₂). The profile for the reactions was measured by integrating the corresponding peaks of the ¹H NMR spectra (e.g., disappearance of the H4 peak at 4.65 ppm for **97** and appearance/disappearance of the H1 peak at 5.28 ppm for **98** and appearance of the H3 peak at 4.10 ppm for **99**).

It is important to also note that in the reaction with 1.2 equiv. of LTBH no diol **99** was ever detected. Reduction of **97** with 2.5 equiv. of LTBH was completed within 1 min showing exclusive formation of lactol **98**. Interestingly, longer reaction time showed a slow disappearance of lactol **133** with increasing formation of diol byproduct **99** [0.5 h, **98** (72%)/**99** (28%); 2 h, **98** (65%)/**99** (35%), see ¹H NMR reaction profile in experimental section 4.6.1., which was also observed in our preliminary reaction parameters. Using 1.2 equiv. of LTBH leads to no diol formation, even if left reacting for long periods of time and at room temperature, but when excess of LTBH is used, such as 2.5 equiv., diol formation requires longer time, making the conditions optimal for fast reaction time.

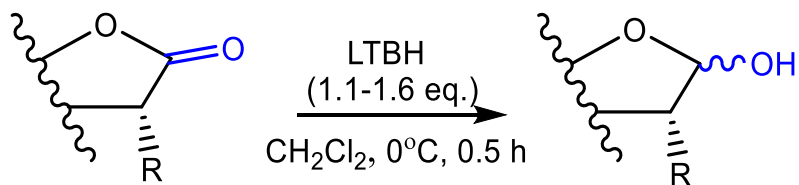
3.2.4. Reduction of several sugar lactones

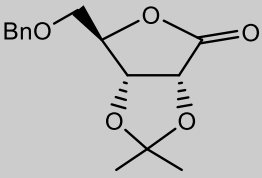
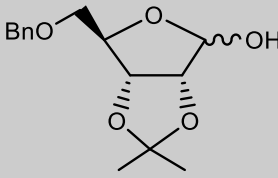
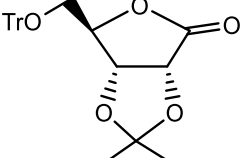
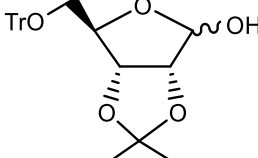
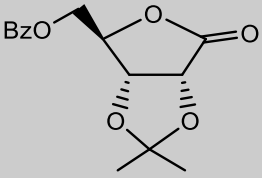
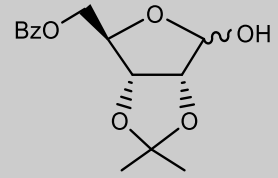
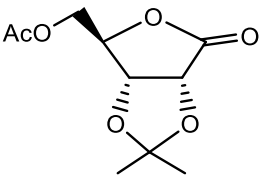
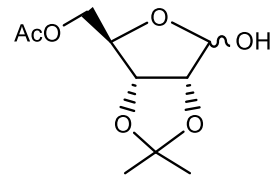
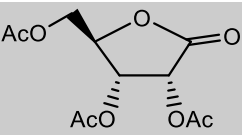
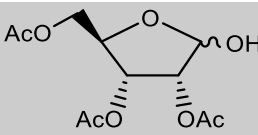
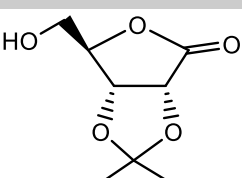
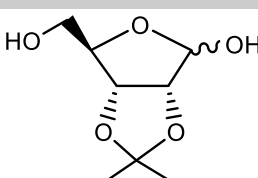
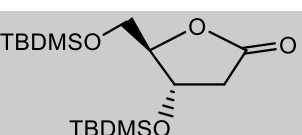
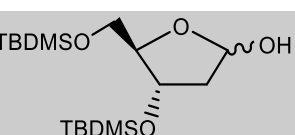
To probe the generality of the reduction of sugar lactones to the corresponding hemiacetals with LTBH, several γ - and δ -lactones were tested (Table 8). Thus, reduction of 2,3-*O*-isopropylidene-ribo-1,4-lactones with trityl (**100**), benzoyl (**102**) or acetyl (**104**) protection at 5-hydroxyl provided the corresponding lactols **101**, **103**, and **105** (entries 2-4). The trityl and benzoyl protection groups were found to be stable under these reducing conditions. Reduction of the 5'-*O*-acetyl lactone **104** yielded also substantial amount of 2,3-*O*-isopropylidene- α/β -D-ribofuranose after 30 min as a result of the reduction of the acetyl ester. However, reduction with 1.1 equiv. of LTBH and shorter reaction time (10 min) provided lactol **105** in 70% yield (entry 4). Reduction of 2,3,5-tri-*O*-acetyl lactone **106** gave hemiacetal **107** but in low yield (30%, entry 5), again, due to the reductions of the acetyl esters. Conversion of 2,3-*O*-isopropylideneribono-1,4-lactone **108** to ribose **109** required an increased amount of LTBH (1.6 equiv.; entry 6). Reduction of the 3,5-*O*-TBDMS-2-deoxy-D-ribo-1,4-lactone **110** also proceeded efficiently to give

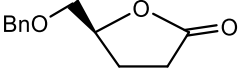
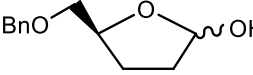
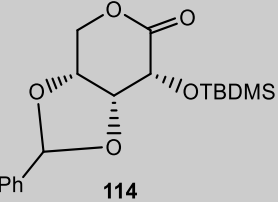
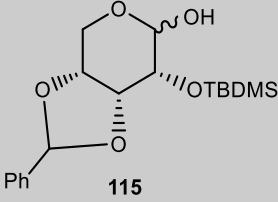
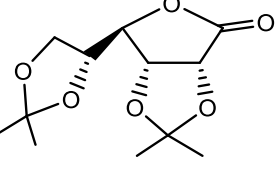
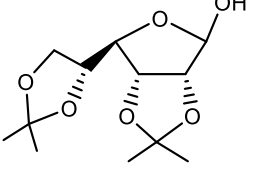
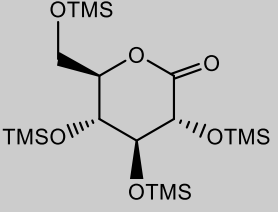
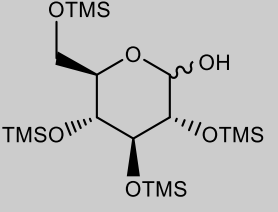
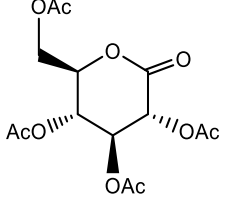
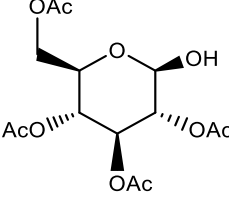
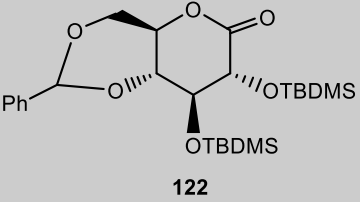
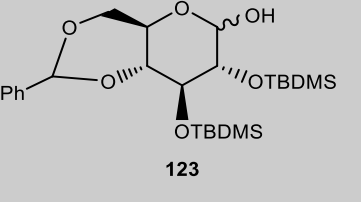
the 2-deoxyribose product **111** when 1.5 equiv. of LTBH was used (entry 7). However, reduction of 5-*O*-TBDMS-2,3-dideoxy-D-ribo-1,4-lactone **112** yielded both the 2,3-dideoxyribose **113** and the corresponding diol byproduct (entry 8). Moreover, reduction of D-ribo-1,5-lactone **114** efficiently produced the corresponding ribopyranose derivative **115** in 88% yield (entry 9).

The lactones derived from hexoses were also efficiently reduced with LTBH to the corresponding hemiacetals. Thus, reduction of 2,3:5,6-Di-*O*-isopropylidene-D-gulono-1,4-lactone **116** gave gulonofuranose **117** (91%, entry 10). Treatment of trimethylsilyl protected glucono-1,5-lactones **118** with LTBH yielded glucopyranose **119** (α/β , 2:1; entry 11). Analogous reduction of the fully acetylated D-glucono-1,5-lactone **120** provided glucose **121** in low yield due to concomitant reduction of the ester protecting group (entry 12). Attempted reduction of the fully benzoylated glucono-1,5-lactone gave similar results (entry 12). However, reduction of glucono-1,5-lactone **122** bearing benzylidene and *tert*-butyldimethylsilyl protection groups proceeded efficiently to give lactol **123** in 80% yield (entry 13). Hence, reduction of sugar lactones with LTBH to lactols appears to have a general character and is clearly compatible with acid-, base- and fluoride-labile protecting groups commonly used in carbohydrate chemistry.

Table 8. Reduction of various sugar lactones with LTBH to lactols^a



Entry	Substrate	Product	LTBH (equiv.)	Yield ^b (%)
1	 97	 98	1.2	90 ^c
2	 100	 101	1.2	89
3	 102	 103	1.2	85
4	 104	 105	1.1	70 ^d
5	 106	 107	1.1	30
6	 108	 109	1.6	90
7	 110	 111	1.5	72

8	 112	 113	1.2	37 ^e
9	 114	 115	1.2	88
10	 116	 117	1.2	91
11	 118	 119	1.2	84
12	 120	 121	1.1	20 ^f
13	 122	 123	1.2	80

^a Reduction was performed on 0.1-1.0 mmol scale of lactones with 1 M solution of LTBH/THF.

^b Isolated yield as a mixture of α/β anomers.

^c Reduction on 1.0 mmol scale.

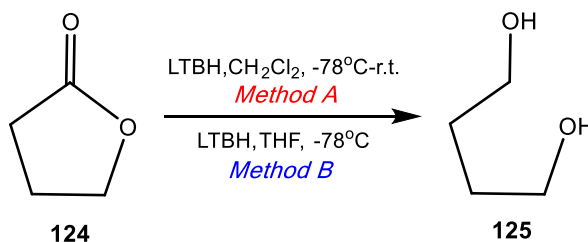
^d With 1.2 equiv. of LTBH the 2,3-*O*-isopropylidene- α/β -D-ribofuranose was isolated in 37% yield.

^e (*R*)-5-(benzyloxy)pentane-1,4-diol (42%) and the residual amount of unchanged **112** (~5%) was also isolated.

^f Analogous reduction of 2,3,4,6-tetra-*O*-benzoylglucono-1,5-lactone¹⁴⁵ yielded 2,3,4,6-tetra-*O*-benzoylglucopyranose (~15-20%; TLC, ¹H NMR).

Reduction of some sugar lactones was also performed with NaBH₄ and DIBAL-H in order to compare our LTBH protocol with these commonly used reducing agents. Thus, reduction of **100** or **110** with NaBH₄ (1.1 equiv.) in EtOH (0 °C) after 30 min showed only a small conversion to the lactol products **101** and **111** (~5-10%) with the unchanged lactones (~80%) and the corresponding diols (~5-10%) present (TLC, ¹H NMR). Increasing the amount of NaBH₄ (5 equiv.) resulted in the formation of the corresponding diols as the major product (~70%). Reduction of **110** with DIBAL-H in CH₂Cl₂ (-78 °C, 30 min.) yielded lactol **111** (90%). However, analogous treatment of 5-*O*-acetyl lactone **104** with DIBAL-H yielded mixture (~2:3) of desired lactol **105** and the lactol **109** as a result of the concomitant reduction of the acetyl ester.

Reduction of γ -butyrolactone **124** with LTBH (1.8 equiv./CH₂Cl₂/0 °C; Method A, Scheme 29] gave 1,4-butanediol **125** as the sole product. Various modifications of the reduction protocol [LTBH (0.5-1.2 equiv.)/CH₂Cl₂/-78 °C or 0 °C or r.t./30 min to 2 h] produced diol **125** in addition to different quantities of the unchanged lactone **124**, but the corresponding lactol was not observed. This is in agreement with the results reported by Brown that reduction of **124** with LTBH (2.0 equiv.; THF/-78 °C; Method B) gave **125** in 94%.¹⁴⁴



Scheme 29. Reduction of γ -butyrolactone with LTBH to 1,4-butanediol

Typically, the reduction of the tested sugar lactones with LTBH in CH₂Cl₂ is higher yielding when the lactone had a larger number of hydroxyl groups (e.g., ribonolactone > 2-deoxyribonolactone >> 2,3-dideoxyribonolactone). The fact that reduction of 2,3-dideoxyribonolactone with LTBH can be controlled to give the lactol product, while under similar conditions γ -butyrolactone is converted to the diol provides support for the assumption that chelation of the borane reagent to the exocyclic sugar hydroxyl group (oxygen) is critical in this reduction process (Figure 40). Buchwald invoked coordination of the titanium center to the lactone's oxygen atoms during reduction of lactones to lactols with titanocene(III) hydrides.¹²¹ The fact that reduction with LTBH gave much better yields in CH₂Cl₂ than in THF (Table 7) may be attributed to the additional coordination of LTBH reagent to the more polar THF solvent which can result in weakening of the LTBH chelation to the lactone oxygens. Our studies also showed that lactones containing an ester protection group (acetyl or benzoyl) can be chemoselectively reduced to the lactols under certain reduction conditions with LTBH/CH₂Cl₂ combination while the ester moiety remains intact.

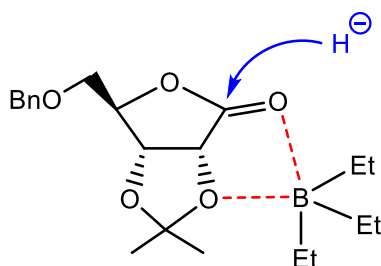


Figure 40. Proposed chelating of borane with exocyclic sugar oxygens

4. EXPERIMENTAL

4.1. General Procedures

The ^1H (400 MHz), ^{13}C (100 MHz), or ^{19}F (376 MHz) NMR spectra were recorded at ambient temperature in solutions of CDCl_3 or MeOH-d_4 , as noted. The reactions were followed by TLC with Merck Kieselgel 60-F254 sheets, and products were detected with a 254 nm light or with Hanessian's stain. Column chromatography was performed using Merck Kieselgel 60 (230–400 mesh). Reagent-grade chemicals were used and solvents were dried by reflux distillation over CaH_2 under nitrogen gas unless otherwise specified. The carboxylic acid and amine derivatives used for the coupling with gemcitabine were either commercially available or prepared as described. 4-(di-*iso*-propylsilyl)benzylalcohol was commercially available from Sigma Aldrich. Reactions were carried out under a N_2 atmosphere. Phenomenex Gemini RP-C18 with an isocratic mobile phase (various % $\text{CH}_3\text{CN}/\text{H}_2\text{O}$) was used for some HPLC purification.

4.2. Synthesis of 4-*N*-Alkyl β -keto sulfonate gemcitabine analogues

***tert*-Butyl *N*-(10-undecenyl) carbamate (57).** di-*tert*-Butyl-dicarbonate (2.20 g, 10.04 mmol) was added to a solution of **56** (1.00 g, 5.91 mmol) in MeOH (20 mL) and stirred at ambient temperature. After 18 h, the volatiles were evaporated under reduced pressure and the resulting residue was then column chromatographed (30% EtOAc/hexane) to give **57**¹⁴⁶ (1.45 g, 92%) as a white solid. ^1H NMR (CDCl_3) δ 1.27 (s, 11H, $\text{C}(\text{CH}_3)_3 + \text{CH}_2$), 1.33-1.38 (m, 10H, $5 \times \text{CH}_2$), 1.56-1.59 (m, 2H, CH_2), 2.03 (dd, $J = 6.8, 14.4$ Hz, 2H, CH_2), 3.10 (t, $J = 7.1$ Hz, 2H, CH_2), 4.48 (br, 1H, NH), 4.96 (m, 2H, CH_2), 5.81 (m, 1H, CH).

***tert*-Butyl *N*-(10,11-Dihydroxyundecan-1-yl) carbamate (58).** 5% mol of OsO_4 (50 μL , cat. amount) and *N*-methylmorpholine-*N*-oxide (87.8 mg, 0.75 mmol) was added to a

solution of **57** (130 mg, 0.50 mmol) in acetone (2 mL) and water (0.2 mL), and the mixture was stirred at 0 °C to ambient temperature under Nitrogen. After 4 h, the reaction mixture was diluted with CH₂Cl₂ (20 mL) and partitioned with H₂O. The organic layer was washed with saturated NaHCO₃/H₂O (15 mL), and brine (15 mL), dried over Na₂SO₄, and evaporated, and the resulting residue was column chromatographed (70% EtOAc/hexane) to give **58** (140 mg, 92 %). ¹H NMR (CDCl₃) δ 1.27 (s, 11H, C(CH₃)₃ + CH₂), 1.35-1.37 (m, 14H, 7 × CH₂), 3.07 (t, *J* = 7.1 Hz, 2H, CH₂), 3.41 (dd, *J* = 7.7, 11.0 Hz, 1H, CH), 3.63 (dd, *J* = 3.0, 11.0 Hz, 1H, CH), 3.67-3.70 (m, 1H, CH).

***tert*-Butyl *N*-(10,11-Dihydroxy-11-*O*-Benzyl-undecane) carbamate (**59**).** Benzyl bromide (47 μL, 67.7 mg, 0.40 mmol) and Ag₂O (115 mg, 0.50 mmol) was added to a solution of **58** (100 mg, 0.33 mmol) in CH₂Cl₂ (4 mL). The mixture was stirred at ambient temperature under Nitrogen. After 18 h, the reaction mixture was diluted with CH₂Cl₂ (20 mL) and washed with saturated NaHCO₃/H₂O (20 mL), and brine (15 mL), dried over Na₂SO₄, and evaporated, and the resulting residue was column chromatographed (30% EtOAc/hexane) to give **59** (66 mg, 51 %). ¹H NMR (CDCl₃) δ 1.26 (s, 11H, C(CH₃)₃ + CH₂), 1.43-1.45 (m, 14H, 7 × CH₂), 3.07-3.10 (m, 2H, CH₂), 3.32 (dd, *J* = 8.0, 9.4 Hz, 1H, CH), 3.50 (dd, *J* = 3.0, 9.4 Hz, 1H, CH), 3.78-3.82 (m, 1H, CH), 4.51 (s, 2H, CH₂), 7.26-7.43 (m, 5H, Ar).

***tert*-Butyl *N*-(11-*O*-Benzyl-10-oxoundecanyl) carbamate (**60**).** A freshly prepared solution of Collins reagent [CrO₃ (100 mg, 1.00 mmol), pyridine (81 μL, 100 mg, 1.00 mmol), and Ac₂O (190 μL, 204 mg, 2.00 mmol) in CH₂Cl₂ (2 mL)] was added to a stirred solution of **59** (100 mg, 0.25 mmol) in CH₂Cl₂ (8 mL) at ambient temperature. The resulting mixture was stirred for 1 h. and was immediately column chromatographed (EtOAc) to

give **60** (84.5 mg, 86 %). $^1\text{H NMR}$ (CDCl_3) δ 1.26 (s, 11H, $\text{C}(\text{CH}_3)_3 + \text{CH}_2$), 1.44 (m, 10H, $5 \times \text{CH}_2$), 1.56-1.59 (m, 2H, CH_2), 2.44 (t, $J = 7.5$ Hz, 2H, CH_2), 3.09 (m, 2H, CH_2), 4.06 (s, 2H, CH_2), 4.59 (s, 2H, CH_2), 7.28-7.42 (m, 5H, Ar).

***tert*-Butyl *N*-(10,11-Dihydroxy-11-*O*-methanesulfonylundecanyl) carbamate (64).** Mesyl chloride (29.8 mg, 20 μL , 0.26 mmol) was added to a solution of **58** (80 mg, 0.26 mmol) in anhydrous CH_2Cl_2 (2 mL) in the presence of Et_3N (39.5 mg, 54 μL , 0.39 mmol). The mixture was stirred at -20 $^\circ\text{C}$. After 20 minutes, the reaction mixture was diluted with CH_2Cl_2 and partitioned with HCl (0.1 M, 15 mL) and H_2O (15 mL). The organic layer was washed with saturated $\text{NaHCO}_3/\text{H}_2\text{O}$ (15 mL), and brine (15 mL), dried over Na_2SO_4 , and evaporated, and the resulting residue was column chromatographed (40% EtOAc/hexane) to give **64** (54 mg, 55 %). $^1\text{H NMR}$ (CDCl_3) δ 1.28 (s, 11H, $\text{C}(\text{CH}_3)_3 + \text{CH}_2$), 1.44 (m, 14H, $7 \times \text{CH}_2$), 3.08 (s, 3H, Ms), 3.09 (m, 2H, CH_2), 3.70 (m, 1H, CH), 4.10 (dd, $J = 7.2, 10.6$ Hz, 1H, CH), 4.25 (dd, $J = 2.9, 10.5$ Hz, 1H, CH).

***tert*-Butyl *N*-(11-*O*-Mesyl-10-oxoundecanyl) carbamate (65).** A freshly prepared solution of Collins reagent [CrO_3 (52 mg, 0.52 mmol), pyridine (8 μL , 52 mg, 0.52 mmol), and Ac_2O (102 μL , 107 mg, 1.04 mmol) in CH_2Cl_2 (2 mL)] was added to a stirred solution of **64** (50 mg, 0.13 mmol) in CH_2Cl_2 (8 mL) at ambient temperature. The resulting mixture was stirred for 1 h. and was immediately column chromatographed (45 % EtOAc/hexane) to give **65** (45 mg, 92 %). $^1\text{H NMR}$ (CDCl_3) δ 1.28 (s, 11H, $\text{C}(\text{CH}_3)_3 + \text{CH}_2$), 1.44 (m, 10H, $5 \times \text{CH}_2$), 1.58 (m, 2H, CH_2), 2.45 (t, $J = 7.4$ Hz, 2H, CH_2), 3.10 (m, 2H, CH_2), 3.20 (s, 3H, Ms), 4.49 (s, 2H, CH_2).

***tert*-Butyl *N*-(11-Fluoro-10-oxoundecanyl) carbamate (66).** To a solution of KF (6.4 mg, 0.11 mmol), K_2CO_3 (15.2 mg, 0.11 mmol), Kryptofix 2.2.2 (41 mg, 0.11 mmol) in

CH₃CN (2 mL), **65** (10.0 mg, 0.026 mmol) was added and stirred at 80 °C. After 25 min, the reaction mixture was quickly cooled in a water bath and filtered. The crude product was evaporated, and the resulting residue was column chromatographed (35% EtOAc/hexane) to give **66** (4.1 mg, 50 %). ¹H NMR (CDCl₃) δ 1.28 (s, 11H, C(CH₃)₃ + CH₂), 1.44 (m, 10H, 5 × CH₂), 1.58 (m, 2H, CH₂), 2.44 (t, *J* = 7.5 Hz, 2H, CH₂), 3.10 (m, 2H, CH₂), 4.75 (d, *J* = 47.7 Hz, 2H, CH₂F). ¹⁹F NMR δ -227.41 (t, *J* = 47.7, 1F).

4-*N*-(*p*-Toluenesulfonyl)-2'-deoxy-2',2'-difluorocytidine (62). TMSCl (2.5 mL) was added to a suspension of Gemcitabine **1** (300 mg, 1.0 mmol) in anhydrous pyridine (5 mL), and the mixture was stirred at ambient temperature under Nitrogen. After 2 h, TsCl (1.80 g, 10.01 mmol) was added, and the reaction mixture was heated to 60°C and kept stirring. After 24 h, volatiles were evaporated, and the resulting residue was treated with MeOH/NH₃ (5 mL) and stirred at ambient temperature for 8 h. The volatiles were then evaporated under reduced pressure, and the resulting residue was column chromatographed (90% EtOAc/Hexane) to give **62**²⁸ (378.7 mg, 90%) as a white-yellow solid. ¹H NMR (CD₃OD) δ 2.42 (s, 3H,CH₃), 3.78 (dd, *J* = 3.4, 12.8 Hz, 1H, H5'), 3.90–3.95 (m, 2H, H4,H5''),4.28 (dt, *J* = 8.4, 12.0 Hz, 1H, H3'), 6.13 (dd, *J* = 5.3, 9.5 Hz,1H, H1'), 6.65 (d, *J* = 8.2 Hz, 1H, H5), 7.36 (d, *J* = 8.0 Hz, 2H, Ar), 7.79 (d, *J* = 8.3 Hz, 2H, Ar), 7.99 (d, *J* = 8.1 Hz, 1H, H6). ¹³C NMR δ 21.43, 60.34 (C5'), 70.21 (dd, *J* = 18.8, 27.2 Hz, C3'), 82.99 (d, *J* = 8.4, C4'), 85.46 (dd, *J* = 23.9, 41.3 Hz, C1'), 98.46 (C5), 123.84 (t, *J* = 258.7 Hz, C2'), 127.58 (Ar), 130.52 (Ar), 140.71 (Ar), 142.62 (C6), 144.66 (Ar), 150.21 (C2), 160.54 (C4). ¹⁹F NMR δ -120.17 (br s, 1F), -119.41 (dd, *J* = 4.1, 12.7 Hz, 1F).

4-*N*-(Uundec-10-en-1-yl)-2'-deoxy-2',2'-difluorocytidine (67). 10-undecene amine (0.49 mL, 2.16 mmol) was added to a suspension of **62** (300 mg, 0.72 mmol) in 1,4-dioxane

(4.1 mL) and Et₃N (0.302 mL, 219 mg, 2.16 mmol) and the mixture was left stirring at 65°C. After 24 h, volatiles were evaporated and the resulting residue was column chromatographed (5% MeOH/CHCl₃) to give **67**²⁸ (254 mg, 85 %). ¹H NMR (CD₃OD) δ 1.30–1.43 (m, 12H, 6 × CH₂), 1.56–1.65 (m, 2H, CH₂), 2.03–2.09 (m, 2H, CH₂), 3.39 (t, *J* = 7.1 Hz, 2H, CH₂), 3.80 (dd, *J* = 3.3, 12.6 Hz, 1H, H5'), 3.89 (td, *J* = 2.8, 8.3 Hz, 1H, H4'), 3.95 (d, *J* = 12.6 Hz, 1H, H5''), 4.26 (dt, *J* = 8.3, 12.1 Hz, 1H, H3'), 4.91–5.02 (m, 2H, CH₂), 5.82 (tdd, *J* = 6.7, 10.3, 17.0 Hz, 1H, CH), 5.87 (d, *J* = 7.6 Hz, 1H, H5), 6.23 (t, *J* = 8.0 Hz, 1H, H1'), 7.74 (d, *J* = 7.6 Hz, 1H, H6). ¹³C NMR δ 28.01, 29.98, 30.12, 30.19, 30.42, 30.51, 30.63, 34.88, 41.75, 60.56 (C5'), 70.67 (dd, *J* = 22.4, 23.8 Hz, C3'), 82.26 (dd, *J* = 3.6, 5.0 Hz, C4'), 85.94 (dd, *J* = 26.0, 38.0 Hz, C1'), 97.33 (C5), 114.68, 124.05 (t, *J* = 258.4 Hz, C2'), 140.16, 140.77 (C6), 158.30 (C2), 165.37 (C4). ¹⁹F NMR δ –119.89 (br d, *J* = 240.1 Hz, 1F), –118.80 (br d, *J* = 240.1 Hz, 1F).

4-*N*-(Uundec-10-en-1-yl)-3',5'-di-*O*-benzoyl-2'-deoxy-2',2'-difluorocytidine (68). BzCl (140 μL, 1.2 mmol) was added to a solution of **67** (200 mg, 0.48 mmol), 2,6-lutidine (223 μL, 1.92 mmol), and 4-dimethylaminopyridine (117.3 mg, 0.96 mmol) in CH₂Cl₂ (10 mL), and the mixture was stirred at 35 °C under Nitrogen. After 6 h, the reaction mixture was diluted with CH₂Cl₂ (40 mL) and partitioned with H₂O, and the aqueous layer was extracted with CH₂Cl₂ (2 × 15 mL). The combined organic layers were sequentially washed with 1 M HCl (15 mL), saturated NaHCO₃/H₂O (15 mL), and brine (15 mL), dried over Na₂SO₄, and evaporated, and the resulting residue (240 mg) was column chromatographed (2% MeOH/CHCl₃) to give **68** (230 mg, 78 %) as a mixture of isomers. The major isomer had the following peaks: ¹H NMR (CDCl₃) δ 1.16–1.41 (m, 12H, 6 × CH₂), 1.49–1.63 (m, 2H, CH₂), 1.93–2.05 (m, 2H, CH₂), 3.37 (t, *J* = 7.1 Hz, 2H, CH₂), 4.48–4.58 (m, 1H, H4'),

4.62-4.82 (m, 2H, H5', H5''), 4.87-5.01 (m, 2H, CH₂), 5.53-5.66 (m, 1H, H3'), 5.76-5.84 (tdd, $J = 6.7, 10.3, 17$ Hz, 1H, CH), 5.73 (d, $J = 7.6$ Hz, 1H, H5), 6.57-6.60 (m, 1H, H1'), 7.29 (dd, $J = 0.6, 7.3$, 1H, H6), 7.37-7.49 (m, 4H, Ar), 7.51-7.66 (m, 2H, Ar), 7.89-8.10 (m, 4H, Ar). ¹³C NMR δ 26.67, 28.65, 28.87, 29.02, 29.28, 29.34, 29.69, 33.78, 43.97, 62.55 (C5'), 71.35 (dd, $J = 17.1, 35.2$ Hz, C3'), 79.57 (C4'), 83.54 (br s, C1'), 91.04 (C5), 114.17, 120.93 (t, $J = 263.1$ Hz, C2'), 126.78, 128.48, 128.73, 128.83, 129.36, 129.63, 129.72, 130.17, 133.58, 134.50, 139.16 (C6), 157.82 (C2), 165.99 (C4), 171.67. ¹⁹F NMR δ -120.35 (br d, $J = 203.2$ Hz, 1F), -115.31 (br d, $J = 246.5$ Hz, 1F).

4-*N*-(10,11-Dihydroxyundecan-1-yl)-3',5'-di-*O*-benzoyl-2',2'-difluorocytidine (69). 5% mol of OsO₄ (100 μ L, catalytic amount) and *N*-methylmorpholine-*N*-oxide (56.20 mg, 0.48 mmol) was added to a solution of **68** (200 mg, 0.32 mmol) in acetone (3 mL) and water (0.3 mL), and the mixture was stirred at 0 °C to ambient temperature under nitrogen. After 2 h, the reaction mixture was diluted with CH₂Cl₂ (30 mL) and partitioned with H₂O (15 mL). The organic layer was washed with saturated NaHCO₃/H₂O (15 mL), and brine (15 mL), dried over Na₂SO₄, and evaporated, and the resulting residue (198 mg) was column chromatographed (90% EtOAc/hexane) to give **69** (202 mg, 96 %) as a mixture of rotamers. The major rotamer had the following peaks: ¹H NMR (CDCl₃) δ 1.21-1.40 (m, 12H, 6 \times CH₂), 1.39-1.43 (m, 2H, CH₂), 1.57-1.60 (m, 2H, CH₂), 3.43-3.45 (m, 2H, CH₂), 3.63-3.66 (m, 1H, CH), 3.71-3.73 (m, 1H, CH₂), 4.54-4.56 (m, 1H, H4'), 4.75 (dd, $J = 4.6, 12.2$ Hz, 1H, H5'), 4.77 (dd, $J = 3.3, 12.1$ Hz, 1H, H5''), 5.60-5.63 (m, 1H, H3'), 5.71 (d, $J = 7.6$ Hz, 1H, H5), 6.59-6.62 (m, 1H, H1'), 7.33 (d, $J = 7.0$, 1H, H6), 7.39-7.51 (m, 4H, Ar), 7.52-7.67 (m, 2H, Ar), 7.98-8.10 (m, 4H, Ar). ¹³C NMR δ 25.28, 26.41, 26.61, 28.57, 28.70, 28.85, 29.19, 33.02, 43.70,

62.55 (C5'), 66.85, 71.61 (m, C3'), 72.22, 77.81, 79.25, 91.34 (C5), 121.14 (t, $J = 263.1$ Hz, C2'), 127.64, 128.70, 128.80, 129.07, 129.71, 130.15, 133.56, 133.72, 134.17, 134.43, 158.82, 164.79, 165.97. ^{19}F NMR δ -120.42 (br d, $J = 243.4$ Hz, 1F), -115.30 (br d, $J = 260.1$ Hz, 1F). HRMS (ESI+) m/z calcd for $\text{C}_{34}\text{H}_{41}\text{F}_2\text{N}_3\text{O}_8$ [M + H] $^+$, 658.2934; found, 658.2930

4-*N*-(10,11-Dihydroxy-11-*O*-methanesulfonylundecanyl)-3',5'-di-*O*-benzoyl-2'-deoxy-2',2'-difluorocytidine (70). Mesyl chloride (14 μL , 20.7 mg, 0.18 mmol) was added to a solution of **69** (100 mg, 0.15 mmol) in anhydrous CH_2Cl_2 (4 mL) in the presence of Et_3N (32 μL , 23 mg, 0.23 mmol). The mixture was stirred at -20 °C. After 20 minutes, the reaction mixture was diluted with CH_2Cl_2 and partitioned with HCl (0.1 M, 15 mL) and H_2O (15 mL). The organic layer was washed with saturated $\text{NaHCO}_3/\text{H}_2\text{O}$ (15 mL), and brine (15 mL), dried over Na_2SO_4 , and evaporated, and the resulting residue was column chromatographed (50% EtOAc/hexane) to give **70** (93 mg, 55%) as a mixture of rotamers. The major rotamer had the following peaks. ^1H NMR (CDCl_3) δ 1.21–1.40 (m, 12H, $6 \times \text{CH}_2$), 1.44–1.47 (m, 2H, CH_2), 1.56–1.59 (m, 2H, CH_2), 3.08 (s, 3H, Ms), 3.48–3.50 (m, 2H, CH_2), 3.91–3.94 (m, 1H, CH), 4.12 (dd, $J = 2.8, 9.9$ Hz, 1H, CH), 4.25 (dd, $J = 3.1, 10.5$ Hz, 1H, CH), 4.50–4.54 (m, 1H, H_4'), 4.65 (dd, $J = 4.5, 12.2$, 1H, H_5'), 4.79 (dd, $J = 3.2, 12.1$, H_5''), 5.58–5.61 (m, 1H, H_3'), 5.69 (d, $J = 7.6$ Hz, 1H, H_5), 6.58–6.61 (m, 1H, H_1'), 7.30 (d, $J = 7.3$, 1H, H_6), 7.39–7.51 (m, 4H, Ar), 7.52–7.67 (m, 2H, Ar), 7.98–8.10 (m, 4H, Ar). ^{13}C NMR δ 25.24, 26.79, 29.08, 29.14, 29.25, 29.28, 29.31, 32.87, 37.69, 41.12, 63.03 (C5'), 69.74, 71.81 (br s, C3'), 73.92, 77.95, 79.27 (C4'), 83.79 (s, C1'), 96.12 (C5), 120.89 (t, $J = 263.2$ Hz, C2'), 126.95, 128.14, 128.75, 128.85, 129.44, 129.86, 130.32,

133.65, 134.33, 140.05, 155.69, 165.09, 166.12. ^{19}F NMR δ -120.26 (br d, J = 222.8 Hz, 1F), -115.21 (br d, J = 246.2 Hz, 1F).

4-*N*-(10,11-Dihydroxy-11-*O*-toluenesulfonylundecanyl)-3',5'-di-*O*-benzoyl-2'-deoxy-2',2'-difluorocytidine (71). Tosyl chloride (29.6 mg, 0.15 mmol) was added to a solution of **70** (100 mg, 0.15 mmol) in anhydrous CH_2Cl_2 (4 mL) in the presence of Et_3N (32 μL , 23 mg, 0.23 mmol). The mixture was stirred at 40 °C. After 15 h, the reaction mixture was diluted with CH_2Cl_2 and partitioned with HCl (0.1 M, 5 mL) and H_2O (15 mL). The organic layer was washed with saturated $\text{NaHCO}_3/\text{H}_2\text{O}$ (15 mL), and brine (15 mL), dried over Na_2SO_4 , and evaporated, and the resulting residue was column chromatographed (45% EtOAc/hexane) to give **71** (76 mg, 62%) as a mixture of rotamers. The major rotamer had the following peaks. ^1H NMR (CDCl_3) δ 1.23–1.31 (m, 12H, 6 \times CH_2), 1.44–1.46 (m, 2H, CH_2), 1.62–1.65 (m, 2H, CH_2), 2.44 (s, 3H, CH_3), 3.46–3.49 (m, 2H, CH_2), 3.82–3.85 (m, 1H, CH), 3.91 (m, 1H, CH), 4.11 (dd, J = 2.9, 9.8 Hz, 1H, CH), 4.51–4.54 (m, 1H, $\text{H}4'$), 4.66 (dd, J = 4.4, 12.2 Hz, 1H, $\text{H}5'$), 4.81 (dd, J = 3.4, 12.3 Hz, 1H, $\text{H}5''$), 5.38–5.41 (m, 1H, $\text{H}3'$), 5.61 (d, J = 7.6 Hz, 1H, $\text{H}5$), 6.64–6.66 (m, 1H, $\text{H}1'$), 7.33–7.36 (m, 3H, $\text{H}6$, Ts), 7.39–7.51 (m, 4H, Ar), 7.52–7.67 (m, 2H, Ar), 7.98–8.10 (m, 4H, Ar). ^{13}C NMR δ 21.80, 25.21, 26.87, 29.32, 29.35, 29.41, 29.58, 29.85, 32.77, 41.17, 63.03 ($\text{C}5'$), 69.62, 71.15 (m, $\text{C}3'$), 74.14, 96.02 ($\text{C}5$), 121.19 (t, J = 262.8 Hz, $\text{C}2'$), 128.11, 128.75, 128.89, 129.45, 129.49, 129.86, 130.10, 130.33, 132.91, 133.65, 134.32, 145.19, 164.85, 165.09, 166.11. ^{19}F NMR δ -120.51 (br d, J = 241.2 Hz, 1F), -115.34 (d, J = 246.8 Hz, 1F).

4-*N*-(11-*O*-Mesyl-10-oxoundecanyl)-3',5'-di-*O*-benzoyl-2'-deoxy-2',2'-difluorocytidine (72). A freshly prepared solution of Collins reagent [CrO_3 (28 mg, 0.28

mmol), pyridine (7 μ L, 28 mg, 0.28 mmol), and Ac₂O (53 μ L, 60 mg, 0.56 mmol) in CH₂Cl₂ (4 mL)] was added to a stirred solution of **71** (50 mg, 0.07 mmol) in CH₂Cl₂ (8 mL) at ambient temperature. The resulting mixture was stirred for 1 h. and was immediately column chromatographed (EtOAc) to give **72** (48 mg, 93%) as a mixture of isomers. The major isomer had the following peaks. ¹H NMR (CDCl₃) δ 1.22–1.35 (m, 12H, 6 \times CH₂), 1.53-1.56 (m, 2H, CH₂), 2.45 (t, J = 7.3 Hz, 2H, CH₂), 3.19 (s, 3H, Ms), 3.48-3.50 (m, 2H, CH₂), 4.51-4.53 (m, 1H, H4'), 4.66 (dd, J = 4.6, 12.3 Hz, 1H, H5'), 4.78 (s, 2H, CH₂), 4.79 (dd, J = 3.6, 12.1 Hz, 1H, H5''), 5.40-5.42 (m, 1H, H3'), 5.60 (d, J = 7.6 Hz, 1H, H5), 6.61-6.63 (m, 1H, H1'), 7.32 (d, J = 7.3, 1H, H6), 7.41-7.52 (m, 4H, Ar), 7.55-7.67 (m, 2H, Ar), 8.02-8.11 (m, 4H, Ar). ¹³C NMR δ 23.14, 26.70, 28.92, 29.02, 29.07, 29.20, 29.83, 38.98, 39.67, 39.78, 44.37, 48.37, 62.91 (C5'), 71.63 (dd, J = 17.2, 35.4 Hz, C3'), 71.79, 79.38 (C4'), 83.85 (br s, C1'), 91.32 (C5), 120.93 (t, J = 263.1 Hz, C2'), 127.79, 128.85, 128.95, 129.24, 129.86, 130.30, 133.56, 133.71, 134.21, 134.42, 138.78 (C6), 146.88 (C4), 158.12, 164.93, 166.09, 203.17. ¹⁹F NMR δ -120.21 (br d, J = 224.5 Hz, 1F), -115.21 (d, J = 245.4 Hz, 1F).

4-N-(11-O-Toluenesulfonyl-10-oxoundecanyl)-3',5'-di-O-benzoyl-2'-deoxy-2',2'-difluorocytidine (73). A freshly prepared solution of Collins reagent [CrO₃ (24.6 mg, 0.246 mmol), pyridine (5 μ L, 24.6 mg, 0.246 mmol), and Ac₂O (45 μ L, 51 mg, 0.493 mmol) in CH₂Cl₂ (2 mL)] was added to a stirred solution of **71** (50 mg, 0.062 mmol) in CH₂Cl₂ (4 mL) at ambient temperature. The resulting mixture was stirred for 1 h. and was immediately column chromatographed (EtOAc) to give **73** (47.2 mg, 94%) as a mixture of isomers. The major isomer had the following peaks. ¹H NMR (CDCl₃) δ 1.23–1.31 (m, 12H, 6 \times CH₂), 1.44-1.46 (m, 2H, CH₂), 2.44 (s, 3H, CH₃), 2.48-2.50 (m, 2H, CH₂), 3.50-

3.52 (m, 2H, CH₂), 4.49 (s, 2H, CH₂), 4.51-4.53 (m, 1H, H_{4'}), 4.67 (dd, $J = 4.4, 12.1$ Hz, 1H, H_{5'}), 4.81 (dd, $J = 3.4, 12.2$ Hz, 1H, H_{5''}), 5.30-5.32 (m, 1H, H_{3'}), 5.58 (d, $J = 7.6$ Hz, 1H, H₅), 6.64-6.66 (m, 1H, H_{1'}), 7.30-7.34 (m, 3H, H₆, Ts), 7.39-7.51 (m, 4H, Ar), 7.52-7.67 (m, 2H, Ar), 7.98-8.10 (m, 4H, Ar). ¹³C NMR δ 21.72, 22.77, 26.77, 28.82, 28.99, 29.00, 29.08, 29.11, 38.93, 41.01, 62.91 (C_{5'}), 71.53 (dd, $J = 17.2, 35.4$ Hz, C_{3'}), 71.83, 77.36 (C_{4'}), 84.01 (br s, C_{1'}), 96.17 (C₅), 120.90 (t, $J = 263.1$ Hz, C_{2'}), 125.99, 128.72, 128.82, 128.94, 129.38, 129.41, 129.45, 129.57, 130.03, 130.54, 130.86, 130.91, 133.16, 134.28, 134.35, 135.12, 135.24, 140.69 (C₆), 146.42 (C₄), 156.51, 164.39, 165.88, 166.99, 203.43. ¹⁹F NMR δ -120.69 (br d, $J = 252.5$ Hz, 1F), -115.28 (d, $J = 248.2$ Hz, 1F).

4-*N*-(11-Fluoro-10-oxoundecanyl)-3',5'-di-*O*-benzoyl-2'-deoxy-2',2'-

difluorocytidine (74). To a solution of KF (2.8 mg, 0.048 mmol), K₂CO₃ (6.5 mg, 0.048 mmol), Kryptofix 2.2.2 (17.9 mg, 0.048 mmol) in CH₃CN (3 mL) **73** (Ts derivative, 10 mg, 0.012 mmol) was stirred at 80 °C. After 25 min, the reaction mixture was quickly cooled in a water bath and filtered. The crude product was evaporated, and the resulting residue was column chromatographed (40% EtOAc/hexane) to give **74** (4.7 mg, 60 %) as a mixture of isomers. The major isomer had the following peaks: ¹H NMR (CDCl₃) δ 1.22-1.35 (m, 12H, 6 \times CH₂), 1.54-1.56 (m, 2H, CH₂), 2.55 (t, $J = 7.3$ Hz, 2H, CH₂), 3.48-3.50 (m, 2H, CH₂), 4.52-4.55 (m, 1H, H_{4'}), 4.65 (dd, $J = 4.6, 12.3$ Hz, 1H, H_{5'}), 4.79 (d, $J = 47.7$ Hz, 2H, CH₂), 4.79 (dd, $J = 3.6, 12.1$ Hz, 1H, H_{5''}), 5.51 (d, $J = 7.6$ Hz, 1H, H₅), 5.62 (m, 1H, H_{3'}), 6.60-6.63 (m, 1H, H_{1'}), 7.32 (d, $J = 7.3$, 1H, H₆), 7.41-7.55 (m, 4H, Ar), 7.56-7.69 (m, 2H, Ar), 8.01-8.12 (m, 4H, Ar). ¹³C NMR δ 22.72, 26.69, 28.68, 28.97, 29.06, 29.21, 29.85, 38.30, 38.32, 38.41, 44.03, 62.66 (C_{5'}), 71.65 (dd, $J = 17.2, 35.4$ Hz, C_{3'}), 79.38 (C_{4'}), 83.91 (br s, C_{1'}), 85.04 (d, $J = 185.2$ Hz, CH₂F), 91.13 (C₅), 120.67 (t,

$J = 263.1$ Hz, C2'), 127.62, 128.89, 128.98, 129.12, 129.85, 130.31, 133.77, 133.45, 134.39, 134.67, 137.68 (C6), 145.20 (C4), 158.00, 164.93, 166.11, 203.34. ^{19}F NMR δ -227.42 (t, $J = 47.7$, 1F), -120.37 (br d, $J = 217.9$ Hz, 1F), -115.21 (dd, $J = 245.1$ Hz, 1F). HRMS (ESI+) m/z calcd for $\text{C}_{34}\text{H}_{38}\text{F}_3\text{N}_3\text{O}_7$ [M + H]⁺, 658.2747; found, 658.2745.

4-*N*-(11-Fluoro-10-oxoundecanyl)-2'-deoxy-2',2'-difluorocytidine (76). Compound **74** (20 mg, .031 mmol) was dissolved in methanolic ammonia (2 mL) and stirred at ambient temperature. After 2 h, volatiles were evaporated under reduced pressure, and the resulting residue was chromatographed (5% MeOH/ CHCl_3) to give **76** (7.5 mg, 55%) as a clear oil. ^1H NMR (MeOD) δ 1.21–1.35 (m, 12H, 6 \times CH_2), 1.53–1.56 (m, 2H, CH_2), 2.41 (t, $J = 7.3$ Hz, 2H, CH_2), 3.35 (t, $J = 7.1$ Hz, 2H, CH_2), 3.74–3.76 (m, 1H, H5), 3.90–3.92 (m, 2H, H4', 5''), 4.21–4.23 (m, 1H, H3'), 4.80 (d, $J = 47.7$ Hz, 2H, CH_2F), 5.99 (d, $J = 7.9$ Hz, 1H, H5), 6.08–6.10 (m, 1H, H1'), 7.96 (d, $J = 7.9$, 1H, H6). ^{13}C NMR δ 23.88, 27.94, 29.94, 30.17, 30.31, 30.72, 38.55, 41.70, 60.56 (C5'), 71.43 (dd, $J = 17.1, 35.4$ Hz, C3'), 82.22 (C4'), 85.04 (d, $J = 185.2$ Hz, CH_2F), 87.96 (C1'), 97.36 (C5), 124.00 (t, $J = 262.8$ Hz, C2'), 140.77 (C6), 158.29 (C2), 165.35 (C4), 202.21. ^{19}F NMR δ -227.44 (t, $J = 47.7$ Hz, 1F), -120.15 (br s, 1F), -119.35 (dd, $J = 4.1, 12.7$ Hz, 1F). HRMS (ESI+) m/z calcd for $\text{C}_{20}\text{H}_{30}\text{F}_3\text{N}_3\text{O}_5$ [M + H]⁺, 450.2210; found, 450.2244.

***N*-(10-undecenyl) benzamide (125).** Benzoyl chloride (0.670 mL, 0.810 g, 5.74 mmol) and Et_3N (1.5 mL, 1.09 g, 10.6 mmol) was added to a solution of **56** (0.810 mL, 4.78 mmol) in CH_2Cl_2 (10 mL) and stirred at ambient temperature. After 8 h, the volatiles were evaporated under reduced pressure and the resulting residue was diluted with CH_2Cl_2 and partitioned with HCl (0.1 M) and H_2O (15 mL). The organic layer was washed with saturated $\text{NaHCO}_3/\text{H}_2\text{O}$ (20 mL), and brine (20 mL), dried over Na_2SO_4 , and the resulting

mixture was then column chromatographed (25% EtOAc/hexane) to give **125** (1.22 g, 93%) as a white solid. ¹H NMR (CDCl₃) δ 1.31-1.35 (m, 10H, 5 × CH₂), 1.61-1.63 (m, 4H, 2 × CH₂), 2.04 (dd, *J* = 6.9, 14.2 Hz, 2H, CH₂), 3.45 (t, *J* = 7.1 Hz, 2H, CH₂), 4.97-4.99 (m, 2H, CH₂), 5.81 (ddt, *J* = 6.7, 10.2, 16.9 Hz, 1H, CH), 6.11 (br s, 1H, NH), 7.44-7.46 (m, 3H, Ar), 7.74-7.77 (m, 2H, Ar).

***N*-(10,11-Dihydroxyundecan-1-yl) benzamide (126)**. 5% mol of OsO₄ (50 μL, cat. amount) and *N*-methylmorpholine-*N*-oxide (87.8 mg, 0.75 mmol) was added to a solution of **125** (137 mg, 0.50 mmol) in acetone (2 mL) and water (0.2 mL), and the mixture was stirred at 0 °C to ambient temperature under Nitrogen. After 4 h, the reaction mixture was diluted with CH₂Cl₂ (20 mL) and partitioned with H₂O. The organic layer was washed with saturated NaHCO₃/H₂O (15 mL), and brine (15 mL), dried over Na₂SO₄, and evaporated, and the resulting residue was column chromatographed (75% EtOAc/hexane) to give **126** (138 mg, 90 %). ¹H NMR (CDCl₃) δ 1.31-1.35 (m, 16H, 8 × CH₂), 3.41 (dd, *J* = 7.7, 11.0 Hz, 1H, CH), 3.44 (t, *J* = 7.1 Hz, 2H, CH₂), 3.63 (dd, *J* = 3.0, 11.0 Hz, 1H, CH), 3.68-3.70 (m, 1H, CH), 6.13 (br s, 1H, NH), 7.44-7.46 (m, 3H, Ar), 7.74-7.77 (m, 2H, Ar).

***N*-(10,11-Dihydroxy-11-*O*-toluenesulfonylundecanyl) benzamide (127)**. Tosyl chloride (65.1 mg, 0.33 mmol) was added to a solution of **126** (100 mg, 0.33 mmol) in anhydrous CH₂Cl₂ (5 mL) in the presence of Et₃N (65 μL, 47 mg, 0.50 mmol). The mixture was stirred at 40 °C. After 18 hours, the reaction mixture was diluted with CH₂Cl₂ and partitioned with HCl (0.1 M) and H₂O (15 mL). The organic layer was washed with saturated NaHCO₃/H₂O (15 mL), and brine (15 mL), dried over Na₂SO₄, and evaporated, and the resulting residue was column chromatographed (50% EtOAc/hexane) to give **127** (91 mg, 60%). ¹H NMR (CDCl₃) δ 1.32-1.35 (m, 14H, 7 × CH₂), 1.59-1.61 (m, 2H, CH₂),

2.45 (s, 3H, CH₃), 3.44 (dd, $J = 7.1, 13.1$ Hz, 2H, CH₂), 3.82 (dd, $J = 2.8, 7.0$ Hz, 1H, CH), 3.87-3.89 (m, 1H, CH), 4.02 (dd, $J = 2.8, 9.8$ Hz, 1H, CH), 6.17 (br s, 1H, NH), 7.35 (d, $J = 8.2$ Hz, 2H, Ts), 7.42 (d, $J = 8.2$ Hz, 2H, Ts), 7.46-7.49 (m, 1H, Ar), 7.75-7.79 (m, 4H, Ar).

***N*-(10-oxo,11-*O*-toluenesulfonylundecanyl) benzamide (128).** A freshly prepared solution of Collins reagent [CrO₃ (52 mg, 0.52 mmol), pyridine (8 μ L, 52 mg, 0.52 mmol), and Ac₂O (102 μ L, 107 mg, 1.04 mmol) in CH₂Cl₂ (2 mL)] was added to a stirred solution of **127** (60 mg, 0.13 mmol) in CH₂Cl₂ (8 mL) at ambient temperature. The resulting mixture was stirred for 1.5 h. and was immediately column chromatographed (45% EtOAc/hexane) to give **128** (56 mg, 94 %). ¹H NMR (CDCl₃) δ 1.29-1.32 (m, 10H, 5 \times CH₂), 1.57-1.59 (m, 4H, 2 \times CH₂), 2.45 (s, 3H, CH₃), 2.48 (t, $J = 7.4$ Hz, 2H, CH₂), 3.44 (dd, $J = 7.1, 13.1$ Hz, 2H, CH₂), 4.48 (s, 2H, CH₂), 6.15 (br s, 1H, NH), 7.36 (d, $J = 8.2, 2H, Ts$), 7.42 (d, $J = 8.2, 2H, Ts$), 7.46-7.49 (m, 1H, Ar), 7.75-7.79 (m, 4H, Ar).

***N*-(10-oxo,11-*O*-Fluoroundecanyl) benzamide (75).** To a solution of KF (26 mg, 0.44 mmol), K₂CO₃ (60 mg, 0.44 mmol), 18-Crown-6 (163 mg, 0.44 mmol) in CH₃CN (6 mL), **128** (50 mg, 0.11 mmol) was stirred at 75°C. After 25 min, the reaction mixture was quickly cooled in a water bath and filtered. The crude product was evaporated, and the resulting residue was column chromatographed (40% EtOAc/hexane) to give **75** (20 mg, 58%). ¹H NMR (CDCl₃) δ 1.29-1.32 (m, 10H, 5 \times CH₂), 1.59-1.62 (m, 4H, 2 \times CH₂), 2.53 (t, $J = 7.4$ Hz, 2H, CH₂), 3.45 (dd, $J = 7.1, 13.1$ Hz, 2H, CH₂), 4.79 (d, $J = 47.7$ Hz, 2H, CH₂F), 6.09 (br s, 1H, NH), 7.46-7.49 (m, 3H, Ar), 7.74-7.77 (m, 2H, Ar). ¹⁹F NMR δ -227.48 (t, $J = 47.7, 1F$).

4.3. Synthesis of 4-*N*-alkanoyl and 4-*N*-alkyl clickable gemcitabine analogues with silicon-fluoride acceptors

Methyl 11-azidoundecanoate (79). Sodium azide (175 mg, 2.7 mmol) was added to a stirred solution of methyl 11-bromoundecanoate **78** (500 mg, 1.8 mmol) in DMF. After 3 hours, the crude mixture was diluted with water and extracted with Et₂O. The organic layer was then washed with brine, dried over Na₂SO₄ and evaporated under reduced pressure to give **79**¹⁴⁷ (420 mg, 97%). ¹H NMR (400 MHz, CDCl₃) δ 1.30 (s, 12H), 1.49-1.66 (m, 4H), 2.29 (t, *J* = 7.5 Hz, 2H), 3.24 (t, *J* = 7.0 Hz, 2H), 3.65 (s, 3H).

11-Azidoundecanoic acid (80). NaOH (1M, 1.5 mL) was added to a solution of **79** (400 mg, 1.7 mmol) in MeOH (1mL) and stirred at ambient temperature. After 2 h, the reaction mixture was diluted with water and was extracted with Et₂O to remove any unreacted starting material. The aqueous layer was then acidified with HCl (1 M) and extracted with fresh portions of Et₂O (2 x 10 mL). The combined organic layer was then washed with brine, dried over Na₂SO₄ and evaporated under reduced pressure to give **80**¹⁴⁷ (350 mg, 88%). ¹H NMR (400 MHz, CDCl₃) δ 1.32 (s, 12H), 1.51-1.71 (m, 4H), 2.35 (t, *J* = 7.5 Hz, 2H), 3.25 (t, *J* = 7.0 Hz, 2H).

4-*N*-(11-Azidoundecanoyl)-2'-deoxy-2', 2'-difluorocytidine (81). *N,N*-Diisopropylethylamine (35 μL, 0.2 mmol), 1-hydroxybenzotriazole (27 mg, 0.2 mmol), **80** (46 mg, 0.2 mmol), and 1-ethyl-3-(3-dimethylaminopropyl)carbodiimide (45 μL, 0.2 mmol) were sequentially added to a stirred solution of gemcitabine hydrochloride (50 mg, 0.17 mmol) in DMF (4 mL) at ambient temperature under Nitrogen. The reaction mixture was then gradually heated to 65 °C (oil-bath) and was kept stirring overnight. The crude mixture was evaporated and column chromatographed (0 → 10% MeOH/CHCl₃) to give

81 (56 mg, 70%): UV (CH₃OH) λ max 299 nm (ϵ 6500), λ min 250 nm (ϵ 12 900); ¹H NMR (CD₃OD) δ 1.24–1.47 (m, 12H, 6 \times CH₂), 1.51–1.75 (m, 4H, 2 \times CH₂), 2.45 (t, J = 7.4 Hz, 2H, CH₂), 3.27 (t, J = 6.9 Hz, 2H, CH₂), 3.81 (dd, J = 2.8, 12.4 Hz, 1H, H5'), 3.89–4.05 (m, 2H, H5', H4'), 4.30 (td, J = 8.5, 12.2 Hz, 1H, H3'), 6.17–6.35 (m, 1H, H1'), 7.50 (d, J = 7.6 Hz, 1H, H5), 8.34 (d, J = 7.6 Hz, 1H, H6); ¹³C NMR δ 25.92, 27.80, 29.90, 30.11, 30.20, 30.33, 30.41, 30.50, 38.17, 52.47, 60.30 (C5'), 70.27 (dd, J = 22.2, 23.6 Hz, C3'), 82.92 (d, J = 8.6 Hz, C4'), 86.42 (dd, J = 26.6, 37.6 Hz, C1), 98.25 (C5), 120.87 (t, J = 259.9 Hz, C2'), 145.96 (C6), 157.68 (C2), 164.83 (C4), 176.00 (CO); ¹⁹F NMR δ -120.05 (d of m, J = 239.7 Hz, 1F), -119.10 (d of m, J = 240.1 Hz, 1F). HRMS (ESI+) m/z calcd for C₂₀H₃₀F₂N₆O₅ [M+Na]⁺ 495.2146; found 495.2141.

4-N-(5-Hexynoyl)-2'-deoxy-2', 2'-difluorocytidine (82). Trimethylsilyl chloride (250 μ L, 2 mmol) was added to a solution of gemcitabine hydrochloride (200 mg, 0.7 mmol) in CH₃CN (2 mL) and pyridine (3 mL) at 0 °C. The mixture was stirred for 4 h from 0 °C to room temperature. A solution of commercially available 5-hexynoic acid (230 μ L, 2.1 mmol) in CH₃CN (2 mL), previously activated by EDC (50 μ L, 1 mmol), was added to the reaction mixture, which was heated at 60 °C for 18 hours. After the solution was cooled down to room temperature, ethanol (5 mL) was added and the mixture was heated at 45 °C for 4 h. After evaporation under vacuum, the resulting residue was column chromatographed (80 \rightarrow 100% EtOAc/hexane) to give **82**⁴⁵ (157.6 mg, 63%): ¹H NMR (CD₃OD) δ 1.83-1.86 (m, 2H, CH₂), 2.25-2.28 (m, 3H, CH₂, CH), 2.60 (t, J = 7.3 Hz, 2H, CH₂), 3.82-3.84 (m, 1H, H5'), 3.89–4.07 (m, 2H, H5'', H4'), 4.31 (dd, J = 12.1, 20.6 Hz, 1H, H3'), 6.24-6.26 (m, 1H, H1'), 7.49 (d, J = 7.6 Hz, 1H, H5), 8.34 (d, J = 7.6 Hz, 1H, H6); ¹³C NMR δ 18.42, 24.96, 33.47, 60.50 (C5'), 68.14 (CH), 70.20 (C) 70.34 (t, J = 23.1

Hz, C3'), 82.35 (d, $J = 8.6$ Hz, C4'), 86.1 (dd, $J = 26.6, 38.3$ Hz, C1'), 96.30 (C5'), 123.91 (t, $J = 259.3$ Hz, C2'), 142.51 (C6), 157.78 (C2), 167.74 (C4), 175.97 (CO); ^{19}F NMR δ -120.14 (d of m, $J = 244.4$ Hz, 1F), -119.23 (d of m, $J = 243.6$ Hz, 1F).

7-Azido-1-aminoheptane (85). *Step A.* Sodium azide (272 mg, 4.0 mmol) was added to a stirred solution of the 1,7-dibromoheptane **83** (424 mg, 1.6 mmol) in DMF at 60 °C (oil bath). After 6 h, the crude mixture was diluted with water and extracted with Et₂O. The organic layer was then washed with brine, dried over Na₂SO₄ and evaporated under reduced pressure to give 1,7-diazidoheptane **84** which was used immediately in next step.

Step B. To a solution of 1,7-diazidoheptane **84** (182 mg, 1 mmol) in Et₂O (1 mL), ethyl acetate (1 mL) and 5% aqueous HCl (3 mL) was added Ph₃P (256 mg, 0.98 mmol) portion wise over 1 h and stirred for 16 h at ambient temperature. The organic layer was discarded and the aqueous layer was washed with (2 × 10 mL) CH₂Cl₂. The resultant aqueous phase was basified with sodium hydroxide (pH>12), and then extracted with (3 × 6 mL) CH₂Cl₂. The combined extracts were dried over Na₂SO₄, filtered and evaporated under reduced pressure to give **85**¹⁴⁸ (130 mg, 83%): ^1H NMR (CDCl₃) δ 1.26-1.48 (m, 10H), 1.57-1.59 (m, 2H), 2.66 (t, $J = 7.0$ Hz, 2H, CH₂), 3.22 (t, $J = 6.9$ Hz, 2H, CH₂).

4-N-(7-Azidoheptanyl)-2'-deoxy-2', 2'-difluorocytidine (86). Freshly prepared 7-Azido-1-aminoheptane **85** (112.5 mg, 0.72 mmol) was added to a suspension of **62** (100 mg, 0.24 mmol) in 1,4-dioxane (5 mL) and Et₃N (0.10 mL, 63 mg, 0.72 mmol) and the mixture was left stirring at 65°C. After 24 h, volatiles were evaporated and the resulting residue was column chromatographed (5% MeOH/CHCl₃) to give **86** (238 mg, 82%): UV (CH₃OH) λ max 267 nm (ϵ 8200), λ min 227 nm (ϵ 7400); ^1H NMR (CD₃OD) δ 1.31-1.41 (m, 12H, 6 × CH₂), 1.51-1.70 (m, 4H, 2 × CH₂), 3.25 (t, $J = 6.9$ Hz, 2H, CH₂), 3.45 (t, J

= 7.0, 2H, CH₂) 3.77–3.83 (m, 1H, H5'), 3.91–3.99 (m, 2H, H5', H4'), 4.25 (dt, $J = 10.5$, 20.8 Hz, 1H, H3'), 5.85 (d, $J = 7.6$ Hz, 1H, H5), 6.23–6.25 (m, 1H, H1') , 7.71 (d, $J = 7.6$ Hz, 1H, H6); ¹³C NMR δ 27.75, 27.86, 29.84, 29.88, 29.92, 41.65, 52.45, 60.56 (C5'), 70.66 (t, $J = 23.1$ Hz, C3'), 82.22 (d, $J = 8.6$ Hz, C4'), 86.26 (dd, $J = 26.6$, 38.3 Hz, C1'), 97.32 (C5), 124.02 (t, $J = 259.2$ Hz, C2'), 140.80 (C6), 158.29 (C2), 165.38 (C4); ¹⁹F NMR δ -119.86 (d of m, $J = 246.2$ Hz, 1F), -119.89 (d of m, $J = 240.2$ Hz, 1F). HRMS (ESI+) m/z calcd for C₁₆H₂₄F₂N₆O₄ [M+H]⁺ 403.1902; found 403.1913.

4-(Azidomethyl)phenyldiisopropylsilane (88). *Step A.* Methanesulfonyl chloride (39 μ L, 0.4 mmol) was added to a stirred solution of 4-(di-*iso*-propylsilyl)benzylalcohol **87** (100 mg, 0.4 mmol) and triethylamine (110 μ L, 81 mg, 0.8 mmol) in CH₂Cl₂ (5 mL) at 0 °C under N₂ atmosphere. After stirring for 5 min, the resulting mixture was allowed to warm up to ambient temperature and kept stirring for 1 h. The reaction mixture was then diluted with CH₂Cl₂ (15 mL) and partitioned between H₂O (20 mL) and the aqueous layer extracted with fresh portions of CH₂Cl₂ (2 x 20 mL). The combined organic layer was then washed with brine (20 mL), dried over Na₂SO₄ and evaporated under reduced pressure to give 4-(*O*-mesylmethyl)phenyldiisopropylsilane (91%) of sufficient purity to use directly in next step: ¹H NMR (400 MHz, CDCl₃) δ 0.99 (d, $J = 7.3$ Hz, 6H), 1.05 (d, $J = 7.3$ Hz, 6H), 1.21–1.30 (m, 2H), 2.92 (s, 3H), 3.94 (t, $J = 3.1$ Hz, 1H), 5.24 (s, 2H), 7.35 (d, $J = 7.7$ Hz, 2H), 7.45 (d, $J = 7.9$ Hz, 2H).

Step B. Sodium azide (34 mg, 0.5 mmol) was added to a stirred solution of the 4-(*O*-mesylmethyl)phenyldiisopropylsilane (105 mg, 0.3 mmol) in DMF. After 6 h, the crude mixture was diluted with water and extracted with Et₂O. The organic layer was then washed with brine, dried over Na₂SO₄ and evaporated under reduced pressure. The resulting

residue was column chromatographed (20% EtOAc/hexanes) to give **88**¹⁴⁹ (118 mg, 95%). ¹H NMR (400 MHz, CDCl₃) δ 0.99 (d, *J* = 7.3 Hz, 6H), 1.07 (d, *J* = 7.3 Hz, 6H), 1.20-1.28 (m, 2H), 3.96 (t, *J* = 3.1 Hz, 1H), 4.36 (s, 2H), 7.30 (d, *J* = 7.7 Hz, 2H), 7.54 (d, *J* = 7.9 Hz, 2H).

Diisopropyl(4-((prop-2-yn-1-yloxy)methyl)phenyl)silane (89). 4-(Di-*iso*-propylsilyl)benzylalcohol **87** (100 mg, 0.4 mmol) was added to a stirred solution of sodium hydride (11.5 mg, 0.48 mmol) in dry THF. After stirring for 2 h at 65 °C, propargyl bromide (80% weight in toluene, 89 μL, 0.8 mmol) was added to the reaction mixture. The stirred solution was stirred at 65 °C overnight. The reaction mixture was cooled at room temperature and extracted with Et₂O (20 mL). The organic layer was then washed with brine, dried over Na₂SO₄ and evaporated under reduced pressure. The resulting residue was column chromatographed (20% EtOAc/hexanes) to give **89** as an oil (85 mg, 82%). ¹H NMR (400 MHz, CDCl₃) δ 0.98 (d, *J* = 7.3 Hz, 6H), 1.06 (d, *J* = 7.3 Hz, 6H), 1.18-1.26 (m, 2H), 2.47 (t, *J* = 2.3 Hz, 1H), 3.94 (t, *J* = 3.1 Hz, 1H), 4.20 (d, *J* = 2.4 Hz, 2H), 4.61 (s, 2H), 7.35 (d, *J* = 7.7 Hz, 2H), 7.51 (d, *J* = 7.8 Hz, 2H); ¹³C NMR δ 10.69, 18.45, 18.64, 57.30, 71.62, 74.65, 79.67, 127.32, 134.87, 135.65, 138.14.

Synthesis of silicon-fluoride acceptors: General procedure for the click reactions

Sodium ascorbate (0.02 mmol), copper sulfate (0.02 mmol) **modified nucleoside** (0.1 mmol) and **silane** (0.1 mmol) were suspended in a mixture of *tert*-butanol/water (3:1 (v/v), 3 mL). The reaction mixture was left at room temperature for 1-6 hours. The reaction mixture was extracted with CHCl₃ (10 mL). The organic layer was washed with sat NH₄Cl (10 mL), brine (10 mL), dried over Na₂SO₄, filtered and evaporated under reduced

pressure. The crude product was purified by chromatography (CHCl₃/MeOH 95:5) to afford the desired triazole adducts:

4-*N*-[11-Undecanoyl-(diisopropylsilyl)-*O*-propargylbenzyltriazol]-2'-deoxy-2', 2'-difluorocytidine (90). Treatment of **81** (30 mg, 0.06 mmol) with **89** (15.6 mg, 0.06 mmol) using procedure reported in section gave **90** (40.5 mg, 92%). UV (CH₃OH) λ max 299 nm (ϵ 6500), 250 nm (ϵ 12900), λ min 278 nm (ϵ 3800); ¹H NMR (CD₃OD) δ 0.96 (d, J = 7.3 Hz, 6H, *i*Pr), 1.05 (d, J = 7.3 Hz, 6H, *i*Pr), 1.24–1.47 (m, 12H, 6 × CH₂), 1.51–1.75 (m, 4H, 2 × CH₂), 2.38 (t, J = 7.3 Hz, 2H, CH₂), 3.81 (dd, J = 2.8, 12.4 Hz, 1H, H5'), 3.89–3.96 (m, 3H, H5', H4', Si-H), 4.30 (td, J = 8.5, 12.2 Hz, 1H, H3'), 4.33 (t, J = 7.1 Hz, 2H), 4.55 (s, 2H, CH₂), 4.61 (s, 2H, CH₂), 6.19 (t, J = 7.5, 1H, H1'), 7.33–7.35 (m, 3H, H5, Ar), 7.51 (d, J = 8.0 Hz, 2H, Ar), 7.74 (s, 1H), 8.10 (d, J = 7.6 Hz, 1H, H6); ¹³C NMR δ 25.92, 27.80, 29.90, 30.11, 30.20, 30.33, 30.41, 30.50, 38.17, 52.47, 60.30 (C5'), 70.27 (dd, J = 22.2, 23.6 Hz, C3'), 82.92 (d, J = 8.6 Hz, C4'), 86.42 (dd, J = 26.6, 37.6 Hz, C1), 98.25 (C5), 120.87 (t, J = 259.9 Hz, C2'), 145.96 (C6), 157.68 (C2), 164.83 (C4), 176.00 (CO); ¹⁹F NMR δ -120.09 (d of m, J = 239.2 Hz, 1F), -119.13 (d of m, J = 240.2 Hz, 1F). HRMS (ESI+) m/z calcd for C₃₆H₅₄F₂N₆O₆Si [M+Na]⁺ 755.3738; found 755.3731.

4-*N*-[6-Hexynoyl-(diisopropylsilyl)-*O*-propargylbenzyltriazol]-2'-deoxy-2', 2'-difluorocytidine (91). Treatment of **82** (35 mg, 0.1 mmol) with **88** (24.7 mg, 0.1 mmol) using procedure reported in section gave **91** (52.6 mg, 87%). UV (CH₃OH) λ max 299 nm (ϵ 6700), 248 nm (ϵ 13000); ¹H NMR (CD₃OD) δ 0.96 (d, J = 7.3 Hz, 6H, *i*Pr), 1.03 (d, J = 7.3 Hz, 6H, *i*Pr), 1.18–1.20 (m, 4H, 2 × CH₂), 2.46 (t, J = 7.3 Hz, 2H, CH₂), 2.71 (t, J = 7.4 Hz, 2H, CH₂), 3.74–3.76 (m, 1H, H5'), 3.89–3.95 (m, 3H, H5', H4', Si-H), 4.24–4.26 (m, 1H, H3'), 5.50 (s, 2H, CH₂), 6.19 (t, J = 7.5 Hz, 1H, H1'), 7.28 (d, J = 8.0 Hz, 2H, Ar),

7.35 (d, $J = 7.6$ Hz, 1H, H5), 7.51 (d, $J = 8.0$ Hz, 2H, Ar), 7.56 (s, 1H), 8.10 (d, $J = 7.6$ Hz, 1H, H6); ^{13}C NMR δ 11.18, 18.65, 18.83, 24.96, 25.17, 37.04, 54.09, 59.93 (C5'), 69.68 (CH), 70.34 (t, $J = 23.1$ Hz, C3'), 81.82 (d, $J = 8.6$ Hz, C4'), 85.70 (dd, $J = 26.6, 38.3$ Hz, C1'), 97.03 (C5'), 122.39 (t, $J = 259.3$ Hz, C2'), 128.07, 134.96, 136.86, 138.11, 145.43 (C6), 148.04, 155.77 (C2), 163.85 (C4), 174.28 (CO); ^{19}F NMR δ -120.10 (d of m, $J = 233.4$ Hz, 1F), -119.20 (d of m, $J = 240.9$ Hz, 1F). HRMS (ESI+) m/z calcd for $\text{C}_{28}\text{H}_{38}\text{F}_2\text{N}_6\text{O}_5\text{Si}$ $[\text{M}+\text{Na}]^+$ 627.2538; found 627.2522.

4-*N*-[7-heptanyl-(diisopropylsilyl)-*O*-propargylbenzyltriazol]-2'-deoxy-2', 2'-difluorocytidine (92). Treatment of **86** (40 mg, 0.1 mmol) with **89** (silane, 26.0 mg, 0.1mmol) using procedure reported in section gave **92** (59.6 mg, 90%). UV (CH_3OH) λ max 267 nm (ϵ 8200), λ min 228 nm (ϵ 7500); ^1H NMR (CD_3OD) δ 0.99 (d, $J = 7.3$ Hz, 6H, *i*Pr), 1.05 (d, $J = 7.3$ Hz, 6H, *i*Pr), 1.31–1.41 (m, 12H, $6 \times \text{CH}_2$), 1.50-1.52 (m, 2H, CH_2), 1.90-1.92 (m, 2H, CH_2), 3.41-3.43 (m, 2H, CH_2), 3.80-3.82 (m, 1H, H5'), 3.91–4.02 (m, 3H, H5', H4', Si-H), 4.41-4.45 (m, 3H, H3', CH_2), 4.60 (s, 2H, CH_2), 4.65 (s, 2H, CH_2), 5.82 (d, $J = 7.6$ Hz, 1H, H5), 6.23-6.25 (m, 1H, H1'), 7.38 (d, $J = 8.0$ Hz, 2H, Ar), 7.48 (d, $J = 8.0$ Hz, 2H, Ar), 7.71 (d, $J = 7.6$ Hz, 1H, H6), 7.99 (s, 1H, CH); ^{13}C NMR δ 11.26, 18.76, 18.96, 27.01, 27.34, 30.93, 40.97, 50.50, 60.31 (C5'), 64.42, 70.26 (t, $J = 23.1$ Hz, C3'), 72.37, 81.75 (d, $J = 8.6$ Hz, C4'), 84.92 (dd, $J = 26.6, 38.3$ Hz, C1'), 95.97 (C5), 124.04 (t, $J = 259.3$ Hz, C2'), 127.88, 133.36, 140.78, 135.56, 136.34, 138.84, 140.78 (C6), 141.02, 155.92 (C2), 164.77 (C4); ^{19}F NMR δ -119.86 (d of m, $J = 246.2$ Hz, 1F), -119.89 (d of m, $J = 240.2$ Hz, 1F). HRMS (ESI+) m/z calcd for $\text{C}_{32}\text{H}_{48}\text{F}_2\text{N}_6\text{O}_5\text{Si}$ $[\text{M}+\text{Na}]^+$ 685.3322; found 685.3324.

General Procedure for Fluorination Reactions

Solid KF (4.7 mg, 0.08 mmol, 4 eq.) was added to a stirred solution of **90** (15 mg, 0.02 mmol,) and 18-Crown-6 ether (21 mg, 0.08 mmol, 4 eq.) in CH₃CN (3 mL) in a round bottom flask under N₂ atmosphere. To this mixture acetic acid (2 μL, 0.02 mmol, 1 eq.) was then added and the resulting reaction mixture was stirred at 80 °C for 25 min. The reaction mixture was then left to cool (~5 min) and filtered to remove the left over 18-crown ether and KF. The filtrate was washed with CH₃CN (2 mL) and the combined mother liquors were then concentrated under reduced pressure to give crude **94**. The resulting residue was chromatographed (MeOH/CHCl₃ 10:90) to give pure **94** (9.5 mg, 63%).

4-*N*-[11-Undecanoyl-((fluoro)diisopropylsilyl)-*O*-propargylbenzyltriazol]-2'-deoxy-2', 2'difluorocytidine (94**).** Treatment of **90** (15 mg, 0.02 mmol) using procedure reported in general procedure section gave **94** (9.5 mg, 63%). UV (CH₃OH) λ max 299 nm (ε 6500), 250 nm (ε 12900), λ min 278 nm (ε 3800); ¹H NMR (CD₃OD) δ 0.99 (d, *J* = 7.3 Hz, 6H, *i*Pr), 1.07 (d, *J* = 7.3 Hz, 6H, *i*Pr), 1.24–1.47 (m, 12H, 6 × CH₂), 1.78-1.80 (m, 2H, CH₂), 1.90-1.92 (m, 2H, CH₂), 2.44 (t, *J* = 7.4 Hz, 2H, CH₂), 3.81 (dd, *J* = 2.8, 12.4 Hz, 1H, H5'), 3.89–3.99 (m, 2H, H5', H4'), 4.29 (t, *J* = 10.4 Hz, 1H, H3'), 4.40 (t, *J* = 7.0 Hz, 2H), 4.60 (s, 2H, CH₂), 4.66 (s, 2H, CH₂), 6.26 (t, *J* = 7.5, 1H, H1'), 7.41 (d, *J* = 7.8 Hz, 2H, Ar), 7.49 (d, *J* = 7.6 Hz, H5), 7.54 (d, *J* = 8.1 Hz, 2H, Ar), 7.99 (s, 1H), 8.34 (d, *J* = 7.6 Hz, 1H, H6); ¹³C NMR δ 13.22, 25.92, 27.80, 29.90, 30.11, 30.20, 30.33, 30.41, 30.50, 38.17, 52.47, 60.30 (C5'), 70.27 (dd, *J* = 22.2, 23.6 Hz, C3'), 82.92 (d, *J* = 8.6 Hz, C4'), 86.42 (dd, *J* = 26.6, 37.6 Hz, C1), 98.25 (C5), 120.87 (t, *J* = 259.9 Hz, C2'), 128.07, 135.53, 135.56, 136.34, 138.84, 145.93 (C6), 148.76, 145.93 (C6), 157.66 (C2), 164.78 (C4), 175.25 (CO); ¹⁹F NMR δ - 188.86 (s, 1F), -120.09 (d of m, *J* = 239.2 Hz, 1F), -119.13 (d

of m, $J = 240.2$ Hz, 1F). HRMS (ESI+) m/z calcd for $C_{36}H_{53}F_3N_6O_6Si$ $[M+H]^+$ 751.3753; found 751.3770.

4-*N*-[6-Hexynyl-((fluoro)diisopropylsilyl)-*O*-propargylbenzyltriazol]-2'-deoxy-2', 2'-difluorocytidine (95). Treatment of **91** (15 mg, 0.025 mmol) using procedure reported in general procedure section gave **95** (10 mg, 65%). UV (CH₃OH) λ max 299 nm (ϵ 6700), 248 nm (ϵ 13000); ¹H NMR (CD₃OD) δ 0.99 (d, $J = 7.3$ Hz, 6H, *i*Pr), 1.06 (d, $J = 7.3$ Hz, 6H, *i*Pr), 1.18-1.20 (m, 2H, CH₂), 1.91-1.93 (m, 2H, CH₂), 2.50 (t, $J = 7.3$ Hz, 2H, CH₂), 2.78 (t, $J = 7.4$ Hz, 2H, CH₂), 3.80-3.82 (m, 1H, H5'), 3.93-4.05 (m, 2H, H5', H4'), 4.29-4.31 (m, 1H, H3'), 5.59 (s, 2H, CH₂), 6.21 (t, $J = 7.5$ Hz, 1H, H1'), 7.35 (d, $J = 7.9$ Hz, 2H, Ar), 7.47 (d, $J = 7.6$ Hz, 1H, H5), 7.57 (d, $J = 8.1$ Hz, 2H, Ar), 7.81 (s, 1H), 8.33 (d, $J = 7.6$ Hz, 1H, H6); ¹³C NMR δ 13.22, 13.35, 16.82, 17.01, 25.46, 25.53, 37.18, 54.70, 60.30 (C5'), 70.01 (CH), 70.34 (t, $J = 23.1$ Hz, C3'), 81.72 (d, $J = 8.6$ Hz, C4'), 82.92 (dd, $J = 26.6, 38.3$ Hz, C1'), 98.27 (C5'), 123.93 (t, $J = 259.3$ Hz, C2'), 128.39, 134.45, 135.53, 135.56, 136.34, 138.84, 145.93 (C6), 148.76, 157.66 (C2), 164.78 (C4), 175.25 (CO); ¹⁹F NMR δ - 188.89 (s, 1F), -120.10 (d of m, $J = 233.4$ Hz, 1F), -119.20 (d of m, $J = 240.9$ Hz, 1F). HRMS (ESI+) m/z calcd for $C_{28}H_{37}F_3N_6O_5Si$ $[M+Na]^+$ 645.2445; found 645.2392.

4-*N*-[7-heptanyl-((fluoro)diisopropylsilyl)-*O*-propargylbenzyltriazol]-2'-deoxy-2', 2'-difluorocytidine (96). Treatment of **92** (15 mg, 0.023 mmol) using procedure reported in general procedure section gave **96** (9 mg, 62 %). UV (CH₃OH) λ max 267 nm (ϵ 8200), λ min 228 nm (ϵ 7500); ¹H NMR (CD₃OD) δ 0.99 (d, $J = 7.3$ Hz, 6H, *i*Pr), 1.05 (d, $J = 7.3$ Hz, 6H, *i*Pr), 1.31-1.41 (m, 12H, 6 \times CH₂), 1.50-1.12 (m, 2H, CH₂), 1.91 (m, 2H, CH₂), 3.39 (m, 2H, CH₂), 3.81 (m, 1H, H5'), 3.91-4.02 (m, 3H, H5', H4', Si-H), 4.25

(m, 1H, H3'), 4.41 (t, $J = 6.9$, 2H, CH₂), 4.60 (s, 2H, CH₂), 4.65 (s, 2H, CH₂), 5.82 (d, $J = 7.6$ Hz, 1H, H5), 6.22 (m, 1H, H1'), 7.41 (d, $J = 8.0$ Hz, 2H, Ar), 7.52 (d, $J = 8.0$ Hz, 2H, Ar), 7.71 (d, $J = 7.6$ Hz, 1H, H6), 8.01 (s, 1H, CH). ¹³C NMR δ 11.26, 18.76, 18.96, 27.01, 27.34, 30.93, 40.97, 50.50, 60.31 (C5'), 64.42, 70.26 (t, $J = 23.1$ Hz, C3'), 72.37, 81.75 (d, $J = 8.6$ Hz, C4'), 84.92 (dd, $J = 26.6, 38.3$ Hz, C1'), 95.97 (C5'), 124.04 (t, $J = 259.3$ Hz, C2'), 127.88, 133.36, 140.78, 135.56, 136.34, 138.84, 140.78 (C6), 141.02, 155.92 (C2), 164.77 (C4); ¹⁹F NMR δ - 188.82 (s, 1F), -119.75 (d of m, $J = 244.1$ Hz 1F), -119.98 (d of m, $J = 239.1$ Hz, 1F). HRMS (ESI+) m/z calcd for C₃₂H₄₇F₃N₆O₅Si [M+Na]⁺ 703.3227; found 703.3234.

4.4. Reduction of sugar lactones to hemiacetals with LTBH

4.4.1. Typical procedure for reduction of the sugar lactones to hemiacetals with LTBH and selected products¹⁵⁰

LTBH (1 M/THF; 0.24 mL, 0.24 mmol) was added to a solution of the appropriate sugar lactone (0.2 mmol) in anhydrous CH₂Cl₂ (3 mL) at 0 °C. After 30 min, the reaction mixture was quenched with MeOH and the volatiles were evaporated. The resulting residue was dissolved in CH₂Cl₂ (10 mL) and washed with NaHCO₃/H₂O. The organic layer was then dried (Mg₂SO₄), evaporated and the residue was column chromatographed (7:3 / 1:1, hexane/ EtOAc, unless stated otherwise) to afford the corresponding sugar hemiacetals.

5-*O*-Benzyl-2,3-*O*-isopropylidene- α/β -D-ribofuranose (98)^{151, 152} Reduction of **97**¹⁵¹ (275 mg, 1.0 mmol) according to the general procedure gave **98** (α/β , 1:4; 250 mg, 90%). Major anomer had: ¹H NMR δ 1.31 and 1.48 (2 x s, 2 x 3H, 2 x CH₃), 3.58 (dd, $J = 2.5, 10.2$ Hz, 1H, H5), 3.66 (dd, $J = 2.5, 10.2$ Hz, 1H, H5'), 4.38 (t, $J = 2.2$ Hz, 1H, H4), 4.52 (d, $J = 5.9$ Hz, 1H, H2), 4.57 (d, $J = 11.7$ Hz, 1H, Bn), 4.65 (d, $J = 11.7$ Hz, 1H, Bn), 4.74

(d, $J = 5.9$ Hz, 1H, H3), 5.28 (d, $J = 6.0$ Hz, 1H, H1), 7.29-7.30 (m, 5H, Ph); ^{13}C NMR δ 24.9 (CH₃), 26.5 (CH₃), 71.2 (C5), 74.1 (Bn), 82.0 (C3), 85.6 (C2), 87.5 (C4), 103.8 (C1), 112.1 (CMe₂), 127.5 (Ar), 128.5 (Ar), 136.2 (Ar); HRMS (TOF-ESI) m/z calcd for C₁₅H₂₀O₅Na⁺ [M+Na]⁺ 303.1197; found 303.1188.

Minor anomer had: ^1H NMR δ 1.38 and 1.55 (2 x s, 2 x 3H, 2 x CH₃), 3.54 (dd, $J = 2.5, 10.2$ Hz, 1H, H5), 3.61 (dd, $J = 2.5, 10.2$ Hz, 1H, H5'), 4.22 (t, $J = 2.2$ Hz, 1H, H4), 4.41 (d, $J = 11.7$ Hz, 1H, Bn), 4.48 (d, $J = 11.7$ Hz, 1H, Bn), 4.57 (dd, $J = 4.4, 6.5$ Hz, 1H, H2), 4.71 (dd, $J = 4.4, 6.5$ Hz, 1H, H3), 5.47 (dd, $J = 3.8, 11.9$ Hz, 1H, H1), 7.29-7.30 (m, 5H, Ph). ^{13}C NMR peaks for the ribose moiety: δ 72.0 (C5), 73.7 (Bn), 79.4 (C3), 79.7 (C2), 81.8 (C4), 97.8 (C1).

5-*O*-Benzyl-2,3-*O*-isopropylidene-D-ribitol (99).¹⁵² Treatment of **97** (55 mg, 0.20 mmol) with 2.5 equiv. of LTBH according to the general procedure gave **98**¹⁵² (19 mg, 34%) followed by **99** (31 mg, 55%). Diol **3** had: ^1H NMR δ 1.33 and 1.38 (2 x s, 2 x 3H, 2 x CH₃), 2.86 (m, 2H, 2 x OH), 3.55 (dd, $J = 6.7, 9.6$ Hz, 1H, H5), 3.74 (dd, $J = 9.6, 3.0$ Hz, 1H, H5'), 3.78 (m, 1H, H1), 3.86 (dd, $J = 7.8, 11.6$ Hz, 1H, H1'), 3.96 (m, 1H, H4), 4.10 (dd, $J = 5.8, 9.6$ Hz, 1H, H3), 4.35 (dt, $J = 5.2, 8.1$ Hz, 1H, H2), 4.59 (s, 2H, Bn), 7.34 (m, 5H, Ph).

4,6-*O*-Benzylidene-2,3-*O*-(tert-butyldimethylsilyl)- α/β -D-glucopyranose (158) Reduction of **157** (50 mg, 0.1 mmol; prepared by standard silylation 4,6-*O*-benzylidene-D-glucopyranose¹⁵³ with TBDMS/imidazole/DMF) according to the general procedure gave **158** (α/β , 1:1, 39 mg, 80%): ^1H NMR δ 0.010-0.17 (6 x s, 12H, MeSi), 0.75-0.98 (2 x s, 18H, *t*-BuSi), 3.92-4.00 (m, 1.5H), 4.13-4.20 (m, 2H), 4.25 (m, 1H), 4.35 (m, 0.5H), 4.44 (m, 1H), 5.07 (m, 0.5H, H1), 5.65 (m, 0.5H, H1), 6.12 (s, 0.5H, *CHPh*),

6.16 (s, 0.5H, *CHPh*), 7.35-7.48 (m, 5H, Ph); ^{13}C NMR δ -5.49, -5.46, -5.44, -5.17, -4.84, -4.77, -4.74, -4.71 (MeSi), 18.1 (*CMe*₃), 18.2 (*CMe*₃), 18.3 (*CMe*₃), 25.7 (Me), 25.8 (Me), 26.0 (Me), 26.1 (Me), 66.3 (C6), 66.4 (C6), 72.6 (C5), 74.7 (C5), 75.2 (C4), 75.3 (C4), 76.2 (C3), 79.8 (C3), 80.0 (C2), 80.7 (C2), 96.0 (*CH-Ph*), 97.5 (*CH-Ph*), 100.1 (C1), 103.8 (C1), 126.1 (Ar), 126.4 (Ar), 128.5 (Ar), 128.6 (Ar), 129.3 (Ar), 129.9 (Ar), 138.2 (Ar), 138.5 (Ar); HRMS (TOF-ESI) *m/z* calcd for $\text{C}_{25}\text{H}_{44}\text{O}_6\text{Si}_2\text{Na}^+$ [*M*+*Na*] $^+$ 519.2569; found 519.2587

4.4.2. ^1H NMR reaction profile for reduction of sugar lactone **97**

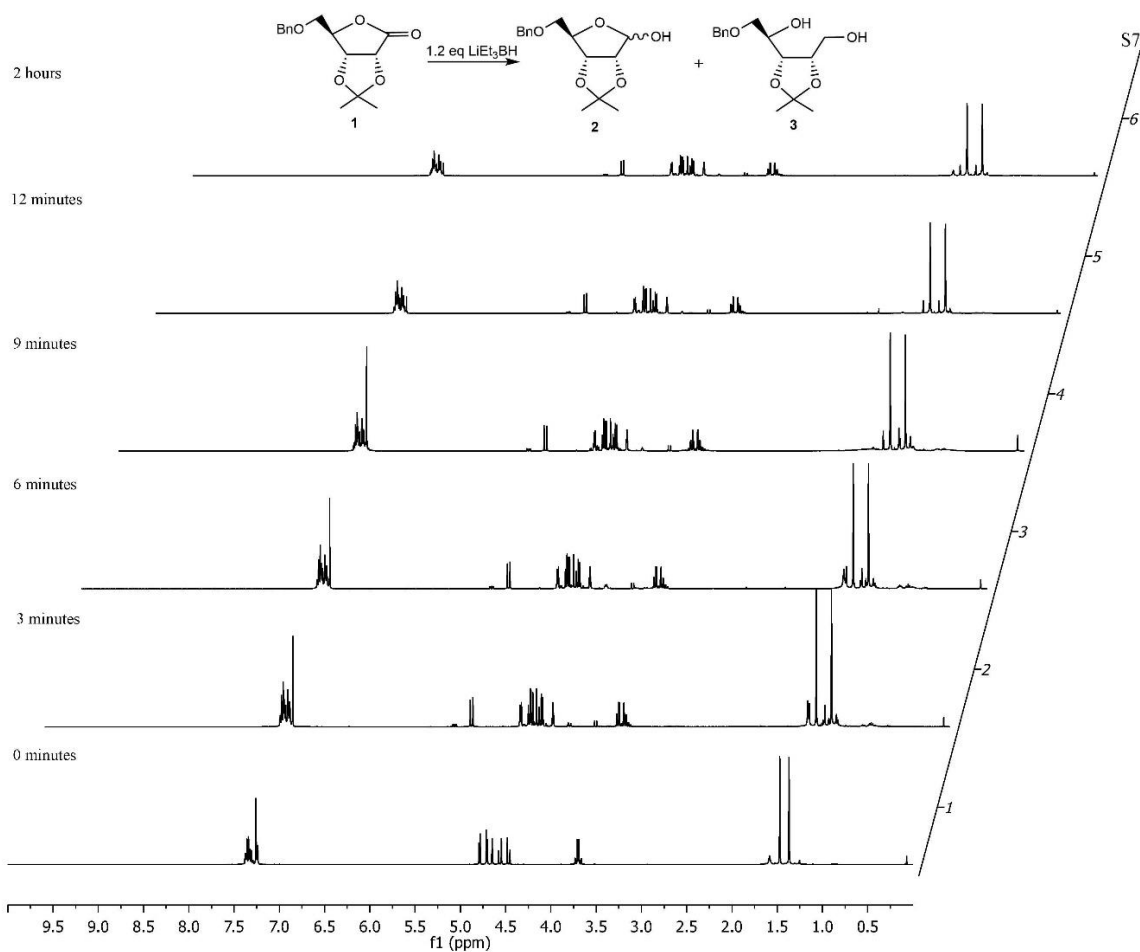


Figure 41. ^1H NMR spectra of reaction profile with 1.2 equiv. of LTBH

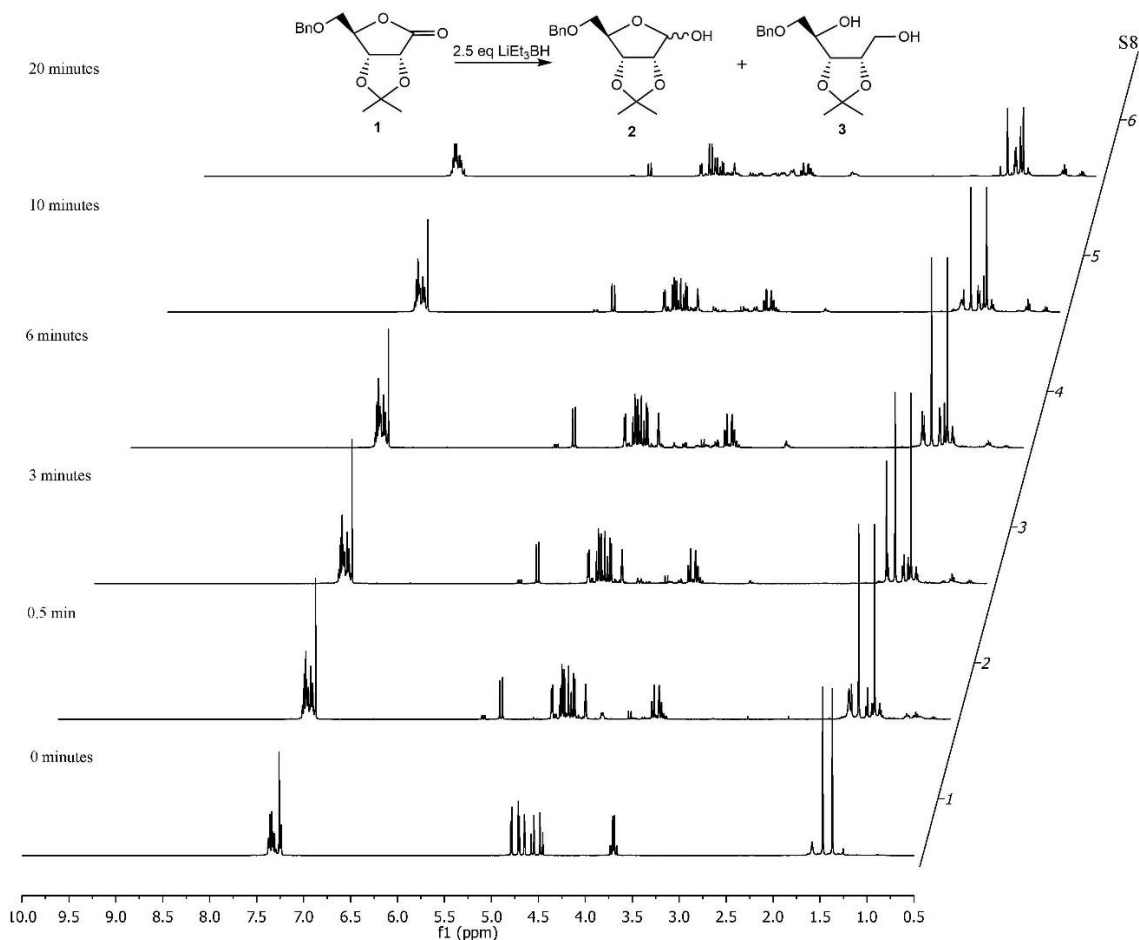


Figure 42. ^1H NMR spectra of reaction profile with 2.5 equiv. of LTBH

4.5. Biological evaluation and studies for 4-*N*-alkanoyl and alkyl gemcitabine analogues

Cytostatic evaluation in L1210 mouse leukemic cells

The L12010 cells were cultured in DMEM medium supplemented with 10% fetal bovine serum and antibiotics (Penicillin and Streptomycin) in a 5% CO_2 incubator maintained at 37 °C. Log phase cells were harvested and plated at 1.0×10^4 cells/well in 96-well microtiter plates. After cell attachment was assured, cells in microtiter plates were treated with increasing concentrations of gemcitabine analogs (0-200 $\mu\text{g}/\text{ml}$) and incubated in the CO_2 incubator at 37 °C for 72 h to induce cell death. MTT assay was performed

using the Cell Proliferation kit I (MTT) from Roche Biochemicals (Indianapolis, IN) and the plates were read in a Bio-Rad Benchmark multiwell plate reader at 570 nm wavelength with a reference wavelength of 655 nm. The percentage of surviving cells (% of control) was calculated and plotted against drug concentrations for estimating the IC (inhibitory concentration) values.

Cytostatic evaluation in HEK 293 cells

HEK 293 cells were cultured in DMEM medium supplemented with 10% fetal bovine serum and antibiotics (Penicillin and Streptomycin) in 5% CO₂ incubator maintained at 37 °C. Log phase cells were harvested and plated at 1.0 x 10⁴ to 1.0 x 10⁵ cells/well in 24-well microtiter plates. After 24 h incubation, cells were treated with increasing concentrations of gemcitabine analogs (0-200 µg/ml) and incubated in the CO₂ incubator at 37 °C for 24 to 72 h. Then, MTT reagent (Roche Diagnostics Corporation, Indianapolis, IN) was added at a final concentration of 50 µg/ml, and further incubated at 37°C and 5% CO₂. Next, the formazan crystals were dissolved in a detergent reagent, and each condition was then quantified via spectrophotometry (Bio-Rad Benchmark multiwell plate reader) at an optical density of 570 nm (OD₅₇₀).

Cell proliferation: HPLC studies with HEK 293 cells

For intracellular localization of **86**, HEK 293 cells were washed twice with PBS and then lysed with cell lysis buffer (50 mM Tris-HCl, 150 mM NaCl, 0.1% SDS, 0.5% sodium deoxycholate, 1% NP-40) in the presence of protease and phosphatase inhibitors. Lysates were collected with cell scrapers and cleared by centrifugation. Prior to HPLC analysis, cell lysates were re-suspended in H₂O, extracted with EtOAc and then subject to RP-HPLC analysis.

HEK 293 Cell Fluorescence Procedure

Cell incubation

HEK 293 cells were seeded in plates containing glass coverslips and incubated overnight. After incubation, fresh media solutions containing **86** (100 μ M) was added and then incubated for various durations (6, 12 and 24 h). Cells were fixed in paraformaldehyde (3.7%) for 15 min at room temperature, quenched, and washed with PBS as essentially described by Neef *et al.*¹³¹

CuAAC-mediated staining in fixed cells

HEK 293 Cells on coverslips were incubated upside-down with 50 μ L of freshly prepared staining mix (10 μ M Fluor alkyne, 1 mM CuSO₄, and 10 mM sodium ascorbate in PBS) for 1 h at room temperature in the dark. Cells were then to be washed with 0.1% Triton X-100 (in order to efficiently dissolve cellular membranes) in PBS, and PBS. Cells were then stained with DAPI for 15 min at room temperature in the dark. After incubation, cells were washing with PBS and coverslips were mounted and viewed on an Olympus FV1200 Laser confocal microscope.

Statistical analysis

All experiments were independently performed in triplicate. The standard error of the mean (SEM) of triplicates was utilized and significance was analyzed by one-way ANOVA. All statistical data were from averages of the three independent experiments. Results with *P<0.01 was considered statistically significant.

4.6. Radiosynthesis of ^{18}F Fluoro-silane probes

Materials

No-carrier-added [^{18}F]fluoride was produced by the $^{18}\text{O}(\text{p},\text{n})^{18}\text{F}$ reaction of [^{18}O]H₂O (84% isotopic purity, Zevacor Pharma, Noblesville, IN, USA) in an RDS-112 cyclotron (Siemens; Knoxville, TN, USA) at 11 MeV using a 1 mL tantalum target with havar foil. Anhydrous grade acetonitrile (CH₃CN), dimethylsulfoxide (DMSO), potassium carbonate (K₂CO₃), 200-proof ethanol (EtOH), and glacial acetic acid (AcOH) were purchased from Sigma-Aldrich (Milwaukee, WI, USA). HPLC grade acetonitrile was purchased from Fisher Scientific (Pittsburg, PA, USA). 4,7,13,16,21,24-Hexaoxa-1,10-diazabicyclo[8.8.8]hexacosane (Kryptofix K₂₂₂) and pre-conditioned quarternary methylammonium (QMA) cartridges were purchased from ABX Advanced Biochemical Compounds (Radeberg, Germany). The t-C18 plus short cartridge (WAT036810) was purchased from Waters (Milford, MA, USA).

For microfluidic radiochemistry chip fabrication, sulfuric acid (96%, cleanroom MB), hydrogen peroxide (30%, cleanroom LP), acetone (99.5%, cleanroom MB), and methanol (99.9%, cleanroom LP) were purchased from XMG Electronic Chemicals Inc. (Houston, TX, USA). Tridecafluoro-1,1,2,2-tetrahydrooctyl trichlorosilane (silane) was purchased from Gelest, Inc. (Morrisville, PA, USA), and Teflon AF 2400 1% solution was purchased from DuPont Fluoroproducts (Wilmington, DE, USA). Tape (TimeMed Label Tape) was obtained from Fisher Scientific.

Chromatography and analytical methods

Purification of [^{18}F]**108** was performed by semi-preparative HPLC using a WellChrom K-501 HPLC pump (Knauer; Berlin, Germany), reversed-phase Gemini-NX (5 μm , 10 x

250 mm, Phenomenex) column, ultraviolet (UV) detector (254 nm, WellChrom Spectrophotometer K-2501, Knauer) and gamma-radiation detector and counter (B-FC-3300 and B-FC-1000; Bioscan Inc.; Washington, DC, USA). Injection was performed using the ELIXYS HPLC injection valve connected to a 5 mL loop. The flow rate was 5 mL/min and a gradient elution of CH₃CN in H₂O was used (5% v/v CH₃CN for 0-5 min, ramp to 20% MeCN at 10 min, ramp to 30% CH₃CN at 20 min). The collected HPLC fraction was diluted with H₂O (30 mL) and trapped on a tC18 plus cartridge previously conditioned with 5 mL of EtOH and 10 mL of H₂O. The cartridge was then rinsed with additional H₂O (5 mL) and eluted with EtOH (1 mL). After complete evaporation of EtOH at 80°C, the purified product was dissolved in 2-3 mL PBS. [¹⁸F]**94** was synthesized but not purified.

Analytical HPLC was used to confirm the identity and radiochemical purity of the synthesized compound. Analytical HPLC was performed on a Knauer Smartline HPLC system with a C18 reverse-phase (Luna column (5 μm, 4.6 x 250 mm, Phenomenex) with in-line Knauer UV (254 nm) and gamma-radiation coincidence detector and counter (B-FC-4100 and B-FC-1000). Injections were performed with a manual injection valve (Rheodyne 7725i) with a 200 μL loop. For analysis of [¹⁸F]**96**, the mobile phase with 60% v/v CH₃CN in H₂O and flow rate was 1 mL/min. Retention times of **92** and **96** were 8.0 and 6.2 min, respectively. For analysis of [¹⁸F]**94**, the mobile phase was 80% v/v CH₃CN in H₂O and flow rate was 1.5 mL/min. Retention times of **90** and **94** were 6.1 and 4.3 min, respectively.

Radio-thin-layer-chromatography (radio-TLC) was performed on precut silica plates (Baker-flex®, J.T.Baker; Phillipsburg, NJ, USA). After spotting a tiny sample volume (~1-

5 μL) using a glass capillary, the plate was developed in the mobile phase. Chromatograms were obtained using a radio-TLC scanner (miniGita Star, Raytest USA, Inc.). The mobile phase was 95% v/v CH_3CN in H_2O . The R_f values for unreacted $[^{18}\text{F}]\text{fluoride}$, $[^{18}\text{F}]\mathbf{94}$ and $[^{18}\text{F}]\mathbf{96}$ were 0.0, 0.64, and 0.72, respectively.

Radiochemical purity (RCP) was determined by using both the radio-TLC and radio-HPLC radiation-detector chromatograms. The radio-TLC chromatogram enabled estimation of the fraction of $[^{18}\text{F}]\text{fluoride}$ that had been converted to product (plus any by-products). The radio-HPLC chromatogram (ignoring the $[^{18}\text{F}]\text{fluoride}$ peak) enabled estimation of the fraction of the desired product among ^{18}F -labeled species. The RCP was computed as the product of these two fractions. Crude radiochemical yield (crude RCY) was computed as the RCP multiplied by the fraction of the starting radioactivity collected at the end of the reaction (corrected for radioactive decay). Isolated RCY was determined by dividing the radioactivity of the purified, formulated product by the starting radioactivity (corrected for radioactive decay).

Macro-scale radiosyntheses of 4-*N*-alkanoyl $[^{18}\text{F}]\mathbf{94}$ and 4-*N*-alkyl $[^{18}\text{F}]\mathbf{96}$

The one-pot syntheses of 4-*N*-alkanoyl $[^{18}\text{F}]\mathbf{94}$ and 4-*N*-alkyl $[^{18}\text{F}]\mathbf{96}$ were adapted from literature^{90, 99} and performed on the ELIXYS FLEX/CHEM radiosynthesizer (Sofie Biosciences, Inc., Culver City, CA, USA). Briefly, $[^{18}\text{F}]\text{fluoride}$ in $[^{18}\text{O}]\text{H}_2\text{O}$ (1.9–37 GBq [50–1000 mCi]; average 15 GBq [400 mCi]) was trapped on a pre-conditioned QMA cartridge and eluted with 0.8 mL of a 3:5 H_2O : CH_3CN (v/v) solution containing 7 mg K_2CO_3 and 23 mg K_{222} into the reaction vessel. This solution was then dried at 110°C under nitrogen stream (7psi) and vacuum. To remove residual water, additional CH_3CN (1.2 mL) was added and the mixed solution again evaporated. This step was repeated a second time

to ensure water was fully removed. 2.5 mg of precursor (**90** or **92**) in DMSO with 1% v/v AcOH was then added to the dried [¹⁸F]KF/K₂₂₂ residue and reacted at 100°C for 25 min. After cooling, 2 mL of HPLC mobile phase was added, and the crude mixture was transferred to a 5 mL injection loop for HPLC purification.

The synthesis of [¹⁸F]**94** was performed only once. The crude radiochemical yield was 0.5% (n = 1) and further purification or synthesis optimization was not pursued. For [¹⁸F]**96**, the radiochemical yield was 6.6 % (n = 5) and the radiochemical purity was >99%. The synthesis time was 84 min, including purification and formulation.

The detailed ELIXYS synthesis program is describe in table 9, and the reagent setup is described in table 10.

Table 9. Details of ELIXYS radiosynthesis program.

Index	Operation	Source	Destination	Duration (s)	Temperature (°C)	Pressure (psi)	Other Parameters
1	Trap radionuclide	Source vial	Reactor 3	90	--	7	
2	Elute radionuclide	Reagent 1	Reactor 3	90	--	7	
3	Evaporate	--	Reactor 3	210	110	7	Stirring (500rpm); Cooling: 35°C
4	Elute radionuclide	Reagent 2	Reactor 3	60	--	7	
5	Evaporate	--	Reactor 3	105	110	7	Stirring (500rpm); Cooling: 35°C
6	Add Reagent	Reagent 3	Reactor 3	15	--	3	Add needle: 1; No stirring
7	Evaporate	--	Reactor 3	105	110	8	Stirring (500rpm); Cooling: 35°C

8	Add Reagent	Reagent 4	Reactor 3	15	--	3	Add needle: 1; No stirring
9	React	--	Reactor 3	1500	100	--	Seal position: 1; Stirring (500rpm); Cooling: 35°C
10	Add Reagent	Reagent 5	Reactor 3	15	--	3	Add needle: 1; Stirring (20s at 500rpm after 15s delay)
11	Transfer	Reactor 3	HPLC	0	--	0	Flow path: out; Loop loading mode: manual; No stirring

Table 10. Details of reagent positions in ELIXYS cassette.

Cassette #	Reagent Position				
	1	2	3	4	5
1	Eluent (7mg K ₂ CO ₃ + 23 mg K222 in 300 μL H ₂ O + 500 μL CH ₃ CN)	CH ₃ CN (1.2 mL)	CH ₃ CN (1.2 mL)	Precursor (2-3 mg in 400 μL DMSO +1% v/v AcOH)	CH ₃ CN/H ₂ O (2 mL, 5/95 v/v)

Microscale radiosyntheses of 4-*N*-alkanoyl [¹⁸F]94 and 4-*N*-alkyl [¹⁸F]96

Microscale radiochemistry chip fabrication

The microscale synthesis was performed in microdroplets on a simple microfluidic chip.^{138, 139} Glass microscope slides were cut into square pieces (25 x 25 x 1 mm), and cleaned by sonication in acetone (5 min), sonication in MeOH (5 min), rinsing with DI

water, and were then dried with nitrogen. Additional cleaning was then performed by submerging the glass pieces into Piranha cleaning solution (3:1 v/v mixture of sulfuric acid (96%) and hydrogen peroxide (30%)) for 15-30 min, then rinsing with DI water and drying with nitrogen. Cleaned substrates were silanized by placing them in a sealed chamber with a few drops of silane under reduced pressure overnight, followed by heating at 110°C for 10 min on a hot plate. Teflon AF solution was spin-coated (Headway PWM 32, Headway Research Inc., Garland, TX, USA) on one side of each chip using the following 3-step program: 500 RPM for 5 s (ramp rate 100 RPM/s), 1000 RPM for 30 s (ramp rate 500 RPM/s) and 0 RPM (ramp rate 1000 RPM/s). After coating, the glass chips were heated on a hotplate at 160°C for 10 min, then at 245°C for 10 min. Finally, the Teflon-coated chips were baked in a Carbolite oven (HTCR6 28 with 3216P1 programmer option, Carbolite Gero Ltd., UK) at 340°C for 3.5 h.

Temperature control

A custom temperature control system was assembled to heat and cool the glass chip. Heating was accomplished on top of a small rectangular 180 W ceramic heater with a built-in thermocouple (CER-1-01-00098 Ultramic heater, Watlow Electric Manufacturing Co., St. Louis, MO, USA). The heater temperature was controlled with a LabView program (National Instruments, Austin, TX, USA) using the thermocouple signal received through a data acquisition module (USB-201, Measurement Computing, Norton, MA, USA) via an on-off algorithm. The heater was affixed to a thermoelectric (Peltier) device for heat insulation and accelerated cooling of the when necessary. The Peltier device was fixed on an aluminum heatsink and fan. A small amount of thermal paste was used for adhesion and better thermal contact between chip and heater, heater and Peltier, and Peltier and heatsink.

On-chip synthesis

The microdroplet synthesis was performed using two Teflon-coated glass chips as shown in Figure 43. The first was placed (Teflon-coated side up) on the heater. [^{18}F]fluoride in [^{18}O]H $_2\text{O}$ (10 μL ; ~ 150 MBq [4 mCi]) was mixed with 12 μL of a 70:30 v/v CH $_3\text{CN}$ /H $_2\text{O}$ solution containing K $_{222}$ (0.23 μg) and K $_2\text{CO}_3$ (0.07 μg) and deposited in the center of the chip. Additional CH $_3\text{CN}$ (10 μL) was added to aid in azeotropic drying, and the chip was heated at 105°C until the droplet on chip shrank to a small volume (~ 1 μL). Next, 0.2 μg precursor (**90** or **92**) in 30 μL of DMSO with 1% v/v AcOH was added to the dried [^{18}F]KF/K $_{222}$ residue, and the reaction droplet was covered with the second glass chip (Teflon-coated side down). Tape affixed to the edges of the top chip resulted in a gap of ~ 150 μm between the substrates. The chip was heated at 100°C for 20 min. Crude product was extracted from chip by adding 20 μL of 1:1 v/v MeOH:H $_2\text{O}$ solution and then collecting the diluted mixture with a pipette. This process was repeated 2x for each substrate (~ 80 μL total volume).

Without purification, the microscale synthesis took ~ 45 min. Decay-corrected crude radiochemical yield for 4-*N*-alkanoyl [^{18}F]**94** was 10 % (n = 1) and for 4-*N*-alkyl [^{18}F]**96** was 24.4% (n = 5). The crude yield for 4-*N*-alkanoyl [^{18}F]**94** was 10% (n = 1) and for 4-*N*-alkyl [^{18}F]**96** was 27.2% (n = 5). Purification and formulation added additional time to the synthesis.

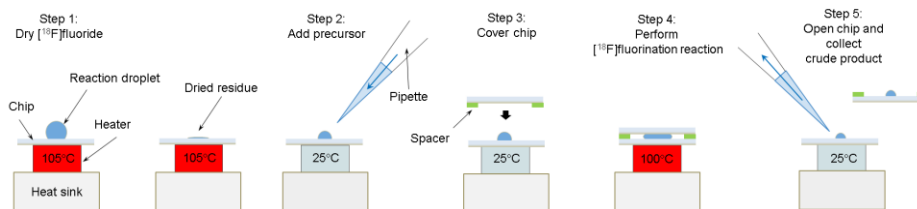


Figure 43. Schematic of the microdroplet radiosynthesis process.

4.7. Biological and PET evaluation of [¹⁸F]-4-*N*-alkyl gemcitabine radioligand 96

Stability in formulation

Methods

After purification, the collected HPLC fraction (3-4 mL) of [¹⁸F]96 was collected in a V-vial. The mobile phase was evaporated to dryness at 75°C with nitrogen stream. The dried residue was then dissolved in 0.3 mL EtOH. 2.7 mL saline was added to the vial, and the mixture was passed through a sterilization filter. Samples of the formulated tracer were analyzed via radio-HPLC (analytical conditions previously described) at various timepoints.

In vivo imaging

Methods

PET/CT was performed on the Genisys 8 PET/CT (Sofie Biosciences, USA). The Genisys 8 PET/CT is an integrated scanner with a PET subsection that consists of 8 detectors with BGO scintillator array arranged in a box geometry and a back section consisting of a rotating CT gantry.

For static PET scans, a WT C57BL/6 mouse was injected with approximately 75 µCi [¹⁸F]96 via tail vein. After 60 min of conscious uptake, mice were anesthetized with 1.5% isoflurane and placed in a dedicated imaging chamber. microPET images were acquired for 600 sec with an energy window of 150-650 keV, reconstructed using maximum-likelihood expectation maximization as recommended by the vendor. All images were corrected for CT-based photon attenuation, detector normalization and radioisotope decay (scatter correction was not applied) and converted to units of percent injected dose per gram (%ID/g).

For dynamic PET scans, a WT C57BL/6 mouse was anesthetized with 2% isoflurane, placed in a dedicated imaging chamber with heating, and catheterized. Dynamic microPET imaging was started concurrently at the beginning of a 10 sec infusion via the catheter with approximately 75 μ Ci of [18 F]**96**. Data was acquired in listmode for 3600 sec with an energy window of 150-650 keV and histogrammed into a frame sequence of 4 x 15 sec, 8 x 30 sec, 5 x 60 sec, 4 x 300 sec, 3 x 600 sec. Images were reconstructed using maximum-likelihood expectation maximization as recommended by the vendor. All images were corrected for photon attenuation, detector normalization and radioisotope decay (scatter correction was not applied) and converted to units of percent injected dose per gram (%ID/g).

All PET acquisitions were immediately followed by CT acquisition. The CT section consists of a gantry and flywheel that uses a 50 kVp, 200 μ A x-ray source and flat-panel detector. The CT acquires images in a continuous-rotation mode and with standard CT acquisition time of 50 s. Standard scans are acquired with 720 projections at 55 ms per projection, and reconstructed using a Feldkamp algorithm.

Metabolite analysis

Methods

In one experiment, mouse blood was incubated with 0.5 mCi of [18 F]**96** for 30 min at 37°C. A sample of this mixture was taken and centrifuged for 5 min. The supernatant (plasma fraction) was collected. The pellet (cell fraction) was washed twice with PBS and the collected liquid mixed with the previous plasma fraction. The radioactivity in each fraction was measured.

In a second experiment, a mouse was injected via tail vein with 1 mCi of [^{18}F]96 and 800 μL was drawn from the mouse 30 min after injection, and was separated and counted as above.

5. CONCLUSION

In this dissertation I reported the synthesis of gemcitabine analogues with 4-*N*-alkanoyl and 4-*N*-alkyl modifications bearing i) β -keto sulfonate moiety or ii) silicon-fluoride acceptor building blocks with both chemotherapeutic properties and ability for the ^{18}F incorporation with possible application as gemcitabine PET radiotracers.

The 4-*N*-alkylgemcitabine analogues with a β -keto sulfonate moieties were synthesized with the goal of overcoming defluorination that can occur with the presence of hydrogens at the β - carbon to the fluorine atom. The presence of these hydrogens have shown to occur in previous PET-imaging results with other 4-*N*-alkylgemcitabine analogues.³⁸ The target analogue was synthesized by coupling the *p*-toluenesulfonamido group in 4-*N*-tosylgemcitabine with an alkyl amine possessing a terminal olefin. This terminal olefin was then modified through several oxidation steps to β -keto with sulfonate groups that have the ability to be fluorinated.

The synthesis of 4-*N*-alkanoylgemcitabines with silicon fluoride acceptor building blocks was achieved by coupling of gemcitabine **1** with the various carboxylic acids using peptide coupling conditions (HOBt/EDC). This method was versatile in that it allowed introduction of aliphatic chains with different terminal functional groups such as azido and alkynes that are compatible for click chemistry. The click reaction with dialkylsilyl-fluoride acceptor building blocks afforded the 4-*N*-alkanoylsilanegemcitabine analogues in short reaction times and high yield. The synthesis of the 4-*N*-alkylgemcitabine with silicon fluoride acceptor building block was achieved by displacement of the *p*-toluenesulfonamido group in 4-*N*-tosylgemcitabine with the corresponding alkyl amine with the terminal azido moiety. Analogously to the alkanoyl analogues, they were coupled

with dialkylsilyl fluoride acceptor building blocks through click chemistry to afford the 4-*N*-alkylsilylanegemcitabine analogue.

Evaluation on mice tumor cell lines (L1210) revealed potent cytotoxic activities for the 4-*N*-alkanoylgemcitabines, with IC₅₀ values in the nM range, comparable to the parent gemcitabine while the 4-*N*-alkylgemcitabines displayed almost no cytotoxic activity. Additionally, biological studies were performed to observe the cellular uptake of 4-*N*-alkyl analogue **86** in HEK293 cells using both HPLC analysis and fluorescence microscopy. These experiments clearly showed that these type of analogues are incorporated into the cell and their lack of hydrolysis into the parent drug inside explain their low cytotoxic activity.

Both 4-*N*-alkanoyl and 4-*N*-alkyl modified gemcitabine analogues were then successfully fluorinated following protocols that are used in radiosynthetic settings using KF and Kryptofix-222 at elevated temperatures. In the case of the analogues bearing the silicon-fluoride acceptors, the protocol did not require harsh deprotection steps after fluorination, but the caution of silicon-fluoride hydrolysis was taken into consideration. The 4-*N*-alkylgemcitabine with β -keto sulfonate analogue was successfully fluorinated via both mesylate and tosylate intermediates followed by a deprotection step. The developed fluorination protocol was then successfully applied for the synthesis of both [¹⁸F]-4-*N*-[11-undecanoyl-(fluoro-di-*iso*-propylsilyl)-*O*-propargylbenzyltriazol]gemcitabine and [¹⁸F]-4-*N*-[7-heptanyl-(fluoro-di-*iso*-propylsilyl)-*O*-propargylbenzyltriazol]gemcitabine radioligands using macroscale and microscale radiolabeling protocols. These radioligands were then evaluated through preliminary stability in formulation studies, *in vivo* PET imaging and metabolite analysis in blood.

Lastly, in studying the efficient reduction of lactones to hemiacetals, I developed an efficient protocol for the reduction of sugar γ - and δ -lactones with LTBH (1.2 equiv.) in CH_2Cl_2 (0°C, 30 min.) to the corresponding hemiacetals. Several ribono- and gulono-1,4-lactone as well as glucono-1,5-lactones were reduced to the corresponding pentose or hexose derivatives in high yields. The reduction with LTBH can be carried out in the presence of protecting groups such as trityl, benzyl, silyl (TMS or TBDMS), isopropylidene/benzylidene and to some extent acyl (Bz, or Ac) that are commonly used in the synthetic carbohydrate chemistry.

REFERENCES

- 1 Gesto, D. S.; Cerqueira, N. M. F. S. A.; Fernandes, P. A.; Ramos, M. J. *Curr. Med. Chem.* **2012**, *19*, 1076-1087.
- 2 Toschi, L.; Finocchiaro, G.; Bartolini, S.; Gioia, V.; Cappuzzo, F. *Future Oncol.* **2005**, *1*, 7-17.
- 3 Brown, K.; Dixey, M.; Weymouth-Wilson, A.; Linclau, B. *Carbohydr. Res.* **2014**, *387*, 59-73.
- 4 Hertel, L. W.; Kroin, J. S.; Misner, J. W.; Tustin, J. M. *J. Org. Chem.* **1988**, *53*, 2406-2409.
- 5 Mackey, J. R.; Mani, R. S.; Selner, M.; Mowles, D.; Young, J. D.; Belt, J. A.; Crawford, C. R.; Cass, C. E. *Cancer Res.* **1998**, *58*, 4349-4357.
- 6 Gandhi, V.; Plunkett, W. *Cancer Res.* **1990**, *50*, 3675-3680.
- 7 Huang, P.; Chubb, S.; Hertel, L. W.; Grindey, G. B.; Plunkett, W. *Cancer Res.* **1991**, *51*, 6110-6117.
- 8 Plunkett, W.; Huang, P.; Xu, Y. Z.; Heinemann, V.; Grunewald, R.; Gandhi, V. *Semin. Oncol.* **1995**, *22*, 3-10.
- 9 Mini, E.; Nobili, S.; Caciagli, B.; Landini, I.; Mazzei, T. *Ann. Oncol.* **2006**, *17*, v7-v12.
- 10 Ewald, B.; Sampath, D.; Plunkett, W. *Oncogene* **2008**, *27*, 6522-6537.
- 11 Wang, J.; Lohman, G. J. S.; Stubbe, J. *Biochem.* **2009**, *48*, 11612-11621.
- 12 Lohman, G. J. S.; Stubbe, J. *Biochem.* **2010**, *49*, 1404-1417.
- 13 Baker, C. H.; Banzon, J.; Bollinger, J. M.; Stubbe, J.; Samano, V.; Robins, M. J.; Lippert, B.; Jarvi, E.; Resvick, R. *J. Med. Chem.* **1991**, *34*, 1879-1884.
- 14 Shipley, L. A.; Brown, T. J.; Cornpropst, J. D.; Hamilton, M.; Daniels, W. D.; Culp, H. W. *Drug Metab. Dispos.* **1992**, *20*, 849-855.
- 15 Veltkamp, S. A.; Beijnen, J. H.; Schellens, J. H. M. *Oncologist* **2008**, *13*, 261-276.
- 16 Horton, N. D.; Young, J. K.; Perkins, E. J.; Truex, L. L. *Cancer Res.* **2004**, *64*, 486-487.

- 17 Veltkamp, S. A.; Pluim, D.; van Tellingen, O.; Beijnen, J. H.; Schellens, J. H. M. *Drug Metab. Dispos.* **2008**, *36*, 1606-1615.
- 18 Hodge, L. S.; Taub, M. E.; Tracy, T. S. *Drug Metab. Dispos.* **2011**, *39*, 2013-2016.
- 19 Moysan, E.; Bastiat, G.; Benoit, J.-P. *Mol. Pharm.* **2013**, *10*, 430-444.
- 20 Song, X.; Lorenzi, P. L.; Landowski, C. P.; Vig, B. S.; Hilfinger, J. M.; Amidon, G. L. *Mol. Pharm.* **2005**, *2*, 157-167.
- 21 Bender, D. M.; Bao, J.; Dantzig, A. H.; Diserod, W. D.; Law, K. L.; Magnus, N. A.; Peterson, J. A.; Perkins, E. J.; Pu, Y. J.; Reutzel-Edens, S. M.; Remick, D. M.; Starling, J. J.; Stephenson, G. A.; Vaid, R. K.; Zhang, D.; McCarthy, J. R. *J. Med. Chem.* **2009**, *52*, 6958-6961.
- 22 Rejiba, S.; Reddy, L. H.; Bigand, C.; Parmentier, C.; Couvreur, P.; Hajri, A. *Nanomedicine* **2011**, *7*, 841-849.
- 23 Krajewska, E.; Shugar, D. *Acta Biochim. Pol.* **1975**, *22*, 185-194.
- 24 Immordino, M. L.; Brusa, P.; Rocco, F.; Arpicco, S.; Ceruti, M.; Cattel, L. *J. Control. Release* **2004**, *100*, 331-346.
- 25 Chung, W. G.; Sandoval, M. A.; Sloat, B. R.; Lansakara, P. D.; Cui, Z. *J. Control. Release* **2012**, *157*, 132-140.
- 26 Couvreur, P.; Stella, B.; Reddy, L. H.; Hillaireau, H.; Dubernet, C.; Desmaele, D.; Lepetre-Mouelhi, S.; Rocco, F.; Dereuddre-Bosquet, N.; Clayette, P.; Rosilio, V.; Marsaud, V.; Renoir, J. M.; Cattel, L. *Nano Lett* **2006**, *6*, 2544-2548.
- 27 Koolen, S. L.; Witteveen, P. O.; Jansen, R. S.; Langenberg, M. H.; Kronemeijer, R. H.; Nol, A.; Garcia-Ribas, I.; Callies, S.; Benhadji, K. A.; Slapak, C. A.; Beijnen, J. H.; Voest, E. E.; Schellens, J. H. *Clin. Cancer Res.* **2011**, *17*, 6071-6082.
- 28 Pulido, J.; Sobczak, A. J.; Balzarini, J.; Wnuk, S. F. *J. Med. Chem.* **2014**, *57*, 191-203.
- 29 May, J. P.; Undzys, E.; Roy, A.; Li, S.-D. *Bioconjugate Chem.* **2016**, *27*, 226-237.
- 30 Dubey, R. D.; Saneja, A.; Gupta, P. K.; Gupta, P. N. *Eur. J. Pharm. Sci.* **2016**, *93*, 147-162.
- 31 Dasari, M.; Acharya, A. P.; Kim, D.; Lee, S.; Lee, S.; Rhea, J.; Molinaro, R.; Murthy, N. *Bioconjugate Chem.* **2013**, *24*, 4-8.

- 32 Han, H.; Jin, Q.; Wang, Y.; Chen, Y.; Ji, J. *Chem. Commun.* **2015**, *51*, 17435-17438.
- 33 Bergman, A. M.; Adema, A. D.; Balzarini, J.; Bruheim, S.; Fichtner, I.; Noordhuis, P.; Fodstad, Ø.; Myhren, F.; Sandvold, M. L.; Hendriks, H. R.; Peters, G. J. *Invest. New Drug.* **2011**, *29*, 456-466.
- 34 Tsume, Y.; Incecayir, T.; Song, X.; Hilfinger, J. M.; Amidon, G. L. *Eur. J. Pharm. Biopharm.* **2014**, *86*, 514-523.
- 35 Faivre, S. J.; Olszanski, A. J.; Weigang-Köhler, K.; Riess, H.; Cohen, R. B.; Wang, X.; Myrand, S. P.; Wickremsinhe, E. R.; Horn, C. L.; Ouyang, H.; Callies, S.; Benhadji, K. A.; Raymond, E. *Invest. New Drug.* **2015**, *33*, 1206-1216.
- 36 Pratt, S. E.; Durland-Busbice, S.; Shepard, R. L.; Heinz-Taheny, K.; Iversen, P. W.; Dantzig, A. H. *Clin. Cancer Res.* **2013**, *19*, 1159-1168.
- 37 Wickremsinhe, E.; Bao, J.; Smith, R.; Burton, R.; Dow, S.; Perkins, E. *Pharmaceutics* **2013**, *5*, 261.
- 38 Pulido, J. In *Design and Synthesis of 4-N-Alkanoyl and 4-N-Alkyl Gemcitabine Analogues Suitable for Positron Emission Tomography*; Florida International University, Miami Florida, 2014; Vol. Chemistry
- 39 Karampelas, T.; Argyros, O.; Sayyad, N.; Spyridaki, K.; Pappas, C.; Morgan, K.; Kolios, G.; Millar, R. P.; Liapakis, G.; Tzakos, A. G.; Fokas, D.; Tamvakopoulos, C. *Bioconjugate Chem.* **2014**, *25*, 813-823.
- 40 Hamsici, S.; Sardan Ekiz, M.; Cinar Ciftci, G.; Tekinay, A. B.; Guler, M. O. *Bioconjugate Chem.* **2017**.
- 41 Lee, G. Y.; Qian, W. P.; Wang, L.; Wang, Y. A.; Staley, C. A.; Satpathy, M.; Nie, S.; Mao, H.; Yang, L. *ACS Nano* **2013**, *7*, 2078-2089.
- 42 Wang, W.; Li, C.; Zhang, J.; Dong, A.; Kong, D. *J. Mater. Chem. B* **2014**, *2*, 1891-1901.
- 43 Hu, X.; Yan, L.; Xiao, H.; Li, X.; Jing, X. *J. Appl. Polym. Sci.* **2013**, *127*, 3365-3373.
- 44 Duangjai, A.; Luo, K.; Zhou, Y.; Yang, J.; Kopeček, J. *Eur. J. Pharm. Biopharm.* **2014**, *87*, 187-196.
- 45 Menard-Moyon, C.; Ali-Boucetta, H.; Fabbro, C.; Chaloin, O.; Kostarelos, K.; Bianco, A. *Chemistry* **2015**, *21*, 14886-14892.

- 46 Kolb, H. C.; Finn, M. G.; Sharpless, K. B. *Angew. Chem., Int. Ed.* **2001**, *40*, 2004-2021.
- 47 Huisgen, R. *Angew. Chem., Int. Ed.* **1963**, *2*, 565-598.
- 48 Scriven, E. F. V.; Turnbull, K. *Chem. Rev.* **1988**, *88*, 297-368.
- 49 Tron, G. C.; Pirali, T.; Billington, R. A.; Canonico, P. L.; Sorba, G.; Genazzani, A. A. *Med. Res. Rev.* **2008**, *28*, 278-308.
- 50 Rostovtsev, V. V.; Green, L. G.; Fokin, V. V.; Sharpless, K. B. *Angew. Chem., Int. Ed.* **2002**, *41*, 2596-2599.
- 51 Tornøe, C. W.; Christensen, C.; Meldal, M. *J. Org. Chem.* **2002**, *67*, 3057-3064.
- 52 Amblard, F.; Cho, J. H.; Schinazi, R. F. *Chem. Rev.* **2009**, *109*, 4207-4220.
- 53 Hein, C. D.; Liu, X.-M.; Wang, D. *Pharm. Res.* **2008**, *25*, 2216-2230.
- 54 El-Sagheer, A. H.; Brown, T. *Chem. Soc. Rev.* **2010**, *39*, 1388-1405.
- 55 Haque, M. M.; Peng, X. *Sci. China Chem.* **2014**, *57*, 215-231.
- 56 Xi, W.; Scott, T. F.; Kloxin, C. J.; Bowman, C. N. *Adv. Funct. Mater.* **2014**, *24*, 2572-2590.
- 57 Nwe, K.; Brechbiel, M. W. *Cancer Biother. Radiopharm.* **2009**, *24*, 289-302.
- 58 Neef, A. B.; Pernot, L.; Schreier, V. N.; Scapozza, L.; Luedtke, N. W. *Angew. Chem., Int. Ed.* **2015**, *54*, 7911-7914.
- 59 Lee, M. H.; Sessler, J. L.; Kim, J. S. *Acc. Chem. Res.* **2015**, *48*, 2935-2946.
- 60 Bhuniya, S.; Lee, M. H.; Jeon, H. M.; Han, J. H.; Lee, J. H.; Park, N.; Maiti, S.; Kang, C.; Kim, J. S. *Chem. Commun.* **2013**, *49*, 7141-7143.
- 61 Maiti, S.; Park, N.; Han, J. H.; Jeon, H. M.; Lee, J. H.; Bhuniya, S.; Kang, C.; Kim, J. S. *J. Am. Chem. Soc.* **2013**, *135*, 4567-4572.
- 62 Yang, Z.; Lee, J. H.; Jeon, H. M.; Han, J. H.; Park, N.; He, Y.; Lee, H.; Hong, K. S.; Kang, C.; Kim, J. S. *J. Am. Chem. Soc.* **2013**, *135*, 11657-11662.
- 63 Liu, L.-H.; Qiu, W.-X.; Li, B.; Zhang, C.; Sun, L.-F.; Wan, S.-S.; Rong, L.; Zhang, X.-Z. *Adv. Funct. Mater.* **2016**, *26*, 6257-6269.
- 64 Gambhir, S. S. *Nat. Rev. Cancer* **2002**, *2*, 683-693.
- 65 Phelps, M. E. *Proc. Natl. Acad. Sci. U.S.A.* **2000**, *97*, 9226-9233.

- 66 Cai, L.; Lu, S.; Pike, V. W. *Eur. J. Org. Chem.* **2008**, 2008, 2853-2873.
- 67 Coenen, H. H. In *Fluorine-18 Labeling Methods: Features and Possibilities of Basic Reactions*; Springer Berlin Heidelberg, Berlin, Heidelberg, 2007. pp 15-50.
- 68 Jacobson, O.; Kiesewetter, D. O.; Chen, X. *Bioconjugate Chem.* **2015**, 26, 1-18.
- 69 Park, B. K.; Kitteringham, N. R. *Drug Metab. Rev.* **1994**, 26, 605-643.
- 70 Orit, J.; Xiaoyuan, C. *Curr. Top. Med. Chem.* **2010**, 10, 1048-1059.
- 71 Neumann, C. N.; Hooker, J. M.; Ritter, T. *Nature* **2016**, 534, 369-373.
- 72 Furuya, T.; Kuttruff, C. A.; Ritter, T. *Cur. Opin. Drug Discov. Devel.* **2008**, 11, 803-819.
- 73 Lemaire, C.; Cantineau, R.; Guillaume, M.; Plenevaux, A.; Christiaens, L. *J. Nucl. Med.* **1991**, 32, 2266-2272.
- 74 Gründer, G.; Siessmeier, T.; Lange-Asschenfeldt, C.; Vernaleken, I.; Buchholz, H.-G.; Stoeter, P.; Drzezga, A.; Lüddens, H.; Rösch, F.; Bartenstein, P. *Eur. J. Nucl. Med.* **2001**, 28, 1463-1470.
- 75 Farwell, M. D.; Pryma, D. A.; Mankoff, D. A. *Cancer* **2014**, 120, 3433-3445.
- 76 Alauddin, M. M. *Am. J. Nucl. Med. Mol. Img.* **2012**, 2, 55-76.
- 77 Britton, T.; Robinson, N. *J. Nucl. Med. Technol.* **2016**, 44, 59-64.
- 78 Pretze, M.; Wangler, C.; Wangler, B. *BioMed Res. Int.* **2014**, 2014, 12.
- 79 Zanzonico, P. In *Prostate Cancer: 16β-[18F] Fluoro-5α-Dihydrotestosterone (FDHT) Whole-Body Positron Emission Tomography*; Springer Netherlands, Dordrecht, 2008. pp 521-530.
- 80 Wagner, M.; Seitz, U.; Buck, A.; Neumaier, B.; Schultheiß, S.; Bangerter, M.; Bommer, M.; Leithäuser, F.; Wawra, E.; Munzert, G.; Reske, S. N. *Cancer Res.* **2003**, 63, 2681-2687.
- 81 Radu, C. G.; Shu, C. J.; Nair-Gill, E.; Shelly, S. M.; Barrio, J. R.; Satyamurthy, N.; Phelps, M. E.; Witte, O. N. *Nat. Med.* **2008**, 14, 783-788.
- 82 Laing, R. E.; Walter, M. A.; Campbell, D. O.; Herschman, H. R.; Satyamurthy, N.; Phelps, M. E.; Czernin, J.; Witte, O. N.; Radu, C. G. *Proc. Natl. Acad. Sci. U.S.A.* **2009**, 106, 2847-2852.

- 83 Schwarzenberg, J.; Radu, C. G.; Benz, M.; Fueger, B.; Tran, A. Q.; Phelps, M. E.; Witte, O. N.; Satyamurthy, N.; Czernin, J.; Schiepers, C. *Eur. J. Nucl. Med. Mol. Imaging* **2011**, *38*, 711-721.
- 84 Hoover, A. J.; Lazari, M.; Ren, H.; Narayanam, M. K.; Murphy, J. M.; van Dam, R. M.; Hooker, J. M.; Ritter, T. *Organometallics* **2016**, *35*, 1008-1014.
- 85 Gens, T. A.; Wethongton, J. A.; Brosi, A. R. *J. Phys. Chem.* **1958**, *62*, 1593-1593.
- 86 Winfield, J. M. *J. Fluorine Chem.* **1980**, *16*, 1-17.
- 87 Rosenthal, M. S.; Bosch, A. L.; Nickles, R. J.; Gatley, S. J. *Int. J. Appl. Radiat. Is.* **1985**, *36*, 318-319.
- 88 Choudhry, U.; Martin, K. E.; Biagini, S.; Blower, P. J. *Nucl. Med. Commun.* **2006**, *27*, 293.
- 89 Schirmacher, R.; Bradtmöller, G.; Schirmacher, E.; Thews, O.; Tillmanns, J.; Siessmeier, T.; Buchholz, H. G.; Bartenstein, P.; Wängler, B.; Niemeyer, C. M.; Jurkschat, K. *Angew. Chem., Int. Ed.* **2006**, *45*, 6047-6050.
- 90 Mu, L.; Hohne, A.; Schubiger, P. A.; Ametamey, S. M.; Graham, K.; Cyr, J. E.; Dinkelborg, L.; Stellfeld, T.; Srinivasan, A.; Voigtmann, U.; Klar, U. *Angew. Chem. Int. Ed. Engl.* **2008**, *47*, 4922-4925.
- 91 Höhne, A.; Yu, L.; Mu, L.; Reiher, M.; Voigtmann, U.; Klar, U.; Graham, K.; Schubiger, P. A.; Ametamey, S. M. *Chem-Eur J.* **2009**, *15*, 3736-3743.
- 92 Schirmacher, E.; Wängler, B.; Cypriak, M.; Bradtmöller, G.; Schäfer, M.; Eisenhut, M.; Jurkschat, K.; Schirmacher, R. *Bioconjugate Chem.* **2007**, *18*, 2085-2089.
- 93 Wängler, C.; Niedermoser, S.; Chin, J.; Orchowski, K.; Schirmacher, E.; Jurkschat, K.; Iovkova-Berends, L.; Kostikov, A. P.; Schirmacher, R.; Wängler, B. *Nat. Protocols* **2012**, *7*, 1946-1955.
- 94 Wängler, C.; Kostikov, A.; Zhu, J.; Chin, J.; Wängler, B.; Schirmacher, R. *Appl. Sci.* **2012**, *2*, 277.
- 95 Tietze, L. F.; Schmuck, K. *Synlett* **2011**, *2011*, 1697-1700.
- 96 Iovkova, L.; Könnig, D.; Wängler, B.; Schirmacher, R.; Schoof, S.; Arndt, H.-D.; Jurkschat, K. *Eur. J. Inorg. Chem.* **2011**, *2011*, 2238-2246.
- 97 Wuest, F.; Berndt, M.; Bergmann, R.; van den Hoff, J.; Pietzsch, J. *Bioconjugate Chem.* **2008**, *19*, 1202-1210.

- 98 Wängler, B.; Kostikov, A. P.; Niedermoser, S.; Chin, J.; Orchowski, K.; Schirmacher, E.; Iovkova-Berends, L.; Jurkschat, K.; Wängler, C.; Schirmacher, R. *Nat. Protocols* **2012**, *7*, 1964-1969.
- 99 Schulz, J.; Vimont, D.; Bordenave, T.; James, D.; Escudier, J.-M.; Allard, M.; Szlosek-Pinaud, M.; Fouquet, E. *Chem-Eur J.* **2011**, *17*, 3096-3100.
- 100 James, D.; Escudier, J.-M.; Amigues, E.; Schulz, J.; Vitry, C.; Bordenave, T.; Szlosek-Pinaud, M.; Fouquet, E. *Tetrahedron Lett.* **2010**, *51*, 1230-1232.
- 101 Chaveriat, L.; Stasik, I.; Demailly, G.; Beaupère, D. *Tetrahedron Asymmetr.* **2005**, *16*, 623-627.
- 102 Lalot, J.; Stasik, I.; Demailly, G.; Beaupère, D. *Carbohydr. Res.* **2003**, *338*, 2241-2245.
- 103 Lalot, J.; Manier, G.; Stasik, I.; Demailly, G.; Beaupère, D. *Carbohydr. Res.* **2001**, *335*, 55-61.
- 104 Takahashi, H.; Hitomi, Y.; Iwai, Y.; Ikegami, S. *J. Am. Chem. Soc.* **2000**, *122*, 2995-3000.
- 105 Wolf, J.; Jarrige, J. M.; Florent, J. C.; Grierson, D. S.; Monneret, C. *Synthesis* **1992**, 773-778.
- 106 Beach, J. W.; Kim, H. O.; Jeong, L. S.; Nampalli, S.; Islam, Q.; Ahn, S. K.; Babu, J. R.; Chu, C. K. *J. Org. Chem.* **1992**, *57*, 3887-3894.
- 107 Chou, T. S.; Heath, P. C.; Patterson, L. E.; Poteet, L. M.; Lakin, R. E.; Hunt, A. H. *Synthesis* **1992**, *1992*, 565-570.
- 108 Choi, W. B.; Wilson, L. J.; Yeola, S.; Liotta, D. C.; Schinazi, R. F. *J. Am. Chem. Soc.* **1991**, *113*, 9377-9379.
- 109 Seyden-Penne, J.; Editor *Reductions by the Alumino- and Borohydrides in Organic Synthesis, Second Edition*; Wiley, 1997.
- 110 Malladi, V. L. A.; Sobczak, A. J.; Meyer, T. M.; Pei, D.; Wnuk, S. F. *Bioorg. Med. Chem.* **2011**, *19*, 5507-5519.
- 111 Malladi, V. L. A.; Sobczak, A. J.; Maricic, N.; Murugapiran, S. K.; Schneper, L.; Makemson, J.; Mathee, K.; Wnuk, S. F. *Bioorg. Med. Chem.* **2011**, *19*, 5500-5506.
- 112 Chbib, C.; Sobczak, A. J.; Mudgal, M.; Gonzalez, C.; Lumpuy, D.; Nagaj, J.; Stokowa-Soltys, K.; Wnuk, S. F. *J. Sulfur. Chem.* **2016**, 307-327.

- 113 Fleming, I. *Comprehensive Organic Synthesis: Selectivity, Strategy and Efficiency in Modern Organic Chemistry, Volume 8: Reduction*; Pergamon, 1992.
- 114 Cragg, G. M. L. *Organoboranes in Organic Synthesis*; Dekker, 1973.
- 115 Abdek-Akher, M.; Hamilton, J. K.; Smith, F. *J. Am. Chem. Soc.* **1951**, *73*, 4691-4692.
- 116 Andriescu, A. *Cellul. Chem. Technol.* **1998**, *32*, 163.
- 117 Santaniello, E.; Ferraboschi, P.; Sozzani, P. *J. Org. Chem.* **1981**, *46*, 4584-4585.
- 118 Brown, H. C.; Rao, B. C. S. *J. Am. Chem. Soc.* **1955**, *77*, 3164-3164.
- 119 Ishii, H.; Dzyuba, S. V.; Nakanishi, K. *Org. Biomol. Chem.* **2005**, *3*, 3471-3472.
- 120 Xavier, N. M.; Rauter, A. P.; Queneau, Y. *Top. Curr. Chem.* **2010**, *295*, 19-62.
- 121 Verdaguer, X.; Hansen, M. C.; Berk, S. C.; Buchwald, S. L. *J. Org. Chem.* **1997**, *62*, 8522-8528.
- 122 Verdaguer, X.; Berk, S. C.; Buchwald, S. L. *J. Am. Chem. Soc.* **1995**, *117*, 12641-12642.
- 123 de Talancé, V. L.; Thiery, E.; Eppe, G.; Bkassiny, S. E.; Mortier, J.; Vincent, S. P. *J. Carbohydr. Chem.* **2011**, *30*, 605-617.
- 124 Hamed, R. B.; Henry, L.; Gomez-Castellanos, J. R.; Mecinović, J.; Ducho, C.; Sorensen, J. L.; Claridge, T. D. W.; Schofield, C. J. *J. Am. Chem. Soc.* **2012**, *134*, 471-479.
- 125 Zanardi, F.; Battistini, L.; Nespi, M.; Rassu, G.; Spanu, P.; Cornia, M.; Casiraghi, G. *Tetrahedron Asymmetr.* **1996**, *7*, 1167-1180.
- 126 Bernard-Gauthier, V.; Wangler, C.; Schirmacher, E.; Kostikov, A.; Jurkschat, K.; Wangler, B.; Schirmacher, R. *BioMed Res. Int.* **2014**, *2014*, 20.
- 127 Sigmond, J.; Honeywell, R. J.; Postma, T. J.; Dirven, C. M. F.; de Lange, S. M.; van der Born, K.; Laan, A. C.; Baayen, J. C. A.; Van Groeningen, C. J.; Bergman, A. M.; Giaccone, G.; Peters, G. J. *Ann. Oncol.* **2009**, *20*, 182-187.
- 128 Cividini, F.; Filoni, D. N.; Pesi, R.; Allegrini, S.; Camici, M.; Tozzi, M. G. *Biochim. Biophys. Acta* **2015**, *1850*, 1354-1361.
- 129 Kim, W.; Le, T. M.; Wei, L.; Poddar, S.; Bazy, J.; Wang, X.; Uong, N. T.; Abt, E. R.; Capri, J. R.; Austin, W. R.; Van Valkenburgh, J. S.; Steele, D.; Gipson, R. M.; Slavik, R.; Cabebe, A. E.; Taechariyakul, T.; Yaghoubi, S. S.; Lee, J. T.; Sadeghi, S.;

- Lavie, A.; Faull, K. F.; Witte, O. N.; Donahue, T. R.; Phelps, M. E.; Herschman, H. R.; Herrmann, K.; Czernin, J.; Radu, C. G. *Proc. Natl. Acad. Sci. U.S.A.* **2016**, *113*, 4027-4032.
- 130 Ho, D. H. W. *Cancer Res.* **1973**, *33*, 2816-2820.
- 131 Neef, A. B.; Luedtke, N. W. *ChemBioChem* **2014**, *15*, 789-793.
- 132 Chang, P. V.; Bertozzi, C. R. *Chem. Commun.* **2012**, *48*, 8864-8879.
- 133 Thirumurugan, P.; Matosiuk, D.; Jozwiak, K. *Chem. Rev.* **2013**, *113*, 4905-4979.
- 134 Ishizuka, T.; Liu, H. S.; Ito, K.; Xu, Y. *Sci. Rep-UK* **2016**, *6*, 33217.
- 135 Gierlich, J.; Burley, G. A.; Gramlich, P. M. E.; Hammond, D. M.; Carell, T. *Org. Lett.* **2006**, *8*, 3639-3642.
- 136 Ngo, J. T.; Schuman, E. M.; Tirrell, D. A. *Proc. Natl. Acad. Sci. U.S.A.* **2013**, *110*, 4992-4997.
- 137 Winz, M.-L.; Samanta, A.; Benzinger, D.; Jäschke, A. *Nucleic Acids Res.* **2012**, *40*, e78-e78.
- 138 Keng, P. Y.; Chen, S.; Ding, H.; Sadeghi, S.; Shah, G. J.; Dooraghi, A.; Phelps, M. E.; Satyamurthy, N.; Chatziioannou, A. F.; Kim, C.-J. C.; van Dam, R. M. *Proc. Natl. Acad. Sci. U.S.A.* **2012**, *109*, 690-695.
- 139 Keng, P. Y.; Dam, R. M. v. *Mol. Imaging* **2015**, *14*, 7290.2015.00030.
- 140 Kamijo, S.; Dudley, G. B. *J. Am. Chem. Soc.* **2006**, *128*, 6499-6507.
- 141 Denolf, B.; Leemans, E.; De Kimpe, N. *J. Org. Chem.* **2007**, *72*, 3211-3217.
- 142 Evans, D. A.; Dow, R. L.; Shih, T. L.; Takacs, J. M.; Zahler, R. *J. Am. Chem. Soc.* **1990**, *112*, 5290-5313.
- 143 Blough, B. E.; Carroll, F. I. *Tetrahedron Lett.* **1993**, *34*, 7239-7242.
- 144 Brown, H. C.; Kim, S. C.; Krishnamurthy, S. *J. Org. Chem.* **1980**, *45*, 1-12.
- 145 Hanessian, S.; Girard, C.; Chiara, J. L. *Tetrahedron Lett.* **1992**, *33*, 573-576.
- 146 Landsmann, S.; Luka, M.; Polarz, S. *Nat. Commun.* **2012**, *3*, 1299.
- 147 Cao, Y.; Galoppini, E.; Reyes, P. I.; Lu, Y. *Langmuir* **2013**, *29*, 7768-7775.
- 148 Roe, S.; Gunaratnam, M.; Spiteri, C.; Sharma, P.; Alharthy, R. D.; Neidle, S.; Moses, J. E. *Org. Biomol. Chem.* **2015**, *13*, 8500-8504.

- 149 Ohkubo, A.; Noma, Y.; Aoki, K.; Tsunoda, H.; Seio, K.; Sekine, M. *J. Org. Chem.* **2009**, *74*, 2817-2823.
- 150 Gonzalez, C.; Kavooosi, S.; Sanchez, A.; Wnuk, S. F. *Carbohydr. Res.* **2016**, *432*, 17-22.
- 151 Elend, M. D.; Fray, J.; Pryde, D. *Arkivoc* **2006**, 114-127.
- 152 Elhalem, E.; Comin, M. J.; Leitofuter, J.; García-Liñares, G.; Rodriguez, J. B. *Tetrahedron Asymmetr.* **2005**, *16*, 425-431.
- 153 Dasgupta, S.; Nitz, M. *J. Org. Chem.* **2011**, *76*, 1918-1921.

VITA

CESAR GONZALEZ

Born, Santiago, Chile

2006-2011

B.A., Chemistry
Florida International University
Miami, Florida

2013-2017

Doctoral candidate
Florida International University
Miami, Florida

2017

SoFLACS Graduate Travel Award

PUBLICATIONS AND PRESENTATIONS

Chbib, C., Sobczak, A. J., Mudgal, M., Gonzalez, C., Lumpuy, D., Nagaj, J., Stokowa-Soltys, K., and Wnuk, S. F. (2016) *S-Ribosylhomocysteine analogues modified at the ribosyl C-4 position*, Journal of Sulfur Chemistry, 307-327.

Gonzalez, C., Kavooosi, S., Sanchez, A., and Wnuk, S. F. (2016) *Reduction of sugar lactones to lactols with lithium triethylborohydride*, Poster presented at 251st ACS National Meeting & Exposition, San Diego, California.

Gonzalez, C., Kavooosi, S., Sanchez, A., and Wnuk, S. F. (2016) *Reduction of sugar lactones to hemiacetals with lithium triethylborohydride*, Carbohydrate Research. 432, 17-22.

Gonzalez, C., Sanchez, A., and Wnuk, S. F. (2017) *Clickable 4-N-alkanoyl and 4-N-alkylgemcitabine analogues with silicon-fluoride acceptors*, Poster presented at 253rd ACS National Meeting & Exposition, San Francisco, California.

de Cabrera, M., Gonzalez, C., Sulimoff, N., and Wnuk, S. F. (2017) *Synthesis of 4-N-Alkyl Gemcitabine Analog Bearing β -Keto Tosylate Moiety Suitable for ^{18}F -Labeling*, Poster presented at 253rd ACS National Meeting & Exposition, San Francisco, California.

Collins J., Lisova, K., Gonzalez, C., Wnuk S.F., and van Dam, M (2017) *Microscale and conventional radiosynthesis of ^{18}F -labeled gemcitabine analog via silicon-fluoride-acceptor chemistry*, oral presentation at 22nd International Symposium on Radiopharmaceutical Sciences, Dresden, Germany.

Gonzalez, C., De Cabrera, M., and Wnuk, S.F. (2017) *Fluorination of 4-N-Alkyl Gemcitabine Analogues with β -Keto Sulfonate Moieties*. Nucleosides, Nucleotides and Nucleic acids (in preparation).

Gonzalez, C., Sanchez, A., Collins, J., Lisova, K., van Dam, M., Barbieri, M. A., Ramachandran, C., and Wnuk, S.F. (2017) *The 4-N-Alkyl Gemcitabine Analogues with Silicon-Fluoride-Acceptor: Application to 18-Fluorine radiolabeling*. Journal of Medicinal Chemistry (in preparation).